Centre for Geo-Information

Thesis Report GIRS-2006-24

Relationships between Leaf Area Index, fAPAR and Spectral Vegetation Indices derived from MERIS across the Netherlands.

Ioakeim Pardalis

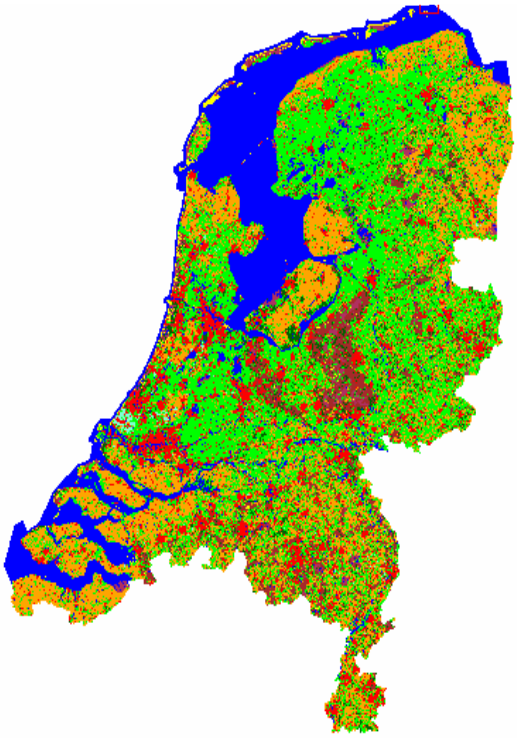

July, 2006

WAGENINGEN UNIVERSITY
WAGENINGEN UR

Relationships between Leaf Area Index, fAPAR and Spectral Vegetation Indices derived from MERIS across the Netherlands.

Pardalis Ioakeim

Registration number: 78 09 10 641 030

<u>Supervisors</u>:

Dr.Ir. J.G.P.W. Clevers

Dr.Ir. Lammert Kooistra

A thesis submitted in partial fulfilment of the degree of Master of Science at Wageningen University and Research Centre, The Netherlands.

July, 2006

Wageningen, The Netherlands

Thesis code number: GRS-80436
Wageningen University and Research Centre
Laboratory of Geo-Information Science and Remote Sensing
Thesis Report: GIRS-2006-24

ACKNOWLEDGEMENT

Many people contributed in different ways to the development of this study and I hereby would like to acknowledge all for their direct or indirect participation. Special emphasis I would like to give to the following people.

First of all, I am deeply indebted to my supervisors Dr. Lammert Kooistra and Dr. J.G.P.W. Clevers for their advice, help and support. Their guidance was critical, continuous and valuable through all the thesis work. Both were dedicated in supporting and discussing my aspirations and keeping me on track in a consistent and constructive way. I am grateful to my study advisor Willy ten Haaf for his advice and arrangement of conditions during my study. I would like to thank all my friends of MGI students for making our time so enjoyable at Alterra. I would also like to take this opportunity to express my gratitude to my family in Greece for their contribution in my study since the beginning.

ABSTRACT

Leaf area index (LAI) and the fraction of absorbed photosynthetically active radiation (fAPAR) are both important vegetation structural variable for the quantitative analysis of biophysical processes in the terrestrial ecosystem. In the context of resource management goals, earth observation (EO) of these variables is the most effective means of collecting data on a regular basis. Estimates of LAI and fAPAR are required for modelling vegetation productivity, studies of land surface climatology, and agricultural resource management .Relationships between LAI, fAPAR and vegetation indices (VI) derived from the different processing data levels (L1b and L2) of MERIS were studied for the Netherlands. The study area consisted of five land cover classes in the Netherlands: deciduous forest, coniferous forest, grassland, natural vegetation and arable land. Several variants of each VI were derived from the MERIS image data (L1b and L2). For each biome, the VIs were derived from radiance (VI_{RAD}), top of aerosol reflectance (VI_{TOAr}), and top of canopy reflectance (VI_{TOC}). To test the effects of spectral data processing and validate the MERIS biophysical products for the main vegetation land cover classes that occur in the Netherlands, ancillary data from the HyMap sensor and the Dutch land use database (LGN5) were used. The strength of the relationships between VI_{MERIS}-VI_{HyMap}, VIMERIS-LAI_{MERIS} and VI_{MERIS}-$fAPAR_{MERIS}$ was examined. Observations in the present study suggest the importance of converting to top of canopy reflectances whenever VIs are estimated for different vegetation land cover types. Image processing reduces the noise in the relationship of VI with biophysical variables and the VI_{HyMap}. The top of the canopy reflectance was found to produce stronger LAI–VI, VI-fAPAR and VI_{MERIS}-VI_{HyMap} relationships for both grass-dominated and arable land-dominated vegetation types of the Millingerwaard test site than the VIs based on top of atmosphere radiance, or top of aerosol reflectance. Thus, atmospheric correction is desirable in the formulation of LAI–VI and fAPAR-VI algorithms based on data derived from MERIS from the site of Millingerwaard. Further studies should include VI derived from digital numbers and TOA reflectance. In addition, a future study could perform a comparison at the multi-pixel (patch) scale, where the derived products might be statistically more stable.

TABLE OF CONTENTS

LIST OF TABLES

LIST OF FIGURES

ABBREVIATIONS AND ACRONYMS

ANN	Artificial Neural Network
APAR	Absorbed Photosynthetically Active Radiation (Wm^{-2})
CEOS-WGCV	Committee Earth Observing Satellites' Working Group on Calibration and Validation
ESA	European Space Agency
fAPAR	Fraction of Absorbed Photosynthetically Active Radiation
LAI	Leaf Area Index
LGN	Land cover database for The Netherlands
LGN5	Land cover database for The Netherlands based on datasets of 2003 and 2004
LUT	Look Up Table
µm	Micrometer
MERIS	Medium Resolution Imaging Spectrometer
MGVI	MERIS Global Vegetation Index
MODIS	Moderate Resolution Imaging Spectrometer
MTCI	MERIS Terrestrial Chlorophyll Index
NDVI	Normalized Difference Vegetation Index
NIR	Near Infrared
nm	Nanometer
NOAA	National Oceanic and Atmospheric Administration
R	Coefficient of correlation
RMSE	Root Mean Square Error
RSR	Reduced Simple Ratio
TOA	Top Of Atmosphere
TOAr	Top Of Aerosol
TOC	Top Of Canopy
TM	Thematic Mapper
VI	Vegetation Index
VITOARAD	Vegetation Index derived from the Top of Atmosphere Radiance

VITOArREF	Vegetation Index derived from the Top of Aerosol Reflectance
VITOCREF	Vegetation Index derived from the Top of Canopy Radiance
ρ	Reflectance values

1. INTRODUCTION

1.1. BACKGROUND

Vegetation and land cover play a key role in terrestrial biogeochemical processes, and changes in land cover induced by human activity have profound implications for climate, the functioning of ecosystems, and biogeochemical fluxes at regional and global scales (Dickinson and Henderson-Sellers 1988, Lean and Warilow 1989). As a consequence, a wide range of problems require reliable and accurate information on global land cover, and in particular, the distribution and properties of vegetation. Estimates of vegetation fractional cover, leaf area index (LAI), and absorbed radiation are required for modelling vegetation productivity (Gower et al. 1999), studies of land surface climatology (Behrenfeld and Sellers 2001), and agricultural resource management (e.g., McVicar and Jupp 1998, Prince 1991a).

Leaf area index (LAI), defined as the projected leaf area per unit of ground area (Ross 1981), is a key biophysical variable influencing land surface processes such as photosynthesis, transpiration, and energy balance (Bonan 1993). It is a dimensionless index used to quantify the single-sided vegetation leaf area per unit of ground area. LAI and the fraction of absorbed, photosynthetically active radiation (fAPAR) (0.4–0.7 μm) strongly control water, carbon and energy exchanges between vegetation and the atmosphere (Agnihothri 1996). On a global scale, both LAI and fAPAR are key variables in many climatic models (Sellers et al. 1996, Sellers et al. 1997) and models of net primary production (NPP) (Running et al. 1999). In the context of resource management goals, earth observation (EO) of these variables is the most effective means of collecting data on a regular basis. On a regional scale, EO estimates of LAI can provide valuable information for hydrological modelling (Andersen et al. 2002, Kite & Pietrorino 1996) and fAPAR is a key variable in the assessment of vegetation productivity (Prince 1991a

and Prince 1991b). Fractional vegetation cover, as first introduced by Deardorff (1978), is an important element for climate modeling.

Remotely sensed data recorded in narrow visible/near infrared wavebands can be used to estimate foliar biochemical content at local to regional scales (Curran 1989, Curran et al. 1997). This information can, in turn, be used to quantify, understand and manage vegetated environments (Johnson 1999, Curran 2001, Lamb et al. 2002). One of the problems addressed in recent years is to relate observations acquired from space to biophysical surface parameters, such as the leaf area index (LAI) and the fraction of absorbed photosynthetically active radiation (fAPAR) (Asner 1998, Hall et al. 1995). The first global maps of LAI and fAPAR were produced from AVHRR data (Sellers et al. 1996, Myneni et al. 1997). Medium spatial resolution satellite sensors operating in the solar domain (400-2500 nm) offer a unique way to monitor terrestrial surfaces over regional to global scales. Several applications are already using these data on an operational basis with a more improved spatial resolution (Baret et al. 2005).

Although remotely sensed data are becoming more available, operational algorithms or procedures to convert radiometric measurements into biophysical variables, such as LAI and fAPAR, are still under deveopment. There are two common approaches to estimating biophysical parameters using remote sensing imagery. The use of empirical relationships between reflectance observed by sensors operating in the spectral, directional, temporal and spatial domain and biophysical properties of the vegetation is illustrated by VI (Baret et al. 1995, Best and Harlan 1985, Curran 1983, Asrar et al. 1985a,b, Peterson et al. 1987, Price and Bausch 1995). Most vegetation indices (VIs) are qualitatively related to the vegetation amount (LAI, % cover,) and have been used as an indicator of vegetation growth (Tucker 1979, Clevers 1989 and Baret and Guyot 1991). Nowadays, these techniques are increasingly being replaced by radiative transfer based models (Sellers et al. 1995, Myneni et al. 1997, Shabanov et al. 2003 , Verhoef and Bach 2003), and progressively complemented by sophisticated methods known as inverse techniques

(Privette et al. 1996, Zarco-Tejada et al. 2003, Gastellu-Etchegorry et al. 2004) and data assimilation (Weiss et al. 2001, Olioso et al. 2002).

There are two major limitations in operational use of a modeling approach. The first one is related to the inversion process of the model. Some models may have multiple solutions, given a set of remote sensing measurements, and the inversion may not always converge (Jacquemoud 1993). This would result in unreliable estimates of biophysical variables. The second limitation is the computation time involved in a large number of inversion processes, which is a major barrier when using large satellite images.

A major limitation of the VI approach is the diversity of proposed equations. These equations vary not only in mathematical form (linear, power, exponential, etc.), but also in their empirical coefficients, depending primarily on vegetation type. Because there is no universal LAI–VI equation applicable to diverse vegetation types, it is difficult to use this approach with large-scale remote sensing images. Another limitation of this approach is the sensitivity of VIs to nonvegetation related factors such as soil background properties (e.g., Huete 1989, Qi et al. 1993), atmospheric conditions (e.g., Kaufman 1989, Vermote et al. 1990), topography (Holben and Justice, 1980; Justice et al., 1981; Pinter et al., 1987), and bidirectional nature of surfaces (Kimes et al. 1985, Deering 1989, Jackson et al. 1990 Roujean et al. 1992, Burgess and Pairman 1997). Of these categories the VI approach, introducing empirical relationships between ground-based biophysical values and various forms of multispectral and hyperspectral data, is the most successful and widely used (Pu et al 2003).

1.2. PROBLEM DESCRIPTION

The Medium Resolution Imaging Spectrometer (MERIS), one of the payloads on the European Space Agency's Envisat, is radiometrically a very accurate imaging spectrometer in space (Curran and Steele 2004). It has 15 programmable (2.5–20 nm

wide) wavebands in the 390–1040 nm region and a spatial resolution of 300 m. Because of its fine spectral and moderate spatial resolution and three-day repeat cycle, MERIS is a valuable sensor for the measurement and monitoring of terrestrial environments at regional to global scales (Verstraete et al. 1999). In the standard band setting, it has five discontinuous wavebands in red and near-infrared (NIR) wavelengths with band centres at 665 nm, 681.25 nm, 708.75 nm, 753.75 nm, 760.625 nm, 778, 865 and 885 nm. Derived products that have been developed (Verstraete et al. 1999) include the MERIS Global Vegetation Index (Gobron et al. 1999) and a MERIS Normalized Difference Vegetation Index. In addition, ESA is also considering the Fraction of Absorbed Photosynthetically Active Radiation (FAPAR) in vegetated areas as described by Govaerts et al. (1999) and a red-edge index as presented by Curran et al. (1995).

Various authors investigated NDVI from remote sensing imagery with the purpose of assessing biophysical plant canopy properties (Pinty et al. 1993), establishing its relationship to Leaf Area Index (Clevers 1988). Although commonly used, several drawbacks of the NDVI were found. The perpendicular vegetation index (PVI; Richardson and Wiegand 1977) was introduced to compensate to background effects. The index assumes that the perpendicular distance between pixels from the soil line (in the red–near-infrared space) is linearly related to the vegetation cover. For a given soil, the red (red) and near-infrared (NIR) reflectances are related by the equation of the soil line as NIR=a×red+b where a is the slope and b is the offset of the soil line. An index related to the PVI is the Weighted Difference Vegetation Index (WDVI) of Clevers (1988). Alternative indices have thus been developed using near-infrared and red bands. Pinty and Verstraete (1991) developed the Global Environmental Monitoring Index (GEMI) to compensate for atmospheric and illumination conditions. Huete (1988) introduced the Soil Adjusted Vegetation Index (SAVI) to take into account the reflectance contributions from background substrates. An alternative vegetation index is developed by Baret et al. (1989) and Baret and Guyot (1991): the Transformed Soil Adjusted Vegetation Index (TSAVI). This index minimizes the soil background effect (Baret et al. 1989). Finally Qi et al. (1994) introduced the Modified Soil Adjusted Vegetation Index (MSAVI) and the second Modified Soil Adjusted Vegetation Index (MSAVI2). For MERIS, a standard

product based on the Global Vegetation Index (MGVI) is developed following a physical and mathematical model description using three MERIS bands (Gobron et al. 1999).

For space observations in the solar spectrum, the presence of the atmosphere substantially modifies the intrinsic contribution of the surface to the signal. Both gaseous absorption and molecular or aerosol scattering reduce the available downward irradiance at ground level, as well as the reflected radiance in the upward path to the sensor. The increasing interest in the extraction of physical parameters from remote sensing data, for comparison of results from different sensors, obtained over different locations or at different times of the year require the need reliable and accurate recovery of surface reflectance.

Most atmospheric correction schemes are based on simplified formulations of the signal in order to ease inversion of Top of Atmosphere (TOA) radiances. Generally, gaseous absorption is separated from the rest. This correction requires integrated values of gas contents in the atmospheric column (mainly water vapour and ozone). The Rayleigh correction requires knowledge of barometric pressure. The correction for aerosols is more problematic, first because of their variable nature and abundance, and second because of their weak contribution to TOA radiances. Of course, this contribution is emphasized over dark surfaces, and the use of so-called Dark Dense Vegetation (DDV) is generally proposed (see, for the AVHRR, Holben et al. (1992)).

Generally, in this study, near-infrared and red band VI were used to investigate the effects of the radiometric processing applied to the MERIS image data on the VIs. The properties of VI depending on whether VI is defined in terms of top of the atmosphere radiances (MERIS Level 1b product), top of the aerosol reflectances, or top of canopy reflectances(MERIS Level 2 product) was examined. Their performance at the spatial scale of observation of MERIS, was investigated in terms of their comparisons with VI derived from the HyMap sensor. Furthermore, the VI relationships with LAI and fAPAR

derived from MERIS and the analysis of the their mutual relations for the vegetation land cover types that occur in the Netherlands was also a scope of our research.

1.3. RESEARCH OBJECTIVES

General objective

- Analysis of the effects of radiometric and spatial characteristics of MERIS on vegetation indices and on the estimation(and their relation with the LAI and fAPAR for the Netherlands) of LAI and fAPAR for the Netherlands

Specific objective

- A comparison of the different vegetation indices derived from the different radiometric MERIS data types (Top of Atmosphere Radiances, Top of Atmosphere Rectified Reflectances and Top of Canopy Reflectances) for the vegetation land cover types of the Netherlands
- Accuracy assessment of the biophysical parameters (LAI, FAPAR) derived from MERIS for the site of Millingerwaard,
- Specify the effects of the different radiometric MERIS data types and of the different vegetation indices to their relationship with the biophysical products (LAI, fAPAR) obtained for the different land cover classes.

Research questions

- What are the effects of atmospheric correction to the derivation of the vegetation indices for the different land cover classes in the Netherlands?
- What is the accuracy of LAI, fAPAR derived from MERIS when we validate these products using the HyMap derived LAI and fAPAR products for the site of Millingerwaad?

- Do the VI values observed at different stages of image processing suggest differential sensitivity to surface biophysical properties (LAI, fAPAR) across different vegetation land cover types?

1.4. STRUCTURE OF THE REPORT

Chapter one of this report comprises an introduction about the general background, overview of the context, definition of the topic and the importance of leaf area index and fAPAR as a key biophysical parameter. Description and definition of the problem is also main part of this chapter. The objectives of this study and research questions are covered in this chapter, as well. Chapter two deals with a review of the relevant literature and discusses similar studies conducted in the field of the study area. The third chapter describes the materials that were used and the methods that were followed in order to achieve the research objectives. The results of this study are presented in chapter four and discussed in chapter five. Conclusion and recommendations are given in the sixth chapter.

2. LITERATURE REVIEW

2.1. Leaf Area Index: Definition and Common Methods of Determination

The Leaf Area Index (LAI) may be described most simply as:

LAI = s/G

where s is the functional (green) leaf area of the canopy standing on ground area G (terminology after Beadle 1993). Because both s and G are normally measured as areas (m^2), LAI is dimensionless, although it is sometimes presented in units of m^2/m^2.

Care should be taken when making comparisons between LAI determinations that may not necessarily use the same methodology or even the same definition of LAI (Chen and Black 1992, Beadle 1993).

LAI is the major factor determining the amount of light intercepted by the plant canopy, but it varies greatly with species and canopy structure. Under optimum conditions for growth, its value for a closed canopy is related to the ability of the lower leaves in the canopy to intercept sufficient light to maintain a positive carbon balance (regardless of whether they are of the same stem, the same species, or competing/coexisting species. Table 1 presents some LAI maxima that have been observed from earlier studies. Many types of vegetation react to stress in the environment by producing canopies with lower LAI. Thus the LAI of a particular plot compared with typical values for such a biome/land cover type may provide an indicator of stresses, such as drought, flooding, nutrient deficiency, excessive heat or cold, as well as disease, phenology, etc.

Table 1. LAI maxima observed from earlier studies

Vegetation type	LAI maxima
Coniferous canopies	>15
Deciduous forests	6-8
Annual crops	6-7

It is important to note that LAI measured for large sample plots or satellite image pixels, comprises the average of a range of point values of LAI, often including different species and canopy types, as well as bare ground. In general, therefore, such area-weighted LAI values may be expected to display lower maximum values and lower variance than point measurements.

According to Barclay (1998), there are at least five common measures of LAI, which partly reflect the different purposes for which LAI is determined (determination of vegetation growth, estimation of potential physiological activity, study of light attenuation under plant canopies, etc.). The four most common of these are defined.

Definition (1): Total LAI is based on the total outside area of the leaves, taking leaf shape into account, per unit area of horizontal land below the canopy.

Definition (2): One-sided LAI is usually defined as half the total LAI, even if the two sides of the leaves are not symmetrical.

Definition (3): Horizontally projected LAI is the area of "shadow" that would be cast by each leaf in the canopy with a light source at infinite distance and perpendicular to it, summed up for all leaves in the canopy.

Definition (4): Inclined projected LAI, or "silhouette" LAI, represents the projected area of leaves taking into account individual leaf inclinations. An additional fifth definition, according to Barclay (1998), is a variation on this approach, counting overlapping leaf areas only once.

Most published values of LAI appear to use definition (2) or definition (3), with an increasing number of definition (4) in the literature (Barclay 1998). Definition (1) is rarely used (see discussion following description of methodologies). Definition (2) suffers from the problem that the meaning of "one-sided" is unclear for coniferous needles, highly clumped foliage, or rolled leaves (Chen and Black 1992). Chen and Black (1992) suggest that the LAI of non-flat leaves should be defined as half the total intercepting area per unit ground area, and that definition (3) should be abandoned. LAI according to definition (2) may exceed LAI according to definition (3) by a factor ranging from 1.28 (hemi-circular cylinders representing conifer needles), through 1.57 (representing cylindrical green branches) to 2.0 (spheres or square bars representing highly clumped shoots and some spruce needles) (Chen and Cihlar 1996). Regrettably, many individual reports of LAI in the literature fail to provide any details of the LAI definition assumed, and a significant fraction do not even describe the methodology used.

In this study, LAI is defined as one half the total leaf area per ground surface area as being used for flat leaves in current studies (Chen and Black 1992, Chen 1996, Liu *et al* 1997, Brown *et al.* 2000, Leblanc et al. 2002).

2.2. FAPAR Definition

FAPAR is inferred from the energy conservation law, and proportional to the difference between the downward solar energy at the top of the canopy plus the energy scattered upward from the soil to the canopy (at the bottom of the canopy) and the energy transmitted through the canopy to the soil plus the upward energy which is scattered by the canopy at its top:

$$f_{\mathrm{APAR}} = A_{\mathrm{PAR}}/Q_{\mathrm{in}} = (Q_{\mathrm{in}} + Q_{\mathrm{b}} - Q_{\mathrm{t}} - Q_{\mathrm{r}})/Q_{\mathrm{in}}. \qquad (1)$$

Where Qin is the incident PAR flux, Qb is the PAR reflected into the canopy from the soil background, Qt is the PAR transmitted through the canopy, and Qr is the above canopy reflected PAR (Hipps et al. 1983, Goward and Huemmrich 1992). PAR fluxes may be measured as energy fluxes (Wm^{-2}) or as counts of photons with units of ($\mu molm^{-2} s^{-2}$).

Productivity of a vegetated surface is closely related, among other factors, to the fraction of incident photosynthetically active radiation (0.4-0.7 μm) absorbed by the photosynthesizing tissue in a canopy (FAPAR). Ground cover and leaf area are perhaps the two most significant variables determining canopy PAR absorption. FAPAR (or its surrogate) can be determined from remote observations of surface spectral reflectance on the premise that surface structural and optical properties govern both these processes (Tucker, 1979).

Earlier studies have provides empirical evidence that fAPAR is related to top of the canopy spectral vegetation indices (Daughtry et al., 1983; Asrar et al., 1984; Hatfield et al., 1984; Gallo et al., 1985; Wiegand et al., 1991, 1992, among others).

2.3. Biophysical Variables Estimation Methods

Satellite remote sensing provides a unique way to obtain LAI over large areas . Current methods for estimating LAI from optical remotely sensed data are classified into several categories :

1) Using the empirical relationship of LAI and vegetation indices (VI);

2) Through the inversion of a radiative transfer (RT) model;

3) Lookup table (LUT) method and Neural network (NN) algorithms.

The two main methods to estimate biophysical variables from RS data are exposed in this section. The first method in becoming operative was the use of “Vegetation Indices”, but since it has many drawbacks a second one is being introduced with success in operational RS applications. This method is known as physically-based model inversion.

2.3.1 Vegetation Indices for LAI-fAPAR Estimation

The theoretical basis for ‘empirical-based’ vegetation indices is derived from examination of typical spectral reflectance signatures of leaves (Figure 1). The reflected energy in the visible is very low as a result of high absorption by photosynthetically active pigments with maximum sensitivity in the blue (470 nm) and red (670 nm) wavelengths. Nearly all of the near-infrared radiation is scattered (reflected and transmitted) with very little absorption, in a manner dependent upon the structural properties of a canopy (LAI, leaf angle distribution, leaf morphology). As a result, the contrast between red and near-infrared responses is a sensitive measure of vegetation amount, with maximum red - NIR differences occurring over a full canopy and minimal contrast over targets with little or no vegetation (Figure 1). For low and medium amounts of vegetation, the contrast is a result of both red and NIR changes, while at higher amounts of vegetation, only the NIR contributes to increasing contrasts as the red band becomes saturated due to chlorophyll absorption.

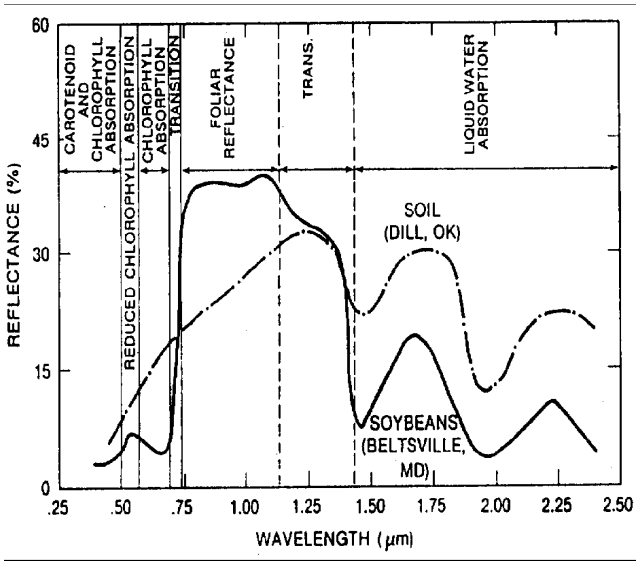

FIGURE 1. SPECTRAL REFLECTANCE SIGNATURE OF A PHOTOSYNTHETICALLY ACTIVE LEAF WITH A SOIL SIGNATURE TO SHOW CONTRAST (TUCKER AND SELLER 1986).

The red-NIR contrast can be quantified through the use of ratios (NIR/red), differences (NIR-red), weighted differences (NIR-k*red), linear band combinations (x1 * red + x2 * NIR), or hybrid approaches of the above. Vegetation indexes are measures of this contrast and thus are integrative functions of canopy structural (%cover, LAI, LAD) and physiological (pigments, photosynthesis) parameters.

Vegetation indices (VIs) are dimensionless, radiometric measures (radiances values, reflectance values and satellite DN) of vegetation exploiting the unique spectral signatures and behaviour of canopy elements, particularly in the red and NIR portions of the spectrum. Data from different wavebands (often visible and near-infrared wavelengths) have been combined to produce spectral VIs, which are sensitive measures of both spatial and temporal variations in vegetation photosynthetic activity and canopy structural variations. Each of the radiometric measurements results into a different, but correct, vegetation index value for the same surface conditions (Jackson and Huete 1991). So in the case of NDVI, (*qNIR-qred*)/(*qNIR+qred*), *q* is reflectance), the values will

differ as a function of the radiometric processing applied to the image data as it is presented in figure 2 (Teillet et al 1997**).**

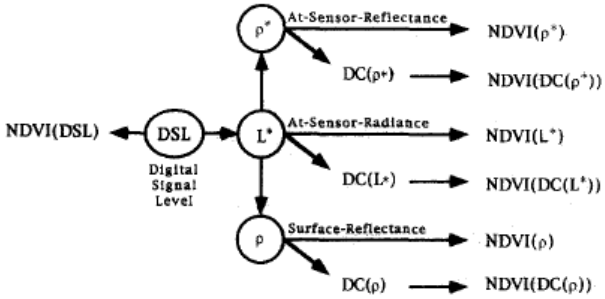

FIGURE 2. DIFFERENT RADIOMETRIC REPRESENTATIONS OF NDVI ILLUSTRATED IN THE CONTEXT OF POSSIBLE DATA PROCESSING FLOWS. (TEILLET ET AL, 1997)

VIs are, therefore, used to assess temporal and spatial variation of biophysical data , such as LAI (Best and Harlan 1985, Friedl et al. 1994, Curran and Williamson 1985) and the fraction of the photosynthetically active radiation absorbed by the plant canopy (Asrar et al. 1984, Epiphanio and Huete 1995).

Myneni et al. (1995) reported that there are more than 12 vegetation indices in the optical region and that they have been correlated with vegetation amount, *f*APAR, unstressed vegetation conductance, and photosynthetic capacity. The choice and suitability of a VI is generally determined by its sensitivity to the characteristics of interest, and/or its sensitivity to disturbing factors (atmosphere, soil background, canopy architecture, topography). According to the effects that they are able to address a general classification is:

- Intristic indices based on the ratios of 2 or more bands. They are difficult to interpret for low LAI values (Rondeaux et al. 1996) and they are very sensitive to soil background
- Soil–line vegetation indices: improving the resistance to soil effects
- Atmospherical resistant indices, by adding to the index atmospheric characteristics for minimizing these effects.

Generally, vegetation indices approach a saturation level asymptotically for a certain range of LAI (Sellers 1985) and respond linearly to fAPAR. However, a biophysical explanation of the relationship between these indices and observable vegetation phenomena is still subject to much discussion. Many studies have concluded that VI to LAI/*f*APAR relationships are canopy structure and land cover dependent, varying with changes in leaf angle distribution, vegetation clumping, row orientation, spacing, and optical properties of canopy components (leaf, stem, etc.) (Asrar et al. 1992, Baret and Guyot 1991, Choudhury 1987, Goward and Huemmrich 1992, Roujean and Breon 1995). Different canopy types exhibit drastic variations in canopy structures and reflectance properties, which can produce different VI values while having identical LAI or fAPAR values. If satellite data are to be used as a measuring tool to determine LAI/fAPAR over large areas where there are differences in canopy characteristics, then an understanding of these relationships specific to a given type of canopy must be developed.

In addition, solar zenith angle, sensor view angle, atmospheric conditions, and background influences from soil and litter alter remotely sensed spectral signatures and the derived vegetation indices significantly (Baret et al. 1991, Huete 1987, Deering et al. 1992, Deering et al. 1994). As noted in numerous studies, darker soil substrates result in much higher vegetation index values for a given amount of vegetation when the ratio vegetation index (qNIR/$q$red, q is reflectance) or the normalized difference vegetation index were used as vegetation measures, while opposite soil brightness influences occur with the perpendicular vegetation index (PVI) (Huete et al. 1985, Elvidge et al. 1985). Atmospheric turbidity generally inhibits reliable measures of vegetation and sometimes renders atmosphere-induced variations on canopy spectra to exceed those due to vegetation development. These effects make the accurate and quantitative translation of VIs more difficult and complicated.

Finally, VIs can estimate only one parameter at a time, because it was specifically developed for each case and parameter. The fitted equation varies not only in mathematical way but also in its empirical coefficients, depending on the studied

parameter and the sensor characteristics (geometry, bands, bandwidth, etc). This disadvantage implies that there is not a universal equation, making it difficult to apply this methodology at large scales (Qi et al. 2000).

2.3.2 Radiative Transfer Models

An alternative to empirical relationships is a modelling approach based on a set of radiative transfer equations or models. In this approach the inversion of a vegetation reflectance model may be used to estimate the biophysical characteristics of the canopy, provided sufficient information can be obtained from the combined remote sensing and ancillary data. Inversion involves adjusting model parameters until the model reflectance best matches the measured reflectance (Goel 1988, Privette et al. 1994).

Inversion of a canopy radiative transfer model is usually achieved numerically by minimizing the difference between measured canopy reflectance samples and modelled values using an optimization routine (Goel 1988, Privette et a*l* 1994). Canopy radiative transfer model inversions are a robust approach to access canopy structural information using remotely sensed data, yet they are limited by the potential lack of reflectance information needed to successfully execute the model inversion (Asner et al. 1998c,d). However, hyperspectral data has been shown to provide sufficient reflectance information from which canopy attributes can be estimated via inverse modelling.

2.4. Validation of MERIS Moderate Resolution Products

Researchers have long been concerned with the need to quantify the accuracy of remotely sensed land cover classifications at the local scale but with the increase in data sets from coarse resolution sensing systems, attention has turned to the challenge of global product ‘validation’ (Justice and Townshend 1994, Justice et al. 1998). ‘Validation’ is the process

of assessing by independent means the accuracy of the data products derived from the system outputs. ‘Validation’ is distinguished from calibration which is the process of quantitatively defining the system response to known, controlled signal inputs (WWW 1). In general, ‘validation’ refers to assessing the uncertainty of higher level, satellite sensor derived products (e.g. VIs, fAPAR, LAI) by analytical comparison to reference data, which is presumed to represent the target value. Intercomparison of data products or model outputs provides an initial indication of gross differences and possibly insights into the reasons for the differences. However independent ‘validation’ data are needed to determine product accuracy. Whereas there are accepted standards for instrument calibration, standards for ‘validation’ of higher order products have yet to be developed.

Currently, the space agencies have several moderate and coarse spatial resolution (250m–4 km) sensing systems in orbit, providing similar land products, e.g. vegetation indices, albedo, leaf area index (LAI), fAPAR e.g. from MERIS, MODIS, AATSR, VEGETATION. Establishing standard methods and protocols for ‘validation’ of these products will enable a broader participation in ‘validation’ campaigns and programs, the sharing and multiple-use of ‘validation’ data, and comparisons and inter-use between products. Common field sites and standard methods for data collection and presenting product accuracy can be expected to foster product standardization and synergy from these various sensors.

Initiated in 1984, the Committee Earth Observing Satellites’ Working Group on Calibration and Validation (CEOS WGCV) pursues activities to coordinate, standardize and advance calibration and validation of civilian satellites and their data (Baret et al. 2005, Morisette et al. 2005). One subgroup of CEOS WGCV, Land Product Validation (LPV), was established in 2000 to define standard validation guidelines and protocols and to foster data and information exchange relevant to the validation of land products.

Having multiple global LAI products and validation activities related to these products it suggests that a direct comparison between ground measurements and corresponding global or large regional satellite products (VIs,LAI, fAPAR) is not recommended because of scale-mismatch, geolocation errors and vegetation heterogeneity at the resolution of the large swath satellite data. Thus, an intermediate step that involves a fine resolution map of the variable of interest is introduced. This map is generated with field data and high resolution satellite data (ETM+, SPOT, ASTER, etc.) When aggregated to the moderate resolution, this map serves as the ground-truth (Tan et al. 2005, Wang et al. 2004). Therefore, the validation of moderate resolution VIs, LAI, fAPAR products includes these steps (Figure 3) - ground sampling of vegetation variables during field campaigns, generation of a fine resolution map of the variables and comparison of the aggregated fine resolution map with moderate products. The achievement of this global validation activity is known as a bottom-up approach (Figure 3).

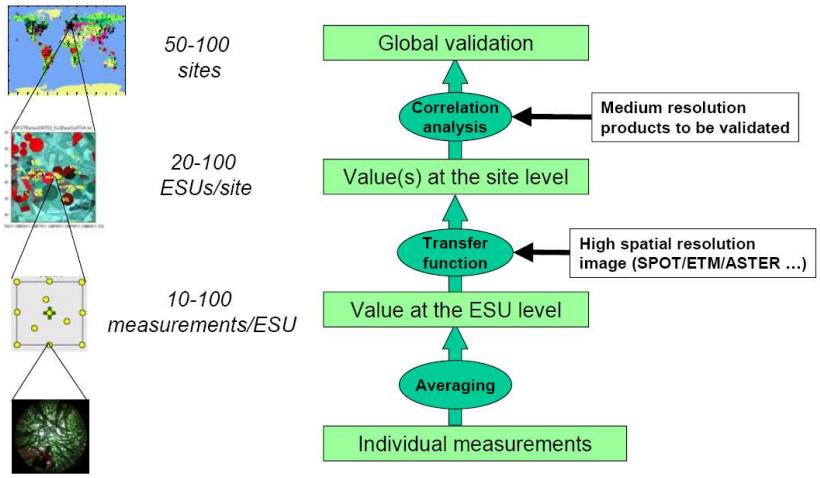

FIGURE 3.THE GENERAL VALIDATION PROCEDURE APPLIED TO LAI ACCORDING TO CEOS LAI INTERCOMPARISON OVERVIEW CAN BE DESCRIBED SCHEMATICALLY (BARET *ET AL.*, 2005; MORISETTE *ET AL.*, 2005)

3. MATERIALS AND METHODS

3.1. Study Area and Methodology

Relationships between LAI, fAPAR and vegetation indices derived from the different processing data levels of MERIS were studied for the Netherlands. The study area consisted of five vegetation classes in the Netherlands: deciduous forest, coniferous forest, grassland, natural vegetation and arable land (Figure 5). The decision to work with these classes was based on the availability of the necessary input data: land cover data and remote sensing data.

The general methodology was divided in three phases: preparation, processing and analysis. In the preparation phase we defined and prepared all necessary input data (remote sensing and land cover data). The processing phase involved the processing of the remote sensing data (MERIS L1b, L2 and HyMap). Four main processing blocks were necessary for our research objectives : 1) estimation of VI from the available L1b and L2 MERIS data, 2) estimation of LAI and fAPAR from MERIS 3) estimation of VI from the HyMap data and finally assessment of the LAI and fAPAR from the HyMap sensor. An overview of the general methodology steps is shown in the Figure 4:

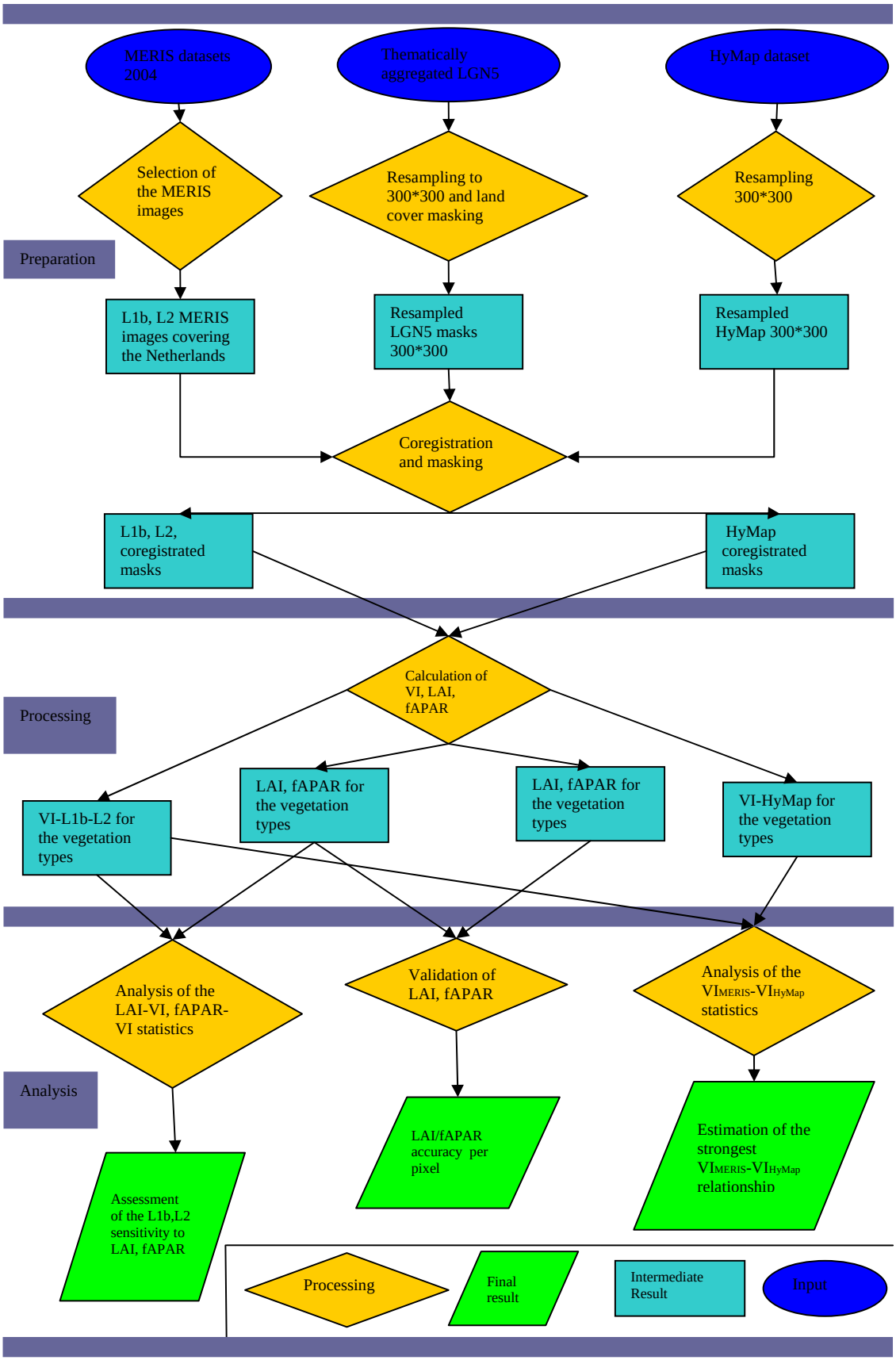
MERIS datasets 2004
Thematically aggregated LGN5
HyMap dataset
Selection of the MERIS images
Resampling to 300*300 and land cover masking
Resampling 300*300
Preparation
L1b, L2 MERIS images covering the Netherlands
Resampled LGN5 masks 300*300
Resampled HyMap 300*300
Coregistration and masking
L1b, L2, coregistrated masks
HyMap coregistrated masks
Calculation of VI, LAI, fAPAR
Processing
VI-L1b-L2 for the vegetation types
LAI, fAPAR for the vegetation types
LAI, fAPAR for the vegetation types
VI-HyMap for the vegetation types
Analysis of the LAI-VI, fAPAR-VI statistics
Validation of LAI, fAPAR
Analysis of the VIMERIS-VIHyMap statistics
Analysis
Assessment of the L1b,L2 sensitivity to LAI, fAPAR
LAI/fAPAR accuracy per pixel
Estimation of the strongest VIMERIS-VIHyMap relationship
Processing
Final result
Intermediate Result
Input

Figure 4. Flowchart of the Methodology

3.2. LGN-5

3.2.1. Description of the Dataset

For the analysis of the relations between the VIs-LAI-fAPAR for specific land use types in the Netherlands, a training dataset, the Dutch land use database (LGN), was used. LGN5 is a geographical database that describes the land use in The Netherlands for the period 2003-2004. It has a grid structure of 25 meters cell size, with an application scale of 1:50.000. The nomenclature of the LGN5 database consists of 39 classes covering urban areas, water, forest, various agricultural and natural land cover types. LGN is produced from multi-temporal classification of satellite imagery with ancillary data. Currently, the version 5 is based on satellite data of the year 2003 for the provinces of the east of the Netherlands and satellite data of 2004 for the provinces of the western part of the country. The overall classification accuracy for all provinces is 78% with values ranging from 46% till 93% (Hazeu 2005). The 39 classes of the LGN5 were recoded into nine classes (grassland, deciduous forest, coniferous forest, arable land, natural vegetation, water, built-up areas, greenhouses, bare-soil) as it is shown in Figure 5.

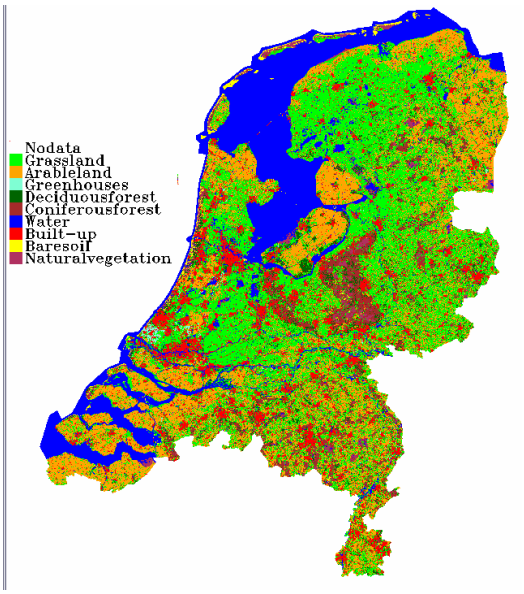

FIGURE 5. THE DUTCH LAND USE DATABASE AGGREGATED TO 9 CLASSES AND 300 M PIXEL SIZE AND FINALLY MASKED FOR THE STUDY AREA.

3.2.2. Preprocessing

The LGN-5 dataset were georeferenced to the map projection UTM (Zone 31 N, geodetic datum WGS84). Subsequently, the LGN5 was aggregated from 25 meters to 300 meters cell size displaying the largest cover type fraction per pixel. The resampling was done by majority fraction with the erdas imagine software.

3.3. MERIS

3.3.1. Description of the Dataset

MERIS is a medium-spectral resolution, imaging spectrometer operating in the solar reflective spectral range. Fifteen spectral bands are routinely acquired in the 390 nm to 1040 nm spectral range (Table 2). MERIS allows a global coverage of the Earth in 3

days. As compared to other medium resolution instruments, the spectral sampling is very unique and the algorithms developed take full advantage of this design.

Table 2 . MERIS spectral characteristics: band centre and width

#	Centre (nm)	Width (nm)	Potential Applications
1	412.5	10	Yellow substance and detrital pigments
2	442.5	10	Chlorophyll absorption maximum
3	490	10	Chlorophyll and other pigments
4	510	10	Suspended sediment, red tides
5	560	10	Chlorophyll absorption minimum
6	620	10	Suspended sediment
7	665	10	Chlorophyll absorption and fluo. reference
8	681.25	7.5	Chlorophyll fluorescence peak
9	708.75	10	Fluo. Reference, atmospheric corrections
10	753.75	7.5	Vegetation, cloud
11	760.625	3.75	Oxygen absorption R-branch
12	778.75	15	Atmosphere corrections
13	865	20	Vegetation, water vapour reference
14	885	10	Atmosphere corrections
15	900	10	Water vapour, land

The MERIS instrument is one of the payload components of the European Space Agency's (ESA) environmental research satellite Envisat, launched in March 2002. It is onboard the ENVISAT platform. It's helio-synchronic near polar orbit definition and some additional instrument characteristics are defined in Table 3 .

Table 3. Characteristics of the ENVISAT instrument and orbit definition

Orbit altitude (km)	799.8
Repeat cycle (days)	35
Period (min)	100.59
Inclination (°)	98.55
Equatorial descending node crossing time (hr)	10:00
Band-to-band registration	<0.1 pixel
Band-centre knowledge accuracy	<1 nm
Polarisation sensitivity	<0.3%
Radiometric accuracy	<2%
Band-to-band accuracy	<0.1%
Dynamic range	Up to albedo 1.0

MERIS scans the Earth's surface by the "push broom" method. CCD arrays provide spatial sampling in the across track direction, while the satellite's motion provides scanning in the along-track direction. The Earth is imaged with a spatial resolution of 300 m (at nadir) that provides the full resolution data (FR). This resolution is reduced to 1200 m (reduced resolution: RR) by the on board combination of four adjacent samples across track over four successive lines. The instrument's 68.5^{o} field of view around nadir covers a swath width of 1150 km.

MERIS data is provided at three levels of processing: level 0, level 1 and level 2. Level 0 consists of the core information recorded in packets by the instrument. This information is not generally available to users and it serves as basis for level 1. Level 1 comprises geo-coded top of atmosphere (TOA) data radiances [$Wsr^{-1}m^{-2}\mu m^{-1}$] and it is the base for level 2. Level 2 provides reflectance values for the different kinds of data products. Level

2 reflectances are different in nature depending on the surface (WWW 2 MERIS-Envisat 2005):

- over clouds, they are TOA reflectances,
- over land, they are Top Of Aerosol (TOAr) reflectances corrected only for Rayleigh diffusion but not corrected for the diffusion by aerosols. The correction for aerosol partially has been addressed by using values in the blue region namely band 2 (442 nm) and one band in the red and near infrared, namely band 8 (681 nm) and band 13 (865 nm).
- over water, they are surface reflectances.

For our study we used the full resolution data L1b products and the products over land of MERIS level 2.

3.3.2. Level 1b

The MERIS Level 1b data products consist of calibrated top of the atmosphere radiances, geolocated and resampled on a regular grid. The full resolution geolocated and calibrated TOA Radiance high-level structure of the product is shown in Appendix 1.

A variety of images from the year 2004 was available for our study. A cloud free image from August 8th 2004 was finally selected as an input for this study (Figure 6). More details concerning this dataset can be observed in Appendix 2.

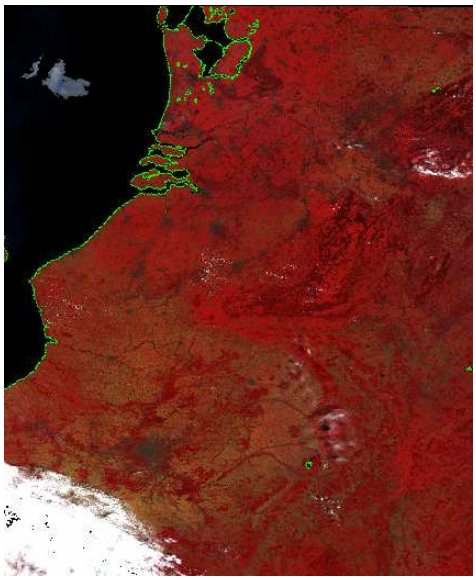

FIGURE 6.MERIS L1B FULL RESOLUTION IMAGES OF AUGUST 8TH 2004. BANDS 14, 8 AND 3 ARE DEPICTED IN RGB.

3.3.3. Level 2

MERIS level 2 land surface products provide TOAr reflectance in 13 bands. Bands 11 and 15 were excluded from the official L2 product for the following reasons:

• **Band 11**. This very narrow band is just located in the oxygen absorption band at the end of chlorophyll absorption. It would bring only marginal additional information on leaf and background optical properties while conveying errors due to uncertainties in oxygen pressure values.

• **Band 15**. This water absorption band will not bring very significant information on canopy characteristics as compared to bands 12 to 13, while also conveying errors due to uncertainties in water vapour values.

The Rayleigh correction is organised in several steps: knowing the surface pressure above a pixel, the Rayleigh optical thickness is computed. With the knowledge of this optical thickness and the geometry of the pixel, the Rayleigh reflectance is then derived from a lookup table (WWW 3). MERIS level 2 has partially addressed the correction for aerosols by using values in the blue region, namely band 2 (442 nm) and one band in the red and near infrared, namely band 8 (681 nm) and band 13 (865 nm). This combination has generated rectified bands that would have been measured in the red and near infrared at the top of canopy (TOC) (Gobron et al. 2004). Reflectance data per pixel is expressed as [%*100].

In addition, MERIS level 2 land surface products includes the MERIS Global Vegetation Index (MGVI) (Gobron et al. 2004), the MERIS Terrestrial Chlorophyll Index (MTCI) (Dash and Curran 2004). The MGVI algorithm is calculated as:

$$MGVI = \frac{l_{0,1}B_1^2 + l_{0,2}B_2^2 + l_{0,3}B_1B_2 + l_{0,4}B_1 + l_{0,5}B_2 + l_{0,6}}{l_{0,7}B_1^2 + l_{0,8}B_2^2 + l_{0,9}B_1B_2 + l_{0,10}B_1 + l_{0,11}B_2 + l_{0,12}} \qquad \textbf{(2)}$$

where B_1 and B_2 are the rectified spectral bands for the red and near infrared, respectively, and $l_{0,n}$ are the coefficients for the polynomial provided in Gobron *et al.* (2004). The design of MGVI is based on a two step procedure where the spectral radiances measured in the red and near-infrared bands are first, rectified in order to ensure their decontamination from atmospheric and angular effects. Second, they are combined together in a mathematical formula that generates fAPAR values (Gobron 2003). The overall scientific objective of the MGVI is to exploit the spectral reflectance measurements acquired by the instrument to provide users with reliable qualitative and qualitative information on the state of the plant cover over terrestrial areas.

In addition the MTCI is defined as:

$$MTCI = \frac{\rho_{band10} - \rho_{band9}}{\rho_{band9} - \rho_{band8}} \quad \textbf{(3)}$$

where ρ are reflectance values for different bands.

For this study the full resolution MERIS level 2 reflectance values, MGVI and MTCI for the Netherlands, from 2004 was used. Specifications of the spectral bands of MERIS Level 2 are given in Table 4.

Table 4. The bands of the MERIS level 2.

Band nr.	Band centre [nm]	Bandwidth [nm]
1	412.5	9.9
2	442.4	10.0
3	489.7	10.0
4	509.7	10.0
5	559.6	10.0
6	619.6	10.0
7	664.6	10.0
8	680.9	7.5
9	708.4	10.0
10	753.5	7.5
12	778.5	15.0
13	864.8	20.0
14	884.8	10
Rectified red	681	7.5
Rectified near infrared	865	20.0

A cloud free image from August 8th 2004 was delivered as an input for this study. Reflectance data per pixel is expressed as [%*100]. More details concerning this dataset can be observed in Appendix 3. The image is shown in Figure 7.

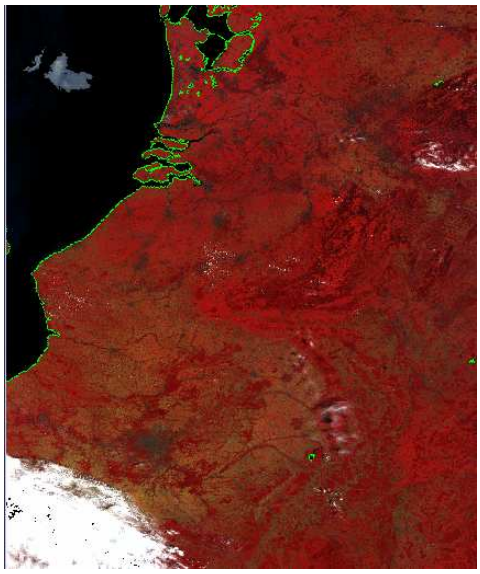

FIGURE 7. MERIS L2 FULL RESOLUTION IMAGES OF AUGUST 8TH 2004. BANDS 14, 8 AND 3 ARE DEPICTED IN RGB.

3.3.4. Preprocessing of the L1b and L2 MERIS Datasets

Effective analysis and treatment of the images required several preprocessing steps. These steps were carried out to assure that the measurements from each sensor (MERIS and HyMap) were as closely comparable as possible. Before any analysis, the satellite images need some correction procedures due to the geometric and radiometric distortions during the acquisition process. These corrections can be divided in two categories: geometric and radiometric corrections. The same procedure was applied for both L1b and L2 MERIS datasets.

Selection of MERIS datasets

Our goal was to acquire image pairs of MERIS and HyMap as nearly time coincident as possible with the July 28th (acquisition date of HyMap dataset), constrained by the requirement that each image needed to be "essentially cloud-free" for the comparison. For the year 2004 a large number of MERIS images were available. The most appropriate MERIS image was the one of August 8th.

Geometric corrections

Geometric corrections are necessary to reduce the effect of geometric distortions and they enable us to match the datasets with the resampled LGN5 database. For both MERIS datasets we assign the map projection UTM (Zone 31 N, geodetic datum WGS84) through the use of the BEAM software. However, observable differences existed between the resampled LGN5 and satellite images. Therefore we performed an image to image co-registration between each MERIS dataset and the resampled LGN5. For each image to image co-registration 27 ground control points were recorded between the two images. At last, a nearest neighbour resampling function was used because it preserves the information of the image pixels most closely.

Radiometric corrections

As we are using radiance and reflectance values from the MERIS level 1b and level 2 products, radiometric corrections are already performed (WWW 3):

Level 1b radiometric processing: the valid MERIS samples are digital counts resulting from the acquisition by MERIS of passive optical spectral radiance remote sensing. The objective of the radiometric processing is to estimate, by an inverse model, the spectral radiance which caused these counts. The radiance sensed by MERIS is, for a given set of target physical parameters and illumination and observation angles, proportional to the extraterrestrial sun spectral fluxx, (WWW 4).

Level 2 corrections: The atmospheric correction scheme is a simple but robust modelling of the signal which yields simple conversions of TOA radiance into surface reflectance. The signal decomposition involves three steps. In the first stage, gaseous absorption is removed from the signal (oxygen, ozone and water vapour).

The second step address corrections related with the Rayleigh scattering: The objectives of the Rayleigh corrections is twofold: first it allows to estimate the Rayleigh reflectance that will eventually be retrieved from the total Top Of Atmosphere signal to have an estimate of the Top Of Aerosol reflectance from which vegetation indices are later retrieved, secondly it allows to estimate all the Rayleigh transmittance factors that are used to bring down the Top Of Atmosphere signal down to the surface.

The correction for aerosols is more problematic, due to their variable nature and abundance, and their weak contribution to TOA radiances. Because their contribution is emphasized over dark surfaces, the use of so-called Dark Dense Vegetation (DDV) is generally proposed (see, for the AVHRR, Holben *et al*. (1992)).

3.4. HyMap Sensor

3.4.1. HyMap sensor characteristics

The HyMap sensor is an airborne imaging system that is used for earth resources remote sensing. It records a digital image of the earth's sunlit surface underneath the aircraft . Unlike standard aerial cameras, the HyMap records images in a large number of wavelengths. In essence, the HyMap sensor is an airborne spectrometer.

The HyMap records an image of the earth's surface by using a rotating scan mirror which allows the image to build line by line as the aircraft flies forward. The reflected sunlight

collected by the scan mirror is then dispersed into different wavelengths by four spectrometers in the system.

For the present study, a single HyMap image is used. The flight was carried out on July 28th, 2004, over the Milingerwaard floodplain along the river Waal near the city of Nijmegen.

The input image for this study was delivered geocoded in the map projection UTM (Zone 31 N, geodetic datum WGS84), band simulated (to MERIS bands), radiometrically and atmospherically corrected. Reflectance data per pixel is expressed as [%*100].

For further processing of the airborne data, data outside the study area was masked out, in order to save memory space and computational time.

3.4.2. Preprocessing

Before any analysis, the satellite image needs some correction procedures due to the geometric and radiometric distortions during the acquisition process. Because the input image for this study was already geocoded in the map projection UTM (Zone 31 N, geodetic datum WGS84), radiometrically and atmospherically corrected and simulated to MERIS bands the preprocessing stage involves only the co-registration.

Aggregation

Comparison of the MERIS and HyMap derived VIs, LAI, fAPAR products, required aggregation of the HyMap measurements to a spatial resolution equivalent to the MERIS measurements. Numerous aggregation methods have been used in remote sensing, including averaging all values, sampling every *n*th pixel and choosing the "dominant" value (Bian 1997). In this case, since we are attempting to approximate the integrated

VIs, LAI, fAPAR that the MERIS instrument measures, we employ the averaging approach.

Geometric corrections

Examining the relative performance of HyMap and MERIS requires, as much as possible, that individual compared pixels are from the same location on the Earth's surface. One of the largest potential sources of error is relief displacement caused by the two sensors viewing the same variable elevation terrain from two different look angles [Bernstein, 1983 and Slama, 1980].

A comparison between the HyMap image resampled to 300m pixel size and LGN-5 image, revealed observable differences. One should note that the resampling of the original HyMap image to the aggregated 300 m pixel size also contribute to the geometric inaccuracy. Therefore, geographic reference points were extracted by locating clearly observed points in the HyMap image and the MERIS image. Nearest neighbour re-sampling was employed in the co-registration process to preserve as much as possible the radiometry of the imagery. Some residual misalignment between HyMap and MERIS is still evident in the resultant products, probably the result of the differing spatial resolution of the HyMap sensor and MERIS instrument.

3.5. Vegetation Indices

The MERIS (L1b, L2) and HyMap reflectance derived VIs was examined in this study. These results can provide a check on the use of MERIS derived VIs and their correlation to the LAI, fAPAR variables for the Netherlands. At the same time a comparison with VI derived from the HyMap sensor is important because it relates to the spatial correlation between the two sensors and can stand as an evaluation of the performance of the TOA Radiances, TOAr Reflectances and TOC reflectances derived vegetation indices The

MERIS derived VIs have a spatial resolution of 300m. The inputs are red and near-infrared, top of atmosphere (TOA) data radiances, top of aerosol (TOAr) reflectances and top of canopy (TOC) data reflectances that corresponds to the bands 8 and 13, respectively. The HyMap derived VI have a spatial resolution of 5m. The 5m VIs are aggregated to 300m by employing the averaging approach.

Among the many different VIs found in the literature, some of the classical ones, soil adjusted and atmospherically resistant ones, were selected. In addition some other VIs specific for being applied to the MERIS bands were also studied.

The vegetation index values were calculated for the MERIS and HyMap scenes for selected vegetation targets: grassland, arable land, deciduous forest, coniferous forest, natural vegetation.

- The Normalized Difference Vegetation Index (NDVI), was calculated by Tucker (1979) as:

  (NIR-RED)/(NIR+RED) **(4)**

- The Weighted Difference Vegetation Index (WDVI), was calculated by Clevers (1988) as:

  NIR-g*Red **(5)**

  Where, g=slope of soil line

The parameter g was calculated and corresponds to 1 for the radiances and 1.2 for the reflectances of L1 and L2 MERIS images, respectively . For the HyMap images the same parameter corresponds to 1.

- The Modified Soil Adjusted Vegetation Index (MSAVI) was calculated by Qi et al.(1994) as:

(2NIR+1-[(2NIR+1) 2 -8(NIR-RED)] 0.5)/2 **(6)**

- The Perpendicular Vegetation Index (PVI) was calculated by Richardson and Wiegand (1977) as:

[NIR-a (RED)-b]/ [1+ (-a) 2] 0.5 **(7)**

Where a=slope of soil line and b is the soil line intercept

- The Global Environmental Monitoring Index (GEMI) was calculated by (Pinty and Verstraete (1991) as:

[eta(1- 0.25×eta)]- [(red- 0.125)/ (1- red)] **(8)**

Where eta is defined as: [2[(NIR)2 –(RED)2] + (1.5 NIR) + (0.5 RED)] / (NIR+RED+0.5)

3.5. Soil Line Concept

The soil line is a linear relationship between the NIR and R reflectance of bare soil originally discovered by Richardson and Wiegand (1977):

$NIR = ß_1 * R + ß_0$ **(9)**

where $ß_1$ is the soil line slope and $ß_0$ is the intercept. The soil line for a particular soil type "...results from the combined variations of its surface status characterized by its roughness and moisture" (Baret et al., 1993). Jasinski and Eagleson (1989) demonstrate that three unique soil lines result by varying soil type, moisture content, and roughness. Soil line slope and intercept are subsequently used in the VI equation to minimize soil background effects. A global soil line representing all soil types is not possible because such a line will only be linear in portions of the entire range due to variations caused by

different soil conditions (soil type, moisture content, organic matter content, soil roughness, etc.)

In this study MERIS images (L1b, L2) and the HyMap image were used to determine the soil line for each case of derived vegetation indices.

3.7. MERIS Measurements of Leaf Area Index and fAPAR

The calculation of the LAI for the study area was implemented by the use of the BEAM software. This MERIS-specific software makes use as inputs the top of atmosphere radiance values as derived from MERIS L1b images. The algorithm that is used for the derivation of LAI is the TOA_VEG algorithm (Baret, Pavageau et al., 2006).

The algorithm is based on the training of neural networks over a data base simulated using radiative transfer models. The SAIL, PROSPECT and SMAC models are coupled and used to simulate the reflectance in the 13 MERIS bands considered (412 nm, 442 nm, 490 nm, 510 nm, 560 nm, 620 nm, 665 nm, 681.25 nm, 708.75 nm, 753.75 nm, 778.75 nm, 865 nm, 885 nm). The oxygen and water absorption bands have not been used because they would convey significant uncertainties associated while providing only marginal information on the surface. The LAI product retrieved from the algorithm represent values for green leaves under direct solar illumination, with LAI being half the total leaf surface area per unit ground area.

The LAI product is sensitive to the green leaves in the canopy. Green leaves have large differences in radiation absorption between the red and near-infrared bands, while in dead leaves and soil, that difference is decreased. The algorithm uses this difference to determine LAI. The simulation in the 13 MERIS bands requires 15 input variables. They were drawn randomly according to an experimental plan aiming at getting a more evenly

populated space of canopy realization. To provide more robust performances of the network, the distributions of each input variable was close to the actual distributions and, when possible realistic co-distributions were also used. Back-propagation neural networks were trained for each variable considered. The use of the MGVI, described at the MERIS L2 product, was the approach for the estimation of fAPAR.

3.8. HyMap Measurements of Leaf Area Index and fAPAR

The LAI map was generated with field data and high resolution satellite data of HyMap based on a model (between that RSR and LAI (Liras 2005) :

$$LAI = -3.86 \ln[1-(RSR/9.5)] \quad \textbf{(10)}$$

When aggregated to the 300m resolution, this map serves as the ground-truth (Tan et al. 2005, Wang et al. 2004).

The fAPAR map was derived based on the MGVI algorithm. In particular, this MERIS algorithm was used, but previously a resampling of the HyMap bands into the MERIS bands took place.

3.9 Validation of Aggregated Fine-Resolution Map and MERIS Product

To investigate the accuracy of individual pixel LAI, fAPAR values, a comparison was made between LAI, fAPAR values in MERIS and those in the matching HyMap image. The LAI values in MERIS images were calculated at 300-m resolution from the TOA_VEG algorithm. The LAI and fAPAR values in the HyMap image were calculated at 5-m resolution and aggregated to 300-m resolution using image-resampling techniques. The main purposes of the validation were to assess the accuracy of the pixel-level LAI,

fAPAR values in terms of the RMSR divided by the average LAI, fAPAR value, respectively.

3.10. Analysis of the LAI, fAPAR, VI_{HyMap}–VI_{MERIS} Relationships

Several variants of each VI were derived from the image data (Table 2). For each biome, the VI was derived from radiance (VI_{RAD}), top of aerosol reflectance (VI_{TOAr}), and top of canopy reflectance (VI_{TOC}). This was done to test the effects of spectral data processing level on the strength of the relationships between VI_{MERIS}-VI_{HyMap} ,VI-LAI and VI-fAPAR. Least squares regression analysis (SAS Institute Inc. 1990) with LAI as the independent variable was used to evaluate the relationships between VI_{HyMap}, LAI, fAPAR and each of the VI_{MERIS}. The models investigated were linear and potential. The results are reported in terms of the R2. To evaluate the relative influence of red and near-infrared reflectance of MERIS (bands 8 and 13) on the LAI–SVI, fAPAR relationships, plots of LAI and fAPAR against Red_{TOC} (Band 8 of MERIS) and NIR_{TOC} (Band 13 of MERIS) were also inspected.

4. RESULTS

4.1. Image Characteristics

The two MERIS datasets (Level 1b and Level 2) and the resampled and aggregated LGN-5 dataset (300m) were georeferenced to UTM (Zone 31 North, geodetic datum WGS 84). However a comparison of the images of the three datasets exposed observable differences. For this reason, we performed an image to image co-registration using 20 ground control points (Figure 8) recorded between the LGN-5 (base image) and each of the MERIS images (warp images). This permitted direct overlay of land cover and LAI data products from MODIS and HyMap. The georegistration showed that both MERIS images have a shift of less a pixel (Table 5).

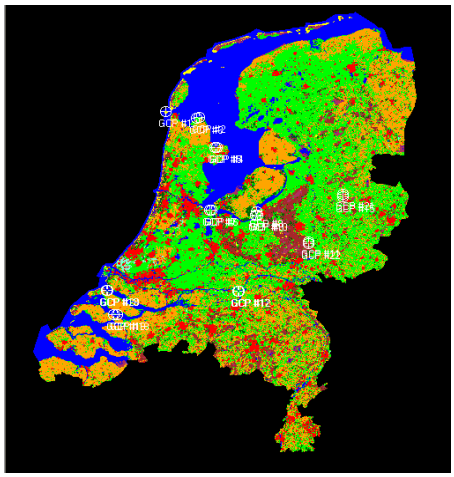

FIGURE 8. THE GROUND CONTROL POINTS OF THE LGN IMAGE THAT WERE SELECTED AS A REFERENCE FOR THE CO-REGISTRATION OF THE MERIS DATASETS.

Table 5. Root mean square errors RMS (in fractions of a pixel) of the georeferencing to the UTM 31 North, WGS-84 coordinate system using the information of 27 image tie points between MERIS images and the aggregated LGN-5.

Images	RMS error (total)
MERIS L1b (08-08-2004)	0.571
MERIS L2 (08-08-2004)	0.480

The calculated to 5m and aggregated to 300m pixel size VIs of the HyMap images were also georeferenced to the UTM (Zone 31 North, geodetic datum WGS 84). A comparison of them with the LGN-5 exposed also some clear and observable differences (Figure 9). In order to achieve a better overlay with the VIs of the MERIS images, we performed an image to image co-registration using 16 ground control points recorded between the VIs of HyMap (aggregated to 300m) and the MERIS images. Although we should do the co-registration of the VIs of HyMap with the LGN-5, the need for direct spatial comparisons between MERIS and HyMap has guide us to make the co-registration of VI_{HyMap} with the MERIS image as a reference.

VI derived from the geocorrected MERIS images exposed also some clear and observable differences. Therefore we performed an image to image co-registration using 16 ground control points recorded between the VIs of HyMap (aggregated to 300m) and the VIs of the MERIS images. Although we can expect modest errors of coregistration, overlay in this way provided confidence in making direct spatial comparisons at the site level of Millingerwaard.

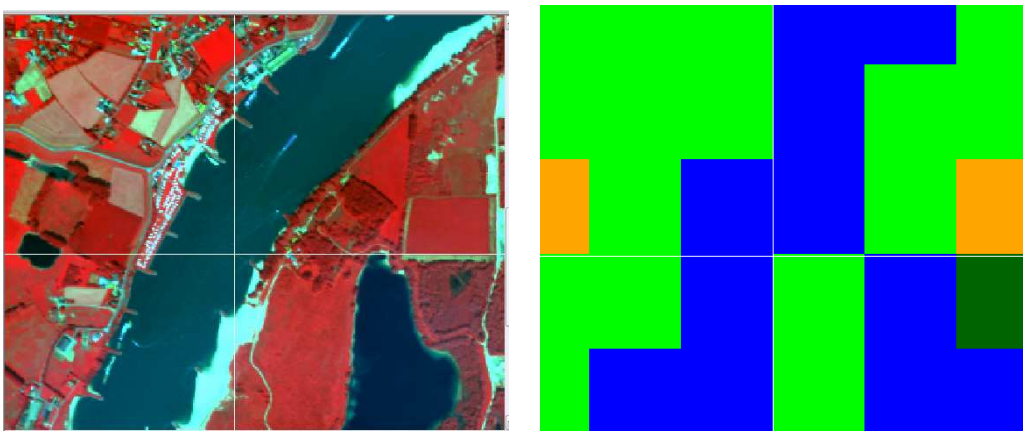

FIGURE 9.COMPARISON OF THE GEOMETRY OF THE HYMAP (5 M PIXEL SIZE) IMAGE AUGUST 28TH , TO THE LEFT AND THE LGN-5 DATABASE (25 M PIXEL SIZE) TO THE RIGHT

Table 5. Root mean square errors RMS [in fractions of a pixel] of the georeferencing to the UTM 31 North, WGS-84 coordinate system using the information of 16 image tie points between the VIs of HyMap (aggregated to 300m) and the VIs of the MERIS images.

Images	RMS error (total)
VIs of HyMap (27-07-2004)	0.699

The georegistration showed that the HyMap image had a shift of less then a pixel (Table 5).

4.2. Effects of the Atmosheric Correction in the Spectral Profiles and Derivation of VI for the Different Vegetation Biomes in the Netherlands

4.2.1 Spectral Profiles

Although all vegetation types have relatively similar spectral properties (large absorption in the red and large reflectance in NIR), different biomes have special characteristics depending on the canopy architecture. These characteristics can be distinguished by

comparing the spectral signatures. Figure 10, presents the mean spectral signatures of the TOAr reflectances in the spectrum of the bands of MERIS as a function of biome type derived MERIS data (TOA radiances and TOC reflectances are shown in Appendix 4 and 5, respectively).

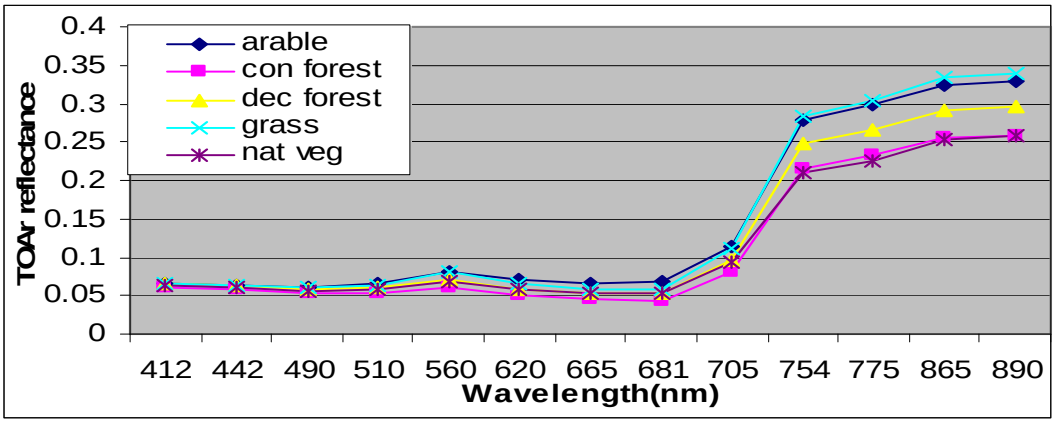

FIGURE 10. SPECTRAL SIGNATURES FOR THE MAIN LGN LAND COVER TYPES DERIVED FROM MERIS LEVEL 2 TOAR REFLECTANCES FOR AUGUST 8TH 2004

After plotting the spectral signatures for the different vegetation land cover types the general pattern of TOA radiance, TOAr reflectance and TOC reflectance was as expected. All vegetation classes showed a steep slope between red and NIR TOA radiances at 762 nm and a steep increase at the 754 nm for the TOAr reflectances (Figure 8 and Appendix 1, respectively).

The spectral profiles have also shown the high degree of correlation for the visible (400 – 700 nm) and NIR (750 – 900 nm) wavelength of MERIS (L1b-L2) spectrum. In order to describe these relations, a correlation matrix for the spectral bands of MERIS was calculated and the results are presented in the Table 5 and Appendix 6. For MERIS TOA radiances bands 11, 15 were not used because at 762nm (band 11) absorption occurs by oxygen of the atmosphere resulting in a dip. Band 15, at 900 nm, is related to the water vapour determination.

Table 5. Correlation matrix for the L1b MERIS image of August 8th, 2004.

Band	1	2	3	4	5	6	7	8	9	10	12	13	14
[nm]	413	443	490	510	560	620	665	681	708	753	778	865	885
1	1												
2	1	1											
3	0.97	0.98	1										
4	0.96	0.98	1	1									
5	0.92	0.94	0.95	0.97	1								
6	0.93	0.95	0.97	0.98	0.97	1							
7	0.92	0.94	0.97	0.97	0.94	1	1						
8	0.92	0.94	0.97	0.97	0.94	0.98	1	1					
9	0.70	0.72	0.75	0.78	0.88	0.82	0.78	0.78	1				
10	-0.30	-0.30	-0.31	-0.28	-0.10	-0.27	-0.34	-0.34	0.21	1			
12	-0.32	-0.32	-0.32	-0.30	-0.13	-0.31	-0.36	-0.37	0.18	1	1		
13	-0.36	-0.36	-0.36	-0.32	-0.14	-0.32	-0.39	-0.39	0.18	0.99	1	1	
14	-0.36	-0.36	-0.36	-0.33	-0.14	-0.32	-0.39	-0.39	0.18	0.99	0.99	1	1

4.2.2. Vegetation Indices Derivation

VI images were determined for the main vegetation biomes of the Netherlands are NDVI, WDVI, PVI, MSAVI and GEMI. Several variants (Table 6) of each SVI were derived from the image data. For each vegetation biome, the VIs were derived from TOA radiances (VI_{TOARAD}), TOAr reflectance ($VI_{TOArREF}$), and TOC reflectance (VI_{TOCREF}).

Table 6. Summary of VIs images prepared by stage of image processing for the vegetation biomes (Grass, Arable land, Deciduous forest, Coniferous forest, Natural vegetation) of the Netherlands.

Stage of image processing		
TOA radiances	TOAr reflectances	TOC reflectances
NDVI	NDVI	NDVI
WDVI	WDVI	WDVI
MSAVI	MSAVI	MSAVI
PVI	PVI	PVI
GEMI	GEMI	GEMI

In order to facilitate the visualization of the 5 vegetation land cover types and compare the effects of the different radiometric MERIS data on the distribution of an index, we choose the WDVI (Figure 11).

a) b)

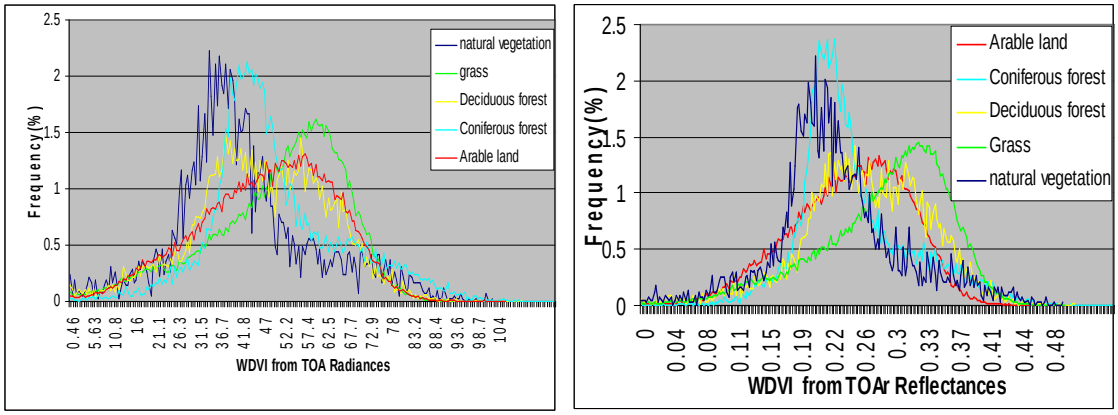

c)

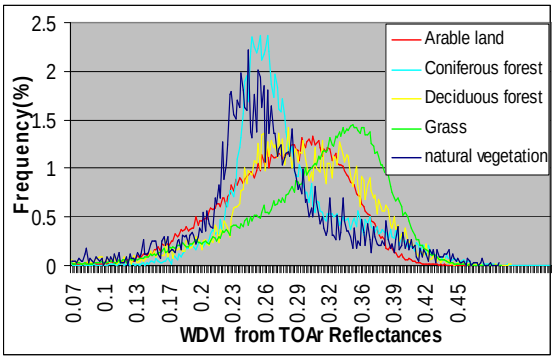

FIGURE 11. HISTOGRAM OF THE WDVI DERIVED FROM THE DIFFERENT RADIOMETRICAL DATA OF MERIS FOR THE BANDS 8 AND 13. a)WDVI from TOA Radiances, b)TOAr Reflectances, c)TOC Reflectances

Table 7 shows a comparison of the mean and standard deviation values of the VIs per biome.

Table 7. Mean values and standard deviation for the VI estimated for the vevegetation biomes of the Netherlands.

	Vegetation Indices								
Biome type	Mean/ Stdev WDVI			Mean/ Stdev MSAVI			Mean / Stdev NDVI		
	TOA Rad.	TOAr Refl.	TOC Refl	TOA Rad.	TOAr Refl.	TOC Refl.	TOA Rad.	TOAr Refl.s	TOC Refl.
Grass	52.15/18	0.26/0.07	0.29/0.07	0.64/0.25	0.47/*0.11*	0.50/0.11	0.37/0.15	0.60/0.13	0.75/0.09
Arable	47.49/18	0.25/0.07	0.27/0.06	0.60/0.23	0.42/0.11	0.45/0.11	0.38/0.16	0.57/0.18	0.69/0.12
Deciduous for	44.82/17	0.23/0.07	0.25/0.07	0.63/0.20	0.41/0.11	0..44/0.10	0.48/0.22	0.69/0.10	0.83/0.10

Coniferous for.	40.20/13	0.21/0.05	0..21/0.05	0.65/0.11	0.37/0.08	0.38/0.09	0.50/0.20	0.71/0.07	0.84/0.07
Natural veg	34.66/19	0.20/0.07	0.21/0.07	0.52/0.20	0.34/0.11	0.37/0.10	0.40/0.19	0.61/0.11	0.78/0.11

	Vegetation Indices					
Biome type	Mean/ Stdev GEMI			Mean/ Stdev PVI		
	TOA Rad	TOAr Refl.	TOC Refl.	TOA Rad.	TOAr Refl.	TOC Refl.
Grass	0.45/0.35	0.72/0.11	0.72/0.11	36.15/18	0.27/0.07	0.33/0.07
Arable	0.46/0.31	0.70/0.11	0.69/0.11	31.48/18	0.25/0.07	0.31/0.06
Deciduous for.	0.58/0.26	0.68/0.10	0.66/0.12	28.80/17	0.24/0.07	0.29/0.07
Coniferous for.	0..50/0.23	0.64/0/08	0.61/0.09	24.20/13	0.22/0.05	0.25/0.05
Natural veg.	0.43/0.25	0.61/0.13	0.58/0.14	76.52/19	0.20/0.07	0.25/0.07

Relationships between the indices

As it is mentioned in the literature review VIs can be clustered into categories according to the effects that they are able to address:

- Intristic indices based on the ratios of 2 or more bands: NDVI, MSAVI
- Soil–line vegetation indices: improving the resistance to soil effects: WDVI, PVI
- Atmospherically resistant indices, by adding to the index atmospheric characteristics for minimizing these effects: GEMI

To test the mutual relationship between these five VIs, they were calculated from the same data set. To minimize the effects of sensor geometry to the derivation of VI, we use a subset of the image in the eastern part. All possible pairs of VIs (ten combinations) were plotted (Figure 12). The Figures show that WDVI, PVI, MSAVI, and GEMI individually differ in concept and contain different information than NDVI, while WDVI and PVI are closely correlated. The comparison of WDVI and PVI with MSAVI, showed a similarity to the information content.

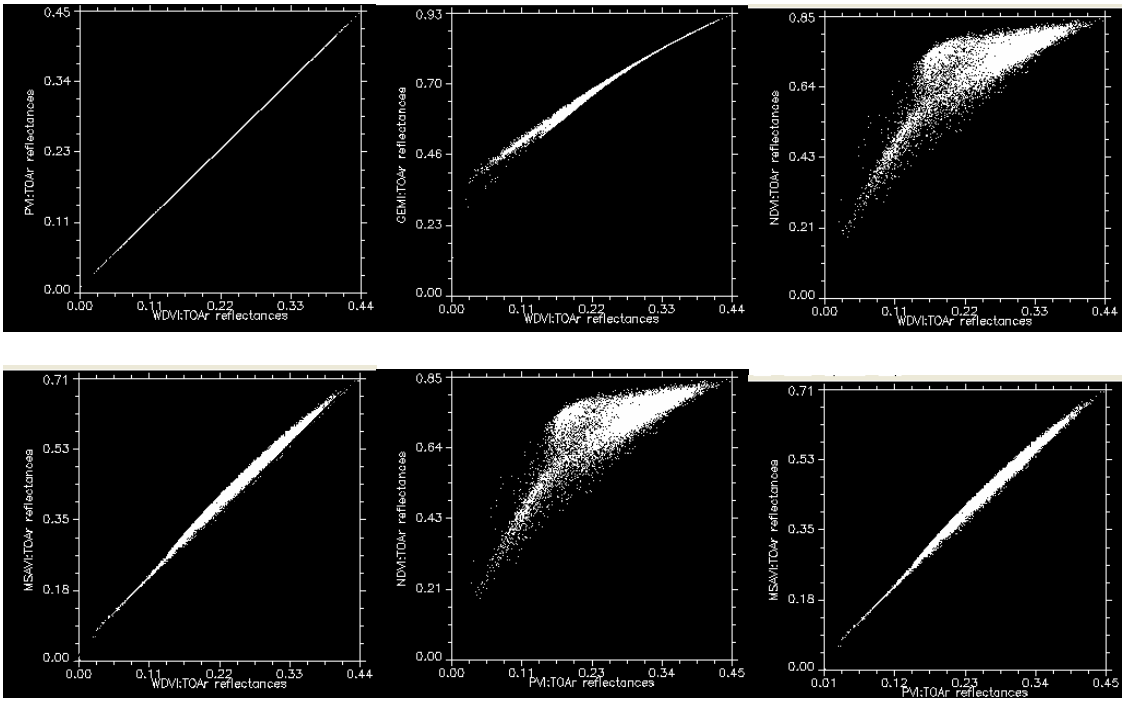

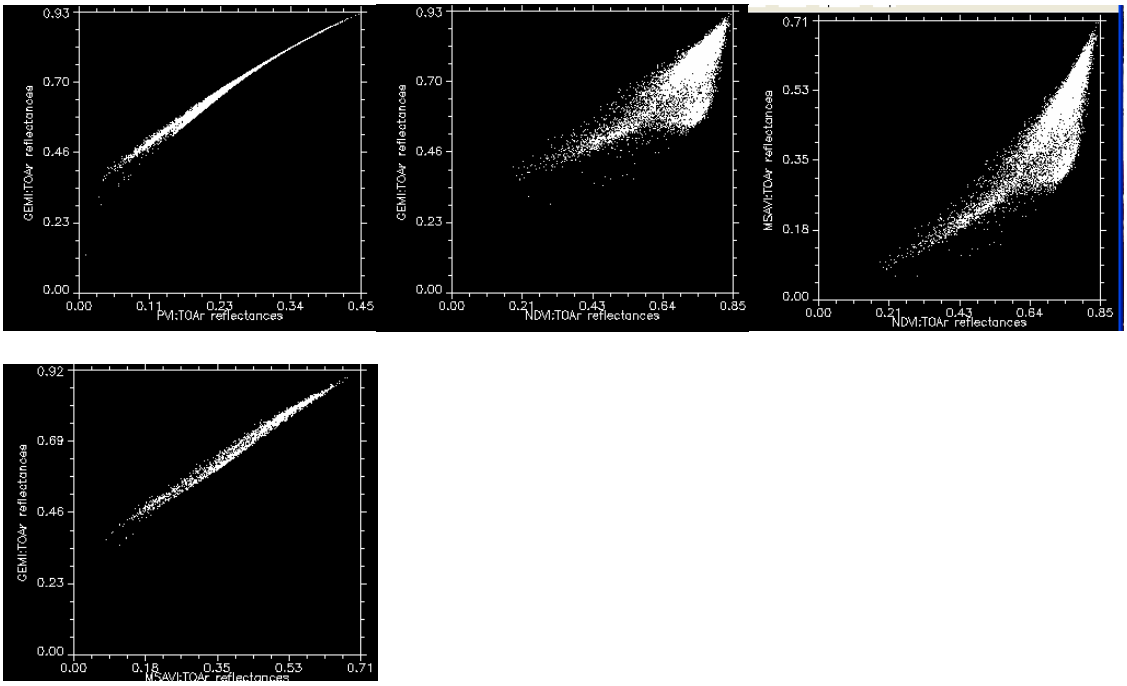

FIGURE 12. GRAPHICAL DETERMINATION OF THE MUTUAL DEPENDENCY OF NDVI, PVI, SAVI, WDVI AND GEMI. EACH DATA POINT CORRESPONDS TO A VI VALUE CALCULATED FOR THE PIXELS OF THE TOAR REFLECTANCE IMAGE.

Beside the investigation of the mutual dependency of the VIs, it is of interest to compare VIs for the TOA radiance, TOAr reflectance and TOC reflectance spectral vegetation indices and investigate how their mutual relationship is influenced due to the atmospheric correction.

We found it appropriate, having in mind the similarities that were revealed in the previous VI comparison, to use for this step three representative VI (NDVI, WDVI, GEMI) that are not functionally equivalent. All possible pairs of VIs (three combinations) were plotted and correlation matrices (Figure 13, Table 8, Appendix 7 and 8) were created for each VI.

a) b)

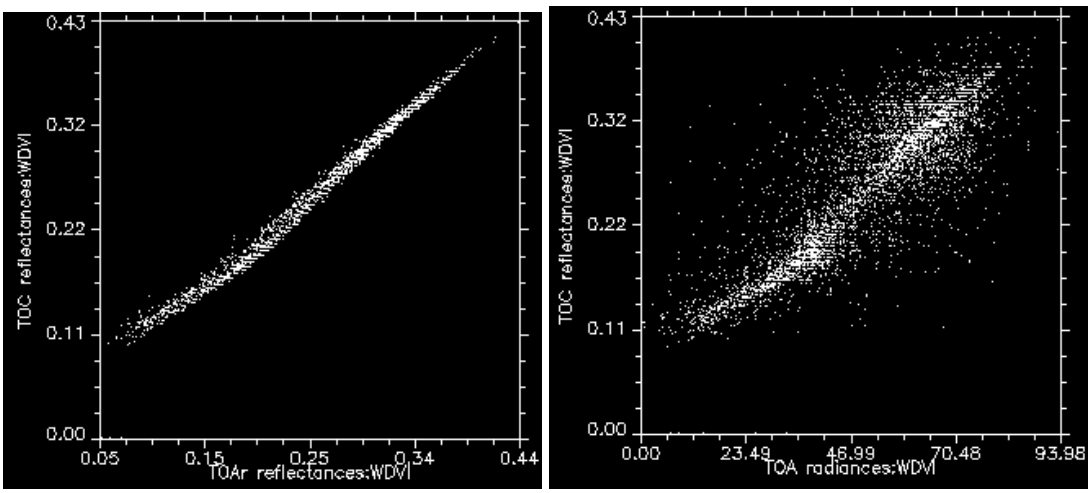

c)

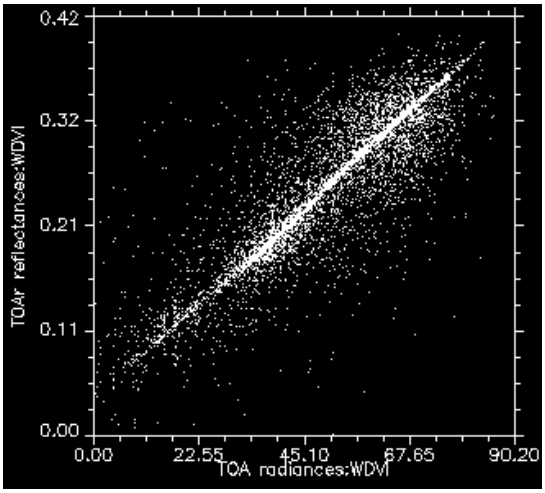

FIGURE 13. SCATTERPLOTS OF THE COMPARISON OF a)$WDVI_{TOArRefl.}$ and $WDVI_{TOC\ Refl.}$, b) $WDVI_{TOA\ Rad.}$ and $WDVI_{TOC\ Refl.}$, c) $WDVI_{TOA\ Rad.}$ and $WDVI_{TOC\ Refl.}$

Table 8. Correlation matrix for the WDVI

Correlation	WDVI TOA Rad.	WDVI TOAr Refl.	WDVI TOC Refl.
WDVI TOA Rad.	1		
WDVI TOAr Refl.	0.96	1	
WDVI TOC Refl.	0.95	0.99	1

In general a high correlation (0.99, Table 13) between $WDVI_{TOC}$ and $WDVI_{TOAr}$ can be observed. In contrast the correlation of $WDVI_{TOC}$ and $WDVI_{TOA}$ seems to be lower (0.95, Table 13).

4.3. Comparison of the VIs Derived from MERIS with the ones of HyMap

Subsequently, the vegetation indices derived from MERIS were related to the ones derived from HyMap for the main vegetation types (arable land and the grass) of the Millingerwaard area. VI derivation affected the result and strength of the VI_{MERIS}-VI_{HyMap} relationships (Table 9, 10, Figure 14, 15 and Appendix 9, 10). This comparison is important because it is used as an evaluation of the performance (r2) of the TOA Radiances, TOAr Reflectances and TOC reflectances from MERIS, although it relates to the spatial correlation between the two sensors due to the different scale that they operate.

The VIs were derived from TOA radiance, TOAr reflectance, and TOC reflectance MERIS data for the arable land dominated and grass-dominated pixels of Millingerwaard. The VI values in MERIS images were calculated at 300-m resolution. The VI values for the HyMap image were calculated at 5-m resolution and aggregated to 300-m resolution.

Two regression analysis results are displayed for each vegetation cover type. One is an "unforced" regression, which tends to create a positive intercept on the vertical axis when data scatter is considerable, and the other is a "forced" regression with the intercept fixed at the origin of the coordinates. Only the R^2 values of the unforced regression are reported to avoid confusion. The best correlation is found for the MSAVI derived from TOC (R2=0.56) for the arable land-dominated biome. Results for MSAVI are presented as a case study in Table 14, 15 and in Figure 12, 13.

Table 9. The Linear model and the R2 for the VIMERIS-VIHyMap Relationship using three Derivations of VIMERIS TOA radiances (TOA rad.), TOAr reflectances (TOAr refl.) and TOC reflectances (TOC refl.) for the arable land-dominated pixels of Millingerwaard.

VI	*TOArad.*	TOAr refl.	TOC refl.
MSAVI	0.07	0.54	0.56
WDVI	0.18	0.46	0.51
PVI	0.18	0.46	0.51
NDVI	0.08	0.48	0.55
GEMI	0.21	0.44	0.46

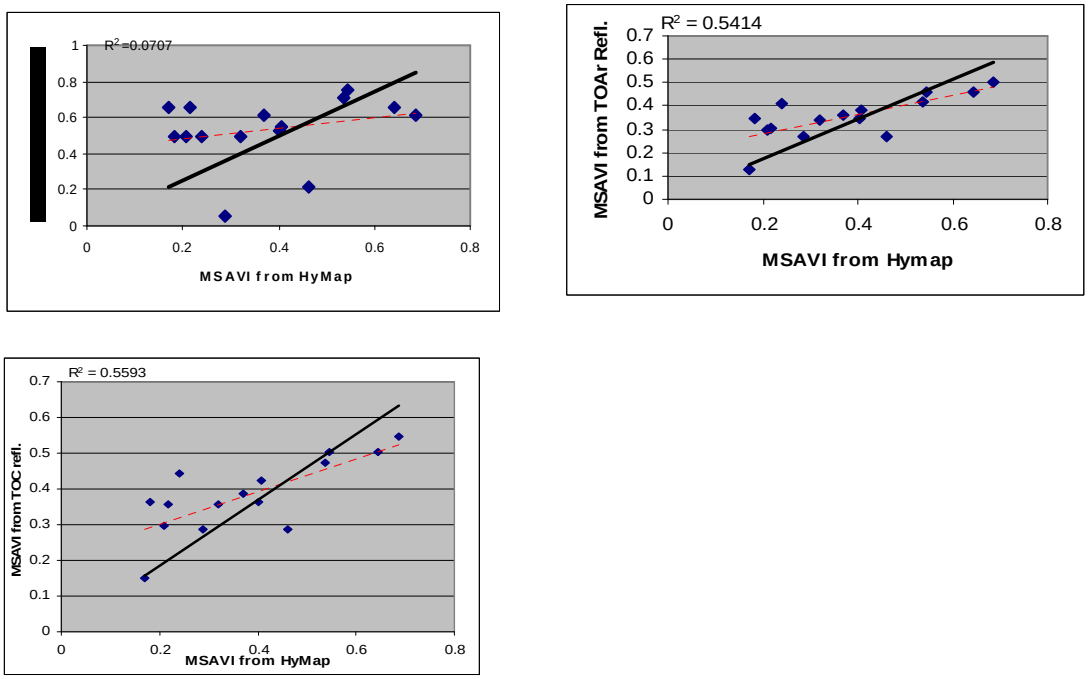

FIGURE 14. SCATTERPLOTS OF THE MSAVI DERIVED FROM MERIS AND HYMAP. RELATIONSHIP USING THREE DERIVATIONS OF MSAVIMERIS: TOA RADIANCES (TOA RAD.), TOAR REFLECTANCES (TOAR REFL.) AND TOC REFLECTANCES (TOC REFL.) FOR THE ARABLE LAND-DOMINATED PIXELS OF MILLINGERWAARD.

Table 10. The Linear model and R^2 for the VIMERIS-VIHyMap Relationship using three Derivations of VIMERIS TOA radiances(TOA rad.), TOAr reflectances (TOAr refl.) and TOC reflectances(TOC refl.) for the grass land-dominated pixels of Millingerwaard.

VI	TOA rad.	*T*OAr refl.	TOC refl.
MSAVI	0.18	0.39	0.44
WDVI	0.21	0.31	0.33
PVI	0.21	0.32	0.34
NDVI	0.12	0.24	0.27
GEMI	0.23	0.33	0.35

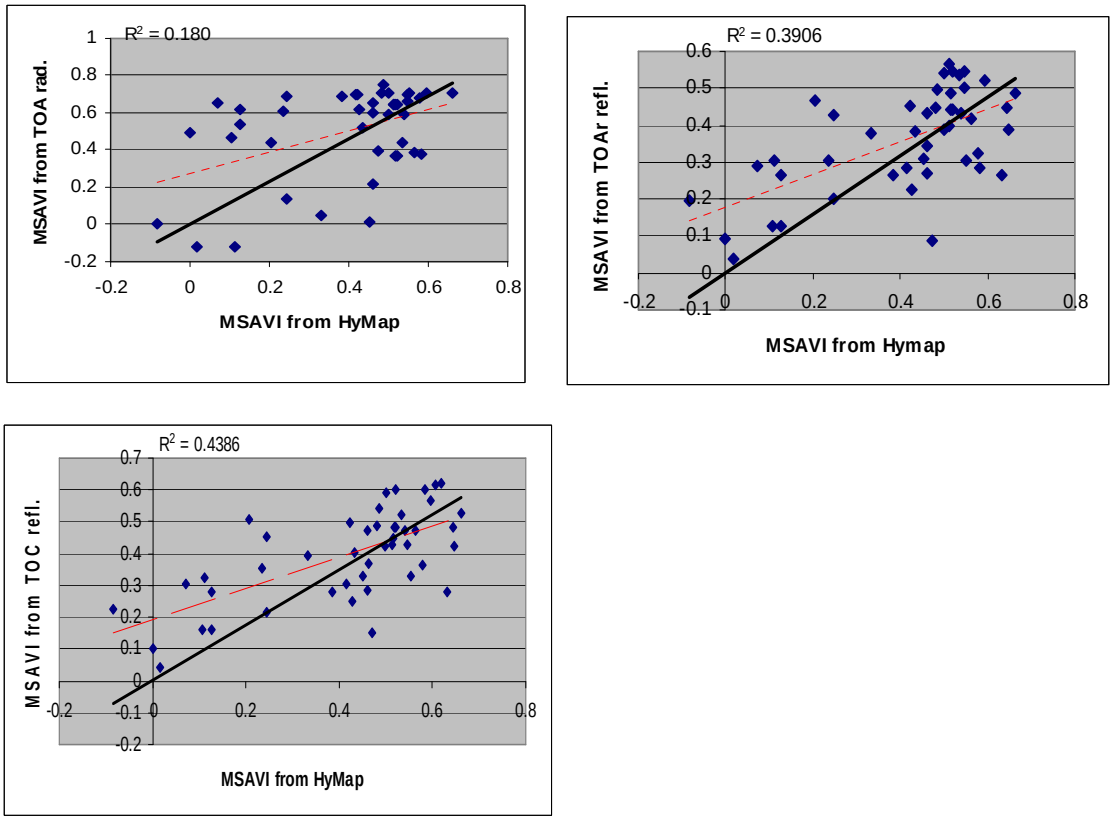

FIGURE 15. SCATTERPLOTS OF THE MSAVI DERIVED FROM MERIS AND HYMAP. RELATIONSHIP USING THREE DERIVATIONS OF MSAVIMERIS: TOA RADIANCES (TOA RAD.), TOAR REFLECTANCES (TOAR REFL.) AND TOC REFLECTANCES (TOC REFL.) FOR THE GRASS-DOMINATED PIXELS OF MILLINGERWAARD.

4.4. LAI Derived from MERIS

After the derivation of LAI (Figure 16) using the plug-in of the BEAM software (Baret 2006), the purpose of validation to assess the accuracy of the pixel-level LAI was implemented.

4.4.1. LAI Map Production

The LAI values across all the vegetation biomes in the Netherlands ranged from 0 to 4 (Table 11). Among the forested areas, the deciduous forest had the highest LAIs. At the same level were the LAI values of grass and arable land. The coniferous forest and the natural vegetation had lower LAIs.

Table 11. Summary of LAI information, derived from Level 1b image (8th August 2004) using BEAM plug-in (Baret 2006), for the Netherlands.

	Vegetation Types	LAI range	Std.Dev.	Mean	Median
Netherlands	Grass	0.01- 4.03	0.67	2.60	2.76
	Coniferous forest	0.09-3.8	0.45	2.16	2.16
	Deciduous forest	0.07-4.04	0.60	2.45	2.53
	Arable land	0-4.05	0.66	2.39	2.48
	Natural vegetation	0-3.66	0.66	1.90	1.92

a)

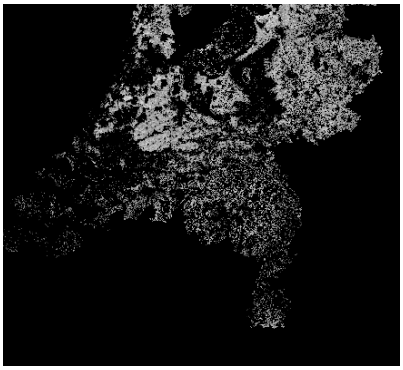

b)

c)

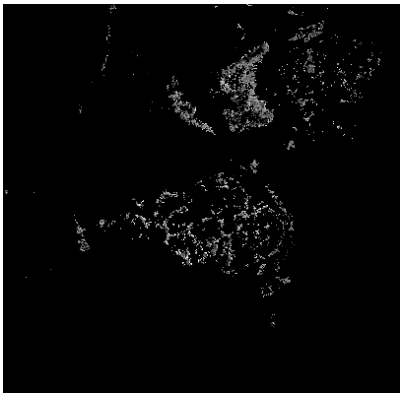

d)

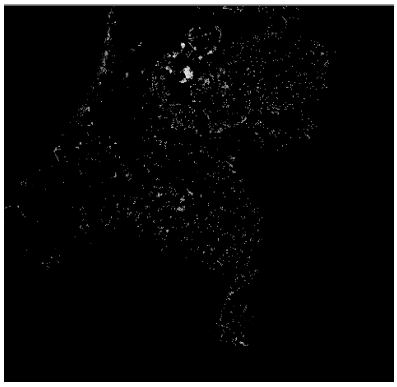

e)

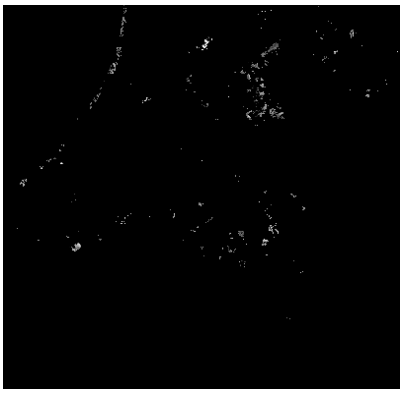

FIGURE16. LAI MAPS DERIVED FROM MERIS IMAGE USING BEAM PLUG-IN (BARET, 2006) FOR a) LAI of grass, b)LAI of Arable land) LAI of Coniferous forest, d) LAI of Deciduous forest, e) LAI of Natural vegetation

4.4.2 Validation of MERIS LAI Using LAI Estimated from HyMap

To investigate the accuracy of individual pixel LAI values derived from MERIS, a comparison was made between LAI values in MERIS images and those in the matching

HyMap image for the Mllingerwaard area. The LAI values in MERIS images were calculated at 300-m resolution. The LAI values in the HyMap image were calculated at 5-m resolution using a function:

$$LAI = -3.86 \ln[1-(RSR/9.5)] \quad \textbf{(11)}$$

between RSR and LAI (Mengesha 2005) and aggregated finally to 300-m resolution. Figure 17, Figure 18 and Table 12 shows this comparison between MERIS and HyMap LAI images with matching dates (August 8th 2004 for MERIS and July 28th 2004 for HyMap composite).

The range of LAIs across Millingerwaard was from 0.16 to 3.19 (Table 12). Among the two main vegetation lands cover types grass had the highest mean LAI (2.13) with a standard deviation of 0.78. The arable land-dominated type had a lower mean value (2.01) but with a bigger standard deviation (0.89).

The error of individual pixel LAI values in the MERIS image is in the range of 35–39%, taken as the ratio of the RMSE to the average LAI of the scene (see Table 13 for the values of RMSE).

Table 12. Summary of LAI statistics of the MERIS and HyMap over the scene of Millingerwaard

		Arable land	Grass
MERIS	Mean	2.01	2.13
	Std. Dev.	0.89	0.78
	LAI range	0.20-3.19	0.16- 3.13
HyMap	Mean	1.60	1.56
	Std. Dev.	0.81	0.83
	LAI range	0.76-3.40	0.04- 3.43

Table13.Correlation of LAI of MERIS with LAI of HyMap in terms of coefficient of determination (R2) and root mean square error (RMSE).

MERIS	R^2	RMSE
Arable land	0.29	0.78
Grass	0.10	0.75

All LAI images are resampled to 300-m resolution before any statistical analysis

a) b)

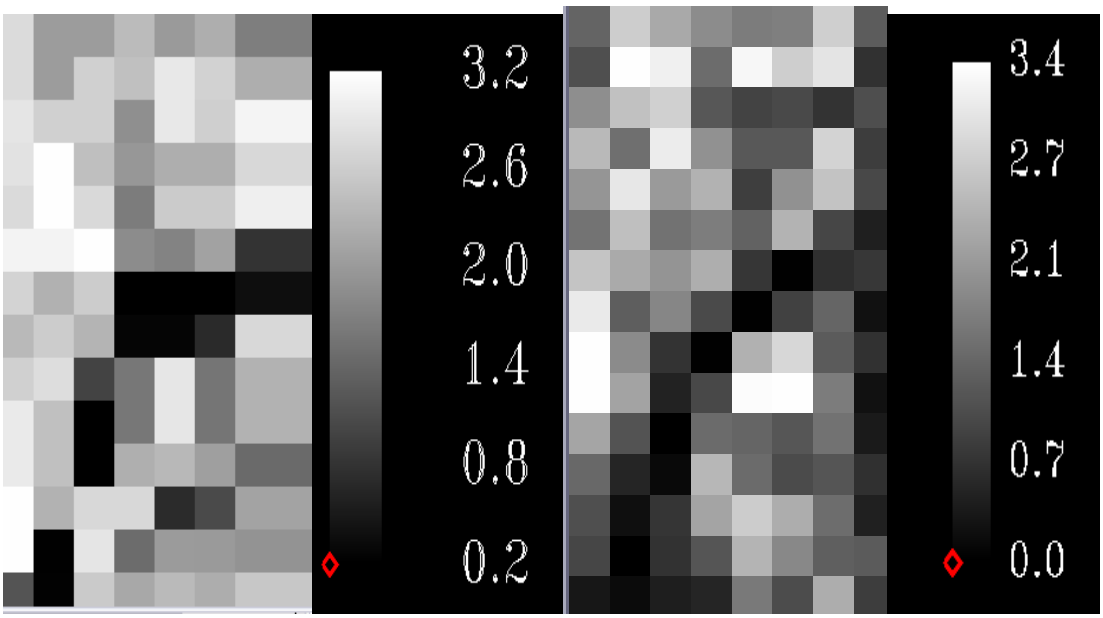

FIGURE17. LAI MAPS FOR THE AREA OF MILLINGERWAARD AS DERIVED FROM A) MERIS 300-M PIXEL SIZE AND B) HYMAP AGGREGATED TO 300-M PIXEL SIZE

a) b)

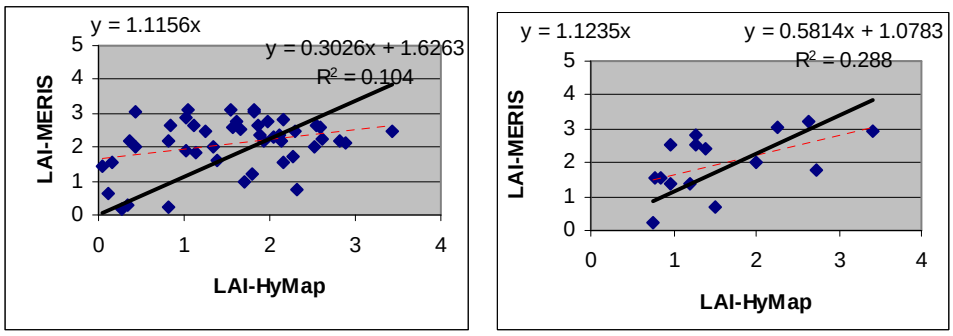

FIGURE 18. COMPARISON OF LAI DERIVED FROM MERIS WITH HYMAP DERIVED LAI FOR THE SCENE OF MILLINGERWAARD RESAMPLED TO THE RESOLUTION OF 300M. a)grass, b)arable land

4.5. FAPAR Derived from MERIS

One of the official vegetation products of the L2 MERIS dataset is the MGVI. The performance of the MGVI is associated to fAPAR values (Gobron 1999). The estimation of MGVI was the basis for the derivation of the fAPAR map for the vegetation types of the Netherlands.

4.5.1. FAPAR Map for Different Biomes

The range of fAPAR across all the vegetation biomes in the Netherlands sites was from 0 to 0.73 (Table 14).

Table 14.Summary of fAPAR information for the Netherlands

	Vegetation Types	fAPAR range	Std. dev.	Mean	Median
Netherlands	Grass	0- 0.73	0.16	0.60	0.63
	Coniferous forest	0.02-0.70	0.13	0.46	0.42
	Deciduous forest	0 -0.72	0.16	0.54	0.53
	Arable land	0-0.73	0.17	0.54	0.55
	Natural vegetation	0-0.70	0.15	0.43	0.40

The resulting maps for the calculation of fAPAR for the different vegetation biomes types are given in Figure 19.

a) b) c)

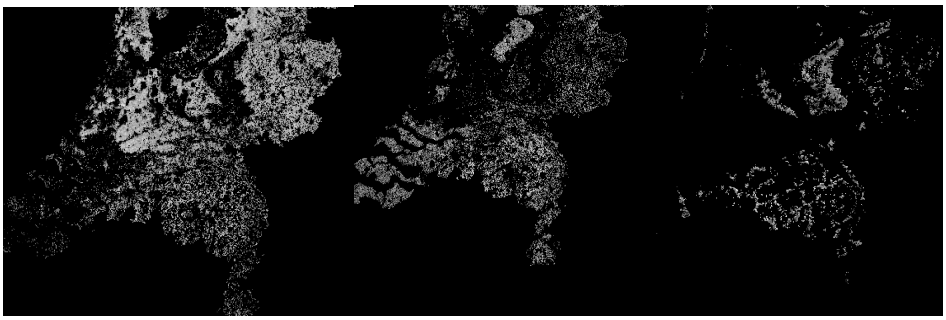

d) e)

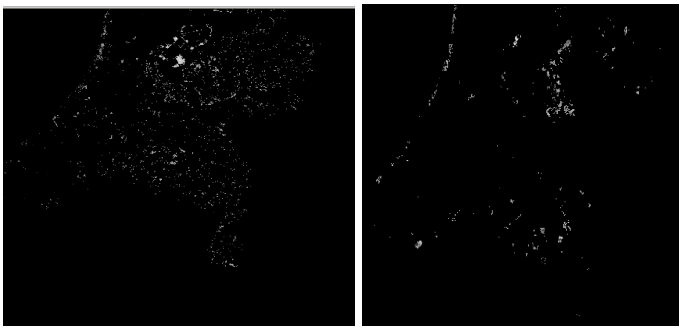

FIGURE19. FAPAR MAPS DERIVED FROM MERIS IMAGE FOR a) grass, b)Arable land, c) Coniferous forest, d)Deciduous forest, e) Natural vegetation

4.5.2. Validation of MERIS FAPAR Using FAPAR Estimated from HyMap

Similarly to LAI, a comparison was made between fAPAR values in the MERIS images and those in the matching HyMap image. The fAPAR values in the MERIS images were calculated at 300-m resolution. The fAPAR values in the HyMap image were calculated at 5-m resolution using the same formula as MGVI and aggregated to 300-m resolution. Figure 20 and 21 shows this comparison between MERIS and HyMap fAPAR images with matching dates (August 8 for MERIS and July 28 for HyMap composite).

The range of fAPAR, derived from MERIS, across Millingerwaard is from 0.14 to 0.78 (Table 15). The fAPAR range in the case of the HyMap sensor is 0.02-1.19. The observed up to 1 value isn't consistent with the nature of fAPAR since its measures in the range 0-1. The cause of this error might occur due to the applied systematic calculation of MGVI (formula, coefficient, etc). This error will influence the validation approach and the results should take this under account.

Among the two main vegetation lands cover types grass had the highest mean fAPAR (0.50) with a standard deviation of 0.17. The arable land-dominated type had a lower mean value (0.43) but with a bigger standard deviation (0.15). The error of individual pixel fAPAR values in the MERIS image is in the range of 23–28% (see Table 16 for RMSE values).

Table 15.Summary of fAPAR statistics from MERIS and HyMap over the scene of Millingerwaard

		Arable land	Grass
MERIS	Mean	0.43	0.50
	Std. Dev.	0.15	0.17
	fAPAR range	0.14-0.68	0.15- 0.78
HyMap	Mean	0.77	0.76
	Std. Dev.	0.28	0.33
	fAPAR range	0.38-1.18	0.02- 1.19

Table 16. FAPAR correlation of MERIS with HyMap in terms coefficient of determination (R2) and root mean square error (RMSE)

MERIS	R^2	RMSE
Arable land	0.50	0.10
Grass	0.29	0.14

All fAPAR images are resampled to 300-m resolution before any statistical analysis.

a) b)

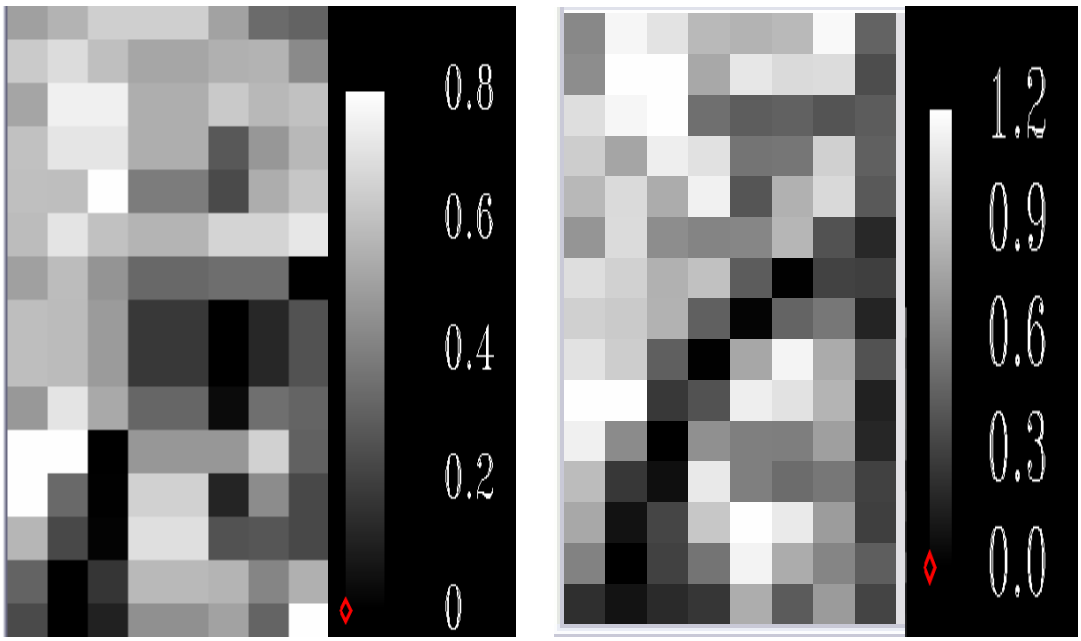

FIGURE20. FAPAR MAPS FOR THE AREA OF MILLINGERWAARD AS DERIVED from a) MERIS 300-m pixel size and b) HyMap aggregated to 300-m pixel size

a) b)

RMSE=0.02 RMSE=0.03

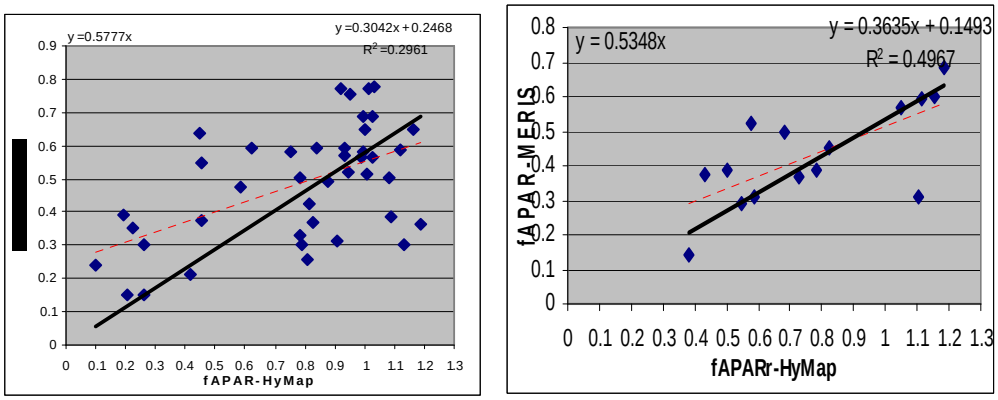

FIGURE 21. COMPARISON OF FAPAR DERIVED FROM MERIS WITH HYMAP DERIVED FAPAR FOR THE SCENE OF MILLINGERWAARD RESAMPLED TO THE RESOLUTION OF 300M. a) grass, b)arable land

4.6. Relationships Between VIS and Biophysical Products

4.6.1. LAI –VI Relationships for the MERIS Image

After correlating the values of the vegetation indices, derived from TOA radiances, TOAr and TOC reflectances, of the pixels with the LAI values for the Millingerwaard site, VI-LAI relationships were built. VI derivation affected the shapes and strength of the LAI–VI relationships. Trends were similar across the VIs. Results that gave the best fit (R^2), with NDVI as a case study are presented in Table 17, Figures 22 and 23. For all derivations, a linear model gave a better fit (R^2) for the LAI–VI relationship than did the potential. In addition TOC gave stronger VI-LAI relationships. The R^2 for NDVI WITH TOC reflectance was higher than those of the other derivations.

Table 17. The Linear model, *R*2 for the VI$_{MERIS}$-VI$_{HyMap}$ Relationship using Three Derivations of VIMERIS TOA radiances (TOA rad.), TOAr reflectances (TOAr refl.) and TOC reflectances(TOC refl.). a) Arable land, b) Grass

a)

VI	TOA rad.	TOAr refl.	TOC refl.
NDVI	0.05	0.40	0.42
MSAVI	0.04	0.33	0.36
WDVI	0.09	0.26	0.34
PVI	0.09	0.25	0.33
GEMI	0.13	0.28	0.23
MTCI	-	-	0.15

b)

VI	TOA rad.	TOAr refl.	TOC refl.
NDVI	0.01	0.28	0. 29
MSAVI	0.01	0.22	0.23
WDVI	0.02	0.12	0.22
PVI	0.02	0.11	0.21
GEMI	0.03	0.25	0.21
MTCI	-	-	0.28

Where y is the SVI and x is the LAI. The parameters of the equations a and b corresponds to:

Linear: $y=ax+b$

Potential: $y= a\, x^{b}$

These models were used in several studies (Holben et al. 1980, Chen and Cihlar 1996, Fassnacht et al. 1997). The potential model was used due to the asymptotic nature that the LAI–VIs may present (Spanner et al.1990, Nemani et al. 1993, Turner et al. 1999).

A similar general pattern in the relationship of LAI to the TOC derived SVI can be observed for all the VIs and for both arable land and grass pixels of Millingerwaard (Figures 22 and 23 and Appendix 11 and 12). For both arable land and grass the VI initially increased at low LAIs, continued to increase at intermediate values, and peaked at the highest LAIs.

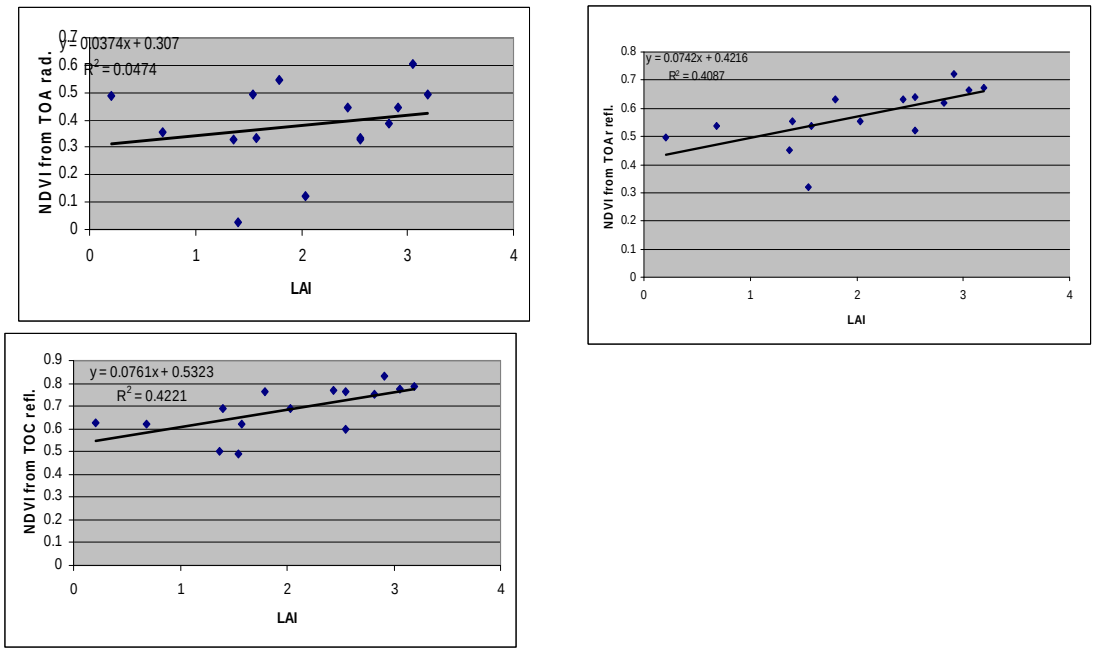

FIGURE 22. EFFECTS OF DIFFERENT STAGES OF MERIS PROCESSING ON THE LAI–NDVI RELATIONSHIP FOR THE ARABLE LAND: a) TOA radiance, b) TOAr reflectance, c) TOC reflectance. See Table 17 for the model R^2 .

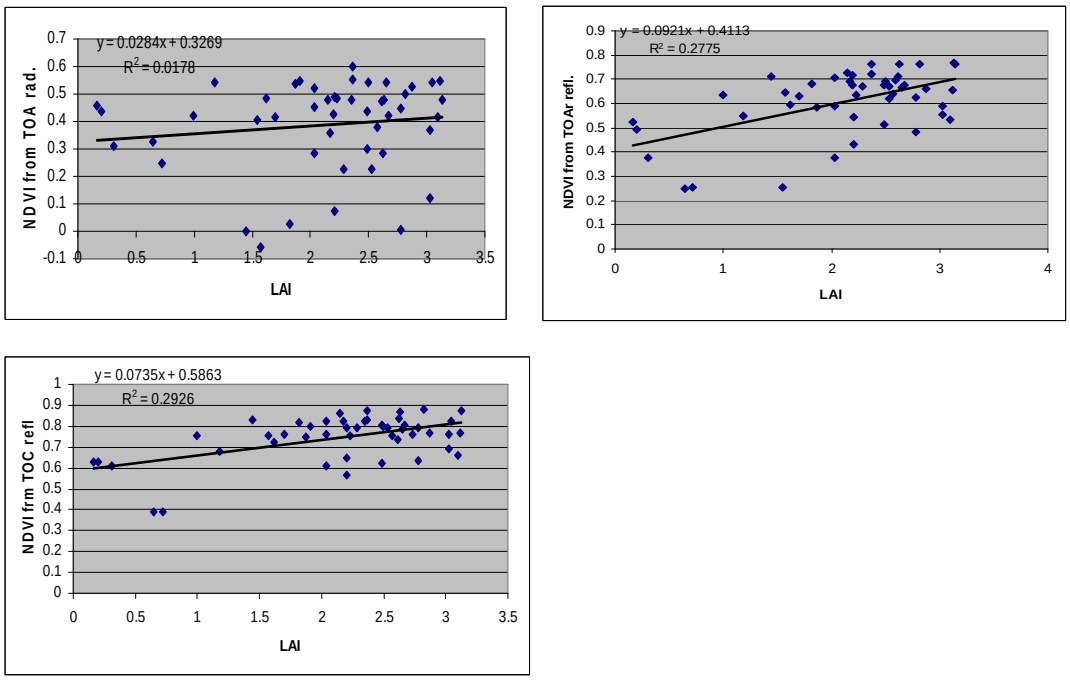

FIGURE 23. EFFECTS OF DIFFERENT STAGES OF MERIS PROCESSING ON THE LAI–NDVI RELATIONSHIP FOR THE GRASS LAND: a) TOA radiance, b) TOAr reflectance, c) TOC reflectance. See Table 17 for the model R^2 in each case.

Figures 24 (a, b) shows the relationship between LAI and surface reflectance for individual bands [RED (Band 8) and NIR (Band 13)].

a) b)

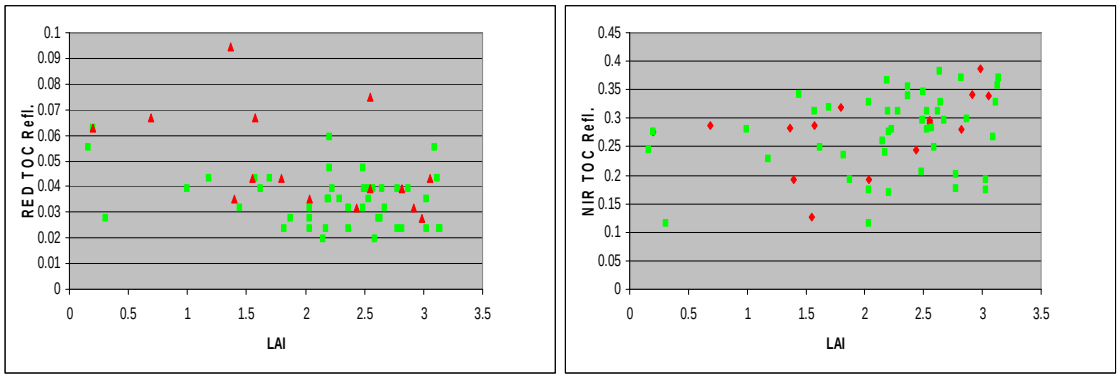

FIGURE 24. RELATIONSHIP ACROSS ALL POINTS FOR LAI AND TOC REFLECTANCE: a) red (MERIS-8), b) near-infrared (MERIS-13).

R2 values at the Table 18 do not reveal strong relationships between NIR-LAI or RED-LAI, although red influence is stronger comparable to the NIR.

Table 18. The Linear model and *R*2 for the REDMERIS-LAIMERIS and NIRMERIS-LAIMERIS relationship for arable land and grass. RED and NIR corresponds to the MERIS bands 8 and 13, respectively

Y	*Model*	R^2
RED (arable)	-0.01x +0.07	0.27
RED (grass)	-0.005x +0.05	0.11
NIR (arable)	0.03x +0.21	0.16
NIR (grass)	0.02x +0.22	0.06

4.6.2. VI-FAPAR Relationships for the MERIS Image

After correlating the values of the vegetation indices, derived from TOA radiances, TOAr and TOC reflectances, of the pixels with the fAPAR values for the Millingerwaard site, VI-fAPAR relationships were also built. Results that gave the best fit (R^2), with MSAVI as a case study are presented in Table 19 and appendix 13 and 14. For the most of the

derivations, the potential model gave a better fit (R^2) for the fAPAR–VI relationship than did the linear. In addition TOC gave stronger VI-fAPAR relationships. The R^2 for MSAVI derived from TOC reflectance was higher than those of the other derivations.

Table 19. The best model fit, in terms of *R*2 for the VIMERIS-MGVI Relationship using Three Derivations of VIMERIS TOA radiances (TOA rad.), TOAr reflectances (TOAr refl.) and TOC reflectances (TOC refl.). a)Arable land b)Grass

a) arable

VI	TOA rad.	TOAr refl.	TOC refl.
MSAVI	0.172	0.96	0.985
GEMI	0.382	0.885	0.939
WDVI	0.367	0.897	0.937
NDVI	0.170	0.776	0.906
PVI	0.358	0.897	0.941
MTCI	-	-	0.816

b) grass

VI	TOA rad.	TOAr refl.	TOC refl.
MSAVI	0.223	0.956	0.989
GEMI	0.41	0.935	0.984
WDVI	0.352	0.945	0.985
NDVI	0.219	0.78	0.906
PVI	0.362	0.943	0.985
MTCI	-	-	0.64

Where y is the SVI and x is the fAPAR. The parameters of the equations a and b corresponds to:

Linear: $y=ax+b$

Potential: $y= a\ x^{b}$

The near linear relationship between VIs and fAPAR has been introduced by a lot of researches (Choudhury 1987, Sellers 1987). Field measurements showed both linear (Wiegand et al., 1991; Daughtry et al., 1992) and non linear relationships (Wiegand et al.1991, 1992, Ridao et al. 1998).

A similar general pattern in the relationship of fAPAR to the TOC derived VI can be observed for all the VIs and for both arable land and grass pixels of Millingerwaard (Appendix 13, 14). For both arable land and grass the VI initially increased at low LAIs, continued to increase at intermediate values, and peaked at the highest fAPARs

The dynamic range for NIR across all plots (Figure 27) had generally increasing values as fAPAR increased. The variation in NIR was the dominant factor contributing to the changes in fAPARs, for both the vegetation types, over the whole range of fAPARs. The dynamic range for NIR across the grass and arable plots was from 14% to 41% with generally increasing values as LAI increased. The range for RED was from 5% to 12%.

a) b)

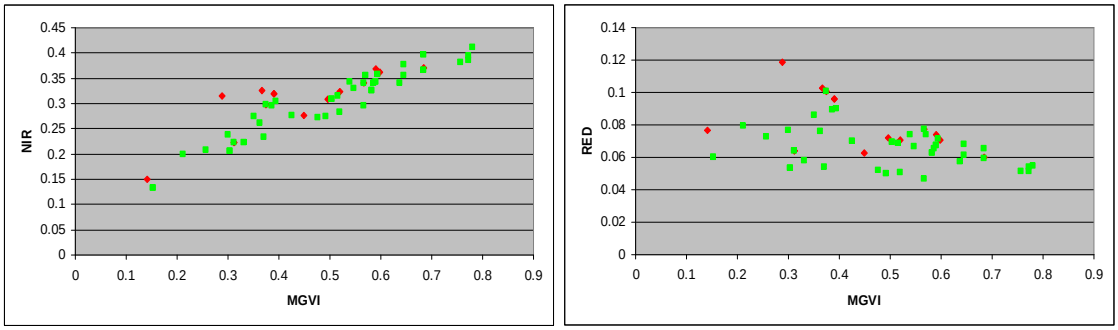

FIGURE 27. RELATIONSHIP ACROSS ALL POINTS FOR MGVI AND TOC REFLECTANCE: A) RED, B) NEAR-INFRARED.

R^2 values given in the Table 20, shows a strong relationship between NIR-fAPAR and a weak for RED-fAPAR.

Table 20. The Linear model, R^2 for the REDMERIS-MGVI and NIRMERIS-MGVI relationship for arable land and grass. RED and NIR corresponds to the MERIS bands 8 and 13, respectively

Y	*Model*	R^2
RED (arable)	- 0.05x +0.10	0.16
RED (grass)	-0.02x +0.08	0.09
NIR (arable)	$0.48\ x^{0.54}$	0.78
NIR (grass)	$0.46\ x^{0.63}$	0.93

5. DISCUSSION

5.1. Image Corrections

The geometric registration that was applied for the geometric correction of the two MERIS images showed that have a shift of less than a pixel compared to the LGN-5 (Table 8). All in all this error appeared to be systematic for both MERIS images. This shift error could be explained by the geolocation inaccuracy during the tie point location in MERIS Level 1 as quoted by the Product Control Facility of ESRIN (Goryl and Saunier 2004). Another element that has to be taken into account is that the resampling of the original LGN-5 dataset with 30m pixel size to the aggregated one with a 300m pixel size also had a geometric inaccuracy of less than a pixel.

In the case of the aggregated 300m VI images derived from HyMap image of the Millingerwaard area, there was also a shift of less than a pixel (Table 9). A possible explanation is the resampling of the original HyMap with 5-m pixel size to the aggregated 300m.

5.2 Effects of the Atmospheric Correction in the Spectral Profiles and Derivation of VI for the Different Vegetation Biomes in the Netherlands

5.2.1. Spectral Profiles

The spectral signatures for the MERIS TOA radiances, TOAr reflectances and TOC reflectances show clear overlap between the land cover types. Grassland and arable land showed a clear vegetation spectrum with high reflectance in the near infrared (NIR). Coniferous forest and natural vegetation had a similar spectrum over the MERIS

wavelengths but their reflectance in the NIR was much lower than the grass and arable land ones. An intermediate spectral behaviour was showed by the spectra of deciduous forest. Both in red and more evidently in NIR part of the spectrum, deciduous forest had a clearly distinguished profile compared to the ones of grass, arable land, coniferous forest and natural vegetation.

Comparing the results from the spectral profiles of TOAr reflectances and TOC reflectances, we conclude that the atmospheric correction at the top of canopy level cause a decrease of reflectance in the red bands and an increase in the NIR bands. This effect occurs for all the vegetation land cover types.

The spectral profiles also showed the high degree of correlation for the visible (400 – 700 nm) and NIR (750 – 900 nm) wavelength bands of MERIS (L1b-L2) spectrum. The only exception was band 9 (708nm and 705nm for L1b and L2 respectively), designed for the red-edge region, witch illustrates a moderate correlation with visible and NIR bands. Clevers et al. (2004) calculated principal component analysis for a MERIS image and showed that most of the information (99.71%) was captured by the first two components meaning the red and NIR. The third component exhibited the contrast between band 9 and other bands, however it contains only 0.16% of the variance of the dataset. Hence, most of the information from a MERIS image could be comprised in two bands: one in the red (TOA radiance or TOAr reflectance or TOC reflectance) and one in the NIR (TOA radiance or TOAr reflectance or TOC reflectance).

5.2.2. Vegetation Indices Derivation

Vegetation indices typically capture the absorption contrast across the 650-850 nm wavelength intervals through combinations of RED and NIR reflectance. They are measures of chlorophyll abundance and energy absorption (Myneni et al. 1995). Figure 9 demonstrates the distribution of WDVI, values derived from MERIS TOA radiance

TOAr reflectances and TOC reflectances data. In general, grass have the highest mean WDVI values, around 52.15, 0.26 and 0.29 for TOA Radiances, TOAr Reflectances and TOC reflectances respectively, followed by arable land, around 47.49, 0.25, 0.278 (Table 12). Natural vegetation and coniferous forest have similar WDVI distributions and their mean and Standard deviation of WDVI values are similar. It would be difficult to distinguish natural vegetation from coniferous forest using only WDVI.

The vegetation indices have been sorted into three categories according to the effects that they are able to address: intrincic vegetation indices (NDVI, MSAVI), soil–line -related vegetation indices (WDVI, PVI) and atmospherically resistant indices (GEMI). Analysis of their differences in concept and contain information revealed a close correlation for WDVI and PVI and MSAVI (Figure 10). All the scatterplots of NDVI showed that all the VI had differences individually in concept and contain different information with NDVI. A conclusion extracted from these comparisons is that WDVI and PVI have a high mutual correlation. Hence, they will not differ significally in their relationships with biophysical products (LAI, fAPAR) or the WDVI and PVI derived from HyMap.

In addition investigation of the TOA radiance, TOAr reflectance and TOC reflectance spectral vegetation indices mutual relationship revealed the influence of the atmospheric correction (Figure 11, Appendices 4, 5, 6 and 7). A similar general pattern, a high mutual dependency, in the scatterplot of TOAr Reflectances and TOC Reflectances was observed for all the VIs. Contrary to this, a low dependency appeared, in the scatterplot of TOA radiance with TOAr Reflectances and TOC Reflectances for all the VIs. Earlier studies (Myneni and Asrart 1994), that used vegetation/atmosphere radiative transfer method have found that relationship between TOA VI and TOC VI is influenced by the soil reflectance, solar zenith angle, and aerosol optical depth. Both WDVI and MSAVI are subject to atmospheric effects. GEMI can compensate for atmospheric and illumination conditions (Pinty and Verstraete 1991). Other factors, such as leaf orientation, leaf optical properties at visible wavelengths, might also introduced variability into the VI_{TOA} – VI_{TOC} relationships, but these influences could not be resolved in this study.

5.3. Comparison of the Vegetation Indices derived from MERIS with the ones of HyMap

The improvement in *R*2 for the VI_{MERIS}–VI_{HyMap} relationship across the vegetation land cover types when using TOC reflectance compared to TOA radiance or TOAr reflectance indicates that the image processing tends to reduce noise in the relationship (Table 14 and 15, Figure 12 and 13). The amount of data scatter in the plots varies among the different VI and the different vegetation biomes (arable land and grass) that occur in the Millingerwaard scene. The R^2 values fall in the range from 0.07 to 0.56. The larger pixel size in MERIS imagery and possible atmospheric influences not completely removed by the image processing may constrain the strong VI–VI correlation. In theory one expects to fit a 1:1 linear relationship through the data, however the best fit is obtained adding an offset of 0.15. The offset is thought to be the result of a) errors in georegistration of these two images, b) averaging effect imposed by the spatial aggregation of Hymap and the simulated MERIS data from airborne HyMap data, c) the effect of surface heterogeneity and mixed pixels, d) the difference in atmospheric corrections for the two sensors and e) the difference in image acquisition dates. The best correlation is found for the MSAVI derived from TOC (R^2=0.56) for the arable land-dominated biome.

5.4. Derivation of MERIS LAI and Validation Using LAI Estimated from HyMap

The range of LAIs across Millingerwaard vegetation types was from 0.16 to 3.19 and 0.04-3.43 for MERIS and HyMap respectively. In both maps the water bodies, urban areas, and generally the non vegetation land cover patterns have been removed (masked out). Despite this masking, the two vegetation types that dominate the site area still include (aggregation had occurred by the use of majority fraction) fractions of non vegetation patterns that corresponds to small LAI values. Among the two main vegetation land cover types grass had the highest LAI values.

The scatter observed in Figure 16, arises from several sources, including: a) errors in georegistration of these two images, b) averaging effect imposed by the spatial aggregation of Hymap and the simulated MERIS data from airborne HyMap data. c) the effect of surface heterogeneity and mixed pixels, e) different image acquisition dates and d) the difference in method of LAI retrieval for the two images. In particular the LAI algorithm for MERIS (TOA__VEG) is not designed to retrieve a deterministic LAI site-specific value, but instead generates a mean LAI value within a specified level of input satellite data and model uncertainties. In addition the algorithm isn't biome specific (Baret 2006). LAI from the HyMap was derived from a site-specific model.

A good agreement between HyMap and MERIS is observed for the leaf area index. The error of individual pixel LAI values in the MERIS image is in the range of 35–39%, taken as the ratio of the RMSE to the average LAI of the scene. In a previous study Gobron (2006) has found a good agreement between the MERIS LAI product and the one of MODIS (RMSE = 0.74).

5.5. Derivation of MERIS FAPAR and Validation Using fAPAR Estimated from HyMap

The range of fAPAR across Millingerwaard vegetation types was from 0.14 to 0.78 and 0.02-1.19 for MERIS and HyMap respectively. Similarly to the LAI maps, the non vegetation land cover patterns have been removed but the two vegetation types that dominate the site still include fractions of non vegetation patterns that correspond to small fAPAR values.

The scatter observed arises from: (1) errors in georegistration of these two images, (2) averaging effect imposed by the spatial aggregation of Hymap and the simulated MERIS data from airborne HyMap data and (3) the effect of surface heterogeneity and mixed pixels.

The best correlation (R2=0.50) is found for arable land. The error of individual pixel fAPAR values in the MERIS image is in the range of 23–28%.

5.6. Relationships between VIs and biophysical products

5.6.1. VIs and LAI Relationships

The significant changes in the VI values observed at different stages of image processing suggest the importance of converting to top of canopy reflectances whenever VI are compared across different biomes. Goward et al. (1991) suggest that whenever VIs are compared across sites ground reflectance should be used. In deriving VIs from TOC reflectances, an increase has been applied to NIR primarily to correct for water vapour absorption (see WWW 6 ESA-ENVISAT), but a decrease has been applied to red to remove the effect of scattering by the atmosphere. Thus, significant differences between VI-TOA radiances and VI-TOC reflectances could be expected depending on atmospheric humidity and haziness.

The improvement in R^2 for the LAI–VI relationship across the vegetation land cover types when using TOC reflectance compared to TOA radiance or TOAr reflectance indicates that the image processing tends to reduce noise in the relationship. Other studies of LAI and remotely sensed VIs have likewise found a better fit in LAI–VI relationships after atmospheric correction of TOA data (Peterson et al. 1987, Spanner et al. 1990).

The LAI–RED relationship was not found to be strong correlated in any case. The TOC reflectance for the vegetation types where LAI measurements were taken ranged from 0.02(TOC refl.), (LAI=2.2, grass) to 0.09(TOC refl), (LAI=1.2, arable land). The relation was inverse linear with a low R^2 (Figure 22), due to the absorption of red reflectance by

pigments. The red spectral response of grass tends to be lower than that for arable land. It is known that canopy structure (LAI, plant height, leaf size, and angle, etc.) affects the target spectral response (Asrar et al. 1985, Bouman 1992, Myneni et al. 1995, 1997). The relation LAI-RED varies among the authors. Peterson et al. (1987) found high correlation (r2~0.89, potential model) in coniferous forest; Holben et al. (1980) found R^2 ~0.57 for soybean (linear model); and Epiphanio et al. (1997) found R^2 ~0.29 for wheat (linear model). A saturation of RED in relation to LAI was not observed in this study.

The LAI–NIR TOC reflectance values ranged from 0.11, (LAI=2.1, grass) to 0.39, (LAI=3, arable land). A high correlation for the LAI–NIR relationship was not observed (Figure 22). Correlations appeared more weak compared to the ones of LAI-red. The NIR spectral response for both vegetation types tends to be similar in range. The observed low correlation for the LAI–NIR relationship was also observed in other studies, i.e. Peterson et al. (1987) with r2~0.04 in coniferous forest, and Nemani et al. (1993) with r2~0.40 also in forest, both using radiance data.

The observed increase in each VI with increasing LAI at low to high LAIs (around 3) is consistent with earlier observations from a variety of ecosystems and predictions from canopy reflectance models (Huemmrich and Goward 1997, Gobron et al. 1997, Myneni et al. 1997). In addition earlier studies have also observed and described the phenomenon of indices saturation when they approach high values of LAI. In particular. Chen and Cihlar (1996) suggested that saturation in VIs for crops and forests would occur approximately for LAI values of 2.5 and 5.0, respectively. Turner et al. (1999) reported that saturation occurred for LAI values between 4.0 and 6.0, for temperate vegetation. The highest LAI value estimated in this study was around 3 and saturation in the LAI–VI relationships was not observed.

The sensitivity of vegetation indices to canopy geometry (leaf angle distribution function, row orientation, and spacing) has been shown by Aase et al. (1984) and Jackson (1986)

among others. In addition, vegetation indices are also sensitive to soil optical properties as shown by Huete and Jackson (1987). They are also affected by the sun position (Asrar et al. 1985b, Huete, 1987b) and the cloudiness (Holben et al., 1986). These results suggest caution in the established relations between vegetation indices and LAI if the effects of these different factors are not known.

Assuming that the image pre-processing has minimized effects of differing Sun–surface–sensor geometry and that LAI estimates are accurate, the observed variation around the best fit LAI– VI relationships over this LAI range are most likely associated with real differences —largely independent of LAI—among the vegetation types in the optical properties of the foliage, canopy, and background. Clevers and Verhoef (1993) used the SAIL canopy and PROSPECT leaf models to show how the main variable that influences vegetation indices is the leaf inclination angle distribution. The more planophile a canopy the greater the vegetation index value for a given LAI. The absence of vegetation free pixels in our study area didn't give us information for describing the influence of background reflectance. Other factors, such as differences in chlorophyll concentration per unit leaf area, differences in leaf clumping, and the relative contribution of branches to canopy reflectance, undoubtedly also introduced variability into the LAI–VI$_{TOC}$ relationships, but these influences could not be resolved in this study.

It can be observed that NDVI values increase faster for lower LAI values (Figures 20 and 21), tending towards stabilization for higher values. Such behaviour was also observed in other studies (Holben et al. 1980 and Turner et al.1999). In this study, the variance was explained better with a linear model for the relationships LAI–VI$_{TOC.}$

At the grassland site, there was little relationship of LAI to the VI in this study. From the indices that were involved in our study NDVI gave the better fit (R^2 =0.29). Strong linear relationships of LAI–VI in grasslands have been reported under well-controlled

conditions with hand-held or boom mounted sensors (Asrar et al., 1984; Middleton, 1991).

Generally, at the arable land of Millingerwaard site, better relations of LAI-VI were derived. NDVI from TOC reflectance was best related to LAI resulting in a R2=0.42.

5.6.2. VIs and fAPAR Relationships

The changes in the VI values observed at different stages of image processing suggest, as in the case of LAI, the importance of converting to top of canopy reflectances whenever VI derived from MERIS are compared with fAPAR across different biomes.

In addition, the improvement in *R*2 for the fAPAR–VI relationship across the vegetation land cover types when using TOC reflectance compared to TOA radiance or TOAr reflectance indicates that the image processing tends to reduce noise in the relationship.

The fAPAR–RED relationship was not found to be strongly correlated in any case (Figure 25). The TOC reflectance for the vegetation types where fAPAR estimations were taken ranged from 0.05 (fAPAR=0.58, grass) to 0.12 (fAPAR=0.3, arable land). The relation was inverse linear with a low R^2, due to the absorption of red reflectance by pigments. The red spectral response of grass tends to be lower than those for arable land. It is known that canopy structure (LAI, plant height, leaf size, and angle, etc.) affects the target spectral response (Asrar et al. 1985, Bouman 1992, Myneni et al. 1995, 1997). A saturation of RED in relation to LAI was not observed in this study.

Figure 25 shows the LAI–NIR. The TOC reflectance values ranged from 0.14, (fAPAR=0.15, grass) to 0.41, (LAI=3, grass). A high correlation to for the fAPAR–NIR relationship was observed (R2=0, 78 and 0, 93 for arable land and grass respectively).

Previous studies have documented differential sensitivity to surface biophysical properties among the VIs (Epiphanio and Huete, 1995; Chen and Cihlar, 1996, White et al., 1997). For the observations in this study, increases in NIR reflectance with increasing fAPAR were more significant than were decreases in red reflectance. Thus the MSAVI, WDVI, PVI (with NIR band in the numerator) were more sensitive than NDVI and GEMI (with NIR band in the denominator) to increasing fAPAR. A fAPAR increase from 0.14 to 0.8 resulted in an increase of the MSAVI, WDVI, and PVI around 80% compared to a 50% increase in the NDVI and a 52% increase for GEMI.

At the grassland site, there was a weak relationship of fAPAR with the VI_{TOC} in this study. From the indices that were involved in our study MGVI gave the better fit. Arable land of the Millingerwaard site had also strong relations of fAPAR-VI. MSAVI from TOC reflectance was best related to fAPAR resulting in a R^2 =0.99 (Table 24).

6. CONCLUSIONS AND RECOMMENDATIONS

6.1. Conclusions

The present study shows that the radiometric processing applied to the image data of MERIS has influence to the derivation of VI for the vegetation land cover types of the Netherlands. In particular the investigation of the TOA radiance, TOAr reflectance and TOC reflectance spectral vegetation indices mutual relationship revealed the influence of the atmospheric correction. A high mutual correlation, for the TOAr Reflectances and TOC Reflectances was observed for all the VIs. Contrary to this high correlation, a lower correlation appeared, in the scatterplot of TOA radiance with TOAr Reflectances and TOC Reflectances for all the VIs and for all the vegetation biomes. In addition the improvement in R^2 for the VI_{MERIS}–VI_{HyMap} relationship across the vegetation land cover types when using TOC reflectance compared to TOA radiance or TOAr reflectance indicates the significancy of the image processing in reducing the noise in the relationship. The best correlation is found for the MSAVI derived from TOC (R^2 =0.56) for the arable land-dominated biome.

The TOA_VEG algorithm (Baret et al. 2006) designed for MERIS and the MGVI as a MERIS L2 product offer an opportunity for producing LAI and fAPAR surfaces. Comparisons of LAI and fAPAR values from these coarse-resolution images with those aggregated from HyMap 5-m pixels suggest that it is feasible to derive LAI and fAPAR using coarse-resolution measurements, but errors due to sensor characteristics and image processing were still considerable. The error in LAI and fAPAR in individual MERIS pixels is found to be about 35% to 39% and 23%-28%, respectively.

Since the level of image processing significantly affects VIs, care must be taken to account for this factor in comparing LAI–VI-fAPAR studies across vegetation biomes. Observations in the present study suggest the importance of converting to top of canopy

reflectances whenever VIs are estimating for different vegetation land cover types. Image processing seems to reduce noise in the relationship of VI with biophysical variables such as LAI, fAPAR. The top of the canopy reflectance was found produces stronger LAI–VI, VI-fAPAR relationships for both grass-dominated and arable land-dominated vegetation types of Millingerwaard than the VIs based on top of atmosphere radiance, or top of aerosol reflectance. Thus, atmospheric correction is desirable in the formulation of LAI–VI and fAPAR-VI algorithms based on data derived from MERIS from the site of Millingerwaard.. Across the main vegetation types that occur in Millingerwaard, the VIs increase with increasing LAI and fAPAR at low to high values.

The impact of the NIR and red spectral band on the relations of VIs with biophysical products has been examined. NIR showed a significant relationship (R^2 ~0.93, 0.78 for grass and arable land, respectively) with fAPAR in contrast to the red (R^2 ~0.16, 0.09 for grass and arable land, respectively). Thus, NIR has more influence on VIs to explain the fAPAR. MSAVI, WDVI, PVI showed a better fit, since they are more sensitive to the NIR. NIR and red did not present a significant relationship with LAI data.

6.2 Recommendations

Based on the present study, the following points are mentioned to be considered for future studies.

Estimation of VIs from the different processing levels of the MERIS data should be further explored by including the VIs derived from digital numbers and TOA reflectance. These results would provide an additional level of comparison between the VIs and the biophysical products.

The current analysis characterizes the trends between the MERIS products (VI, LAI, fAPAR) and explores the relationships with HyMap derived products in terms of what we

understand to be happening at the pixel level. The comparison between these two fields provides an analysis of the MERIS VI, LAI, fAPAR products. However, this pixel by pixel comparison has some disadvantages. First, the actual spatial location of the corresponding pixels in the two sensor maps may not match well because of geolocation uncertainties and pixel-shift errors due to point spread function. Second, the LAI algorithm is not designed to retrieve a deterministic LAI value, but instead generates a mean LAI value from all possible solutions within a specified level of input satellite data and model uncertainties. Therefore, a future study could perform a comparison at the multi-pixel (patch) scale, where the derived products might be statistically more stable.

REFERENCES

Aase, J. K., F. H.Siddoway, and J. P. Millard 1984, Spring wheat leaf phytomass and yield estimates from airborne scanner and hand-held radiometer measurements, *International Journal of Remote Sensing,* **5,** 771-781.

Agnihothri, V.P., 1996, Current sugarcane scenario and management strategies, Indian Phytopathology , **49**, 109 –126.

Andersen, J., G. Dybkjaer, K.H. Jensen, J.C. Refsgaard, and K. Rasmussen, 2002. Use of remotely sensed precipitation and leaf area index in a distributed hydrological model. Journal of Hydrology **30**, pp. 34–50.

Asner, G.P. 1998a, Biophysical and biochemical sources of variability in canopy reflectance, *Remote Sensing of Environment,* **64,** 234–253.

Asner, G.P., C.A. Wessman, and S. Archer. 1998b, Scale dependence of absorption of photosynthetically active radiation in terrestrial ecosystems. *Ecological Applications* 8,906-925.

Asner, G.P., C.A. Wessman, D.S. Schimel, and S. Archer, 1998c, Variability in leaf and litter optical properties: implications for canopy BRDF model inversions using AVHRR, MODIS, and MISR, *Remote Sensing of Environment* 63,200-215.

Asrar, G., R. B.Myneni, and B.J. Choudhury, 1992, Spatial heterogeneity in vegetation canopies and remote sensing of Absorbed Photosynthetically Active Radiation: a modeling study, *Remote Sensing of Environment,* **41,** 85-101**.**

Asrar,E. T. Kanemasu, R. D. Jackson, and P. J. Pinter, 1985a, Estimation of total above ground phytomass production using remotely sensed data. *Remote Sensing of Environment,* **17,** 211–220.

Asrar, G., E. T. Kanemasu, and M. Yoshida, 1985b, Estimates of leaf area index from spectral reflectance of wheat under different cultural practices and solar angle, *Remote Sensing of Environment,* **17,**1-11

Asrar, G., M. Fuchs, E. T. Kanemasu, and Hatfield, J. L. 1984, Estimating absorbed photosynthetic radiation and leaf area index from spectral reflectance in wheat. *Agron. J.* **76,**300–306.

Barclay, H. J. 1998. Conversion of total leaf area to projected leaf area in lodgepole pine and Douglas-fir, *Tree Physiology*, **18,**185–93.

Baret, F. , M. Weiss, B. Bacour, Berthelot, M. C. Gonzalez, "Report on the validation of MERIS TOA_VEG land products", 2006. INRA, Avignon, France.

Baret, F., M. Weiss and S. G. Denis Allard, Marc Leroy, Hervé Jeanjean, R. Fernandes, R. Myneni, J. Privette, J. Morisette Hervé Bohbot, Roland Bosseno, Gérard Dedieu, Carlos Di Bella, Benoit Duchemin, Marisa Espana, Valery Gond, Xing Fa Gu1, Dominique Guyon, Camille Lelong, Philippe Maisongrande, Eric Mougin, Tiit Nilson, Frank Veroustraete, Roxana Vintilla 2005, VALERI: a network of sites and a methodology for the validation of medium spatial resolution land satellite products, www. avignon.inra.fr/valeri/

Baret, F., S. Jacquemond, and J.F. Hanocq. 1993. The soil line concept in remote sensing, **7,** 65–82.

Baret, F., and G. Guyot, 1991, Potentials and limits of vegetation indices for LAI and APAR assessment, *Remote Sensing of Environment,*, **35**, 161–173.

Baret, F., G. Guyot and D. Major, 1989, TSAVI: a vegetation index which minimizes soil brightness effects on LAI and APAR estimation. Proceedings of the 12th Canadian Symposiumon Remote Sensing and IGARSS90, 10–14 July 1989 (Vancouver: IGARSS).

Beadle, C. L. 1993, Growth analysis. pp. 36–46. In D. O. Hall, Scurlock, J.M.O., Bolhar-Nordenkampf, H.O., Legood, R.C. and Long, S.P., 1993) et al. (eds.), Photosynthesis and Production in a Changing Environment: A Field and Laboratory Manual. Chapman and Hall, London.

Behrenfeld, M.J., J.T. Randerson, C.R. McClain, G.C. Feldman, S.O. Los, C.J. Tucker, P.G. Falkowski, C.B.Field, R. Frouin, W.E. Esaias, D.D. Kolber, and N.H. Pollack, 2001, ENSO-scale variations in biospheric photosynthesis, Science 291, pp. 2594–2597

Bernstein, R. 1983, Beyond Objectivism and Relativism: Science, Hermeneutics, and Praxis. Philadelphia: University of Pennsylvania Press.

Best, R.G., and J.C. Harlan. 1985, Spectral estimation of green leaf area index of oats. *Remote Sensing of Environment,* **17,** 27–36.

Bian, L., 1997, Multiscale nature of spatial data in scaling up environmental models. In: D.A.Q.a.M.F. Goodchild (Editor), Scale in remote sensing and GIS, 13-26.

Bonan, G.B., 1993, Importance of leaf area index and forest type when estimating photosynthesis in boreal forests, *Remote Sensing of Environment*, **43**, 303-314

Bouman, B. A. 1992, Accuracy of estimating the leaf area index from vegetation indices derived from crop reflectance characteristics, a simulation study, *International Journal of Remote Sensing,* **13,** 3069–3084.

Brown, L., J. M. Chen, S. G. Leblanc and J. Cihlar, 2000, A shortwave infrared modification to the simple ratio for LAI retrieval in boreal forests: An image and model analysis, *Remote Sensing of Environment* **71,** 16**.**

Burgess, D.W., D. Pairman, 1997, Bidirectional reflectance effects in NOAA AVHRR data , *International Journal of Remote Sensing,* **18** , 2815-2825

Chen, J. M., and J. Cihlar. 1996, Retrieving leaf area indexes of boreal conifer forests using Landsat TM images, *Remote Sensing of Environment,* **55,**153–162.

Chen, J. M. 1996. Optically-based methods for measuring seasonal variation in leaf area index in boreal conifer stands, *Agricultural and Forest Meteorology,* **80,**135–63.

Chen, J. M., and T. A. Black. 1992, Defining leaf area index for non-flat leaves, *Plant Cell Environment,* **15,** 421–29.

Chen, J. M. and T. A. Black 1991,Measuring leaf area index of plant canopies with branch architecture, *Agricultural and Forest Meteorology,* **57**(1-3): 1.

Choudhury, B. J. 1987, Relationships between vegetation indices, radiation absorption, and net photosynthesis evaluated by a sensitivity analysis, *Remote Sensing of Environment,* **22,** 209-233.

Clevers, J.G.P.W., R. Zurita Milla, M., Schaepman, & H. Bartholomeus, 2004, Using MERIS on ENVISAT for Land Cover Mapping. In Envisat Symposium. ESA, Salzburg.

Clevers, J. G. P. W., W. Verhoef 1993, LAI estimation by means of the WDVI: A sensitivity analysis with a combined PROSPECT-SAIL model, *Remote Sensing of Environment*, **7,** 43–64.

Clevers, J. G. P. W. (1989). "The Application of a Weighted Infrared-Red Vegetation Index for Estimating Leaf Area Index by Correcting for Soil Moisture." Remote Sensing of Environment **21**: 25-37.

Clevers, J. P. G. W., 1988, The derivation of a simplified reflectance model for the estimation of Leaf Area Index, *Remote Sensing of Environment*, **25**, 53–69.

Curran, P. J., and C. M. Steele, 2004, MERIS: the re-branding of an ocean sensor, *International Journal of Remote Sensing (submitted).*

Curran, P. J., 2001, Imaging spectrometry for ecological applications. *International Journal of Applied Earth Observation and Geoinformation*, ***3,*** 305–312.

Curran, P. J., J. A. Kupiec, and G. M. Smith, 1997, Remote sensing the biochemical composition of a slash pine canopy. *IEEE Transactions on Geoscience and Remote Sensing*, **35**, 415–420.

Curran, P. J., W. R Windham, and H. L. Gholz, 1995, Exploring the relationship between reflectance red edge and chlorophyll content in slash pine leaves, *Tree Physiology*, **15**, 203–206.

Curran, P. J., 1989, Remote sensing of foliar chemistry, *Remote Sensing of Environment*, **30**, 271–278.

Curran, P.J., and H.D. Williamson, 1985, The accuracy of ground data used in remote sensing investigations, *International Journal of Remote Sensing*, **6,** 1637-1651.

Daughtry, C. S. T., K. P. Gallo, S. N. Goward, S. D. Prince, and W. P. Kustas, 1992, Spectral estimates of absorbed radiation and phytomass production in corn and soybean canopies, *Remote Sensing of Environment*,, **39,** 141–152

Daughtry, C. S. T., K. P. Gallo, and M. E. Bauer. 1983, Spectral estimates of solar radiation intercepted by corn canopies, *Agronomy Journal*, **75**, 27-531.

J. Dash and P.J. Curran, 2004. The MERIS terrestrial chlorophyll index, *International Journal of Remote Sensing*,. **25**, 23:5403-5413.

Deering, D. W., T. F. Eck, and E. Middleton, 1994, Reflectance anisotropy for a forest canopy. *Remote Sensing of Environment*, **47**, 242–260.

Deering, D. W., Middleton, E. M., Irons, J. R., Blad, B. L., Walter-Shea, E. A., Hays, C. J., Walthall, C., Eck, T. F., Ahmad, S. P., and Banerjee, B. P. ,1992, Prairie grassland bidirectional reflectance measured by different instruments at the FIFE site, *Journal of Geophysical Research*, **97**, 18,887-18,903.

Deering, D W. 1989. Field measurements of bidirectional reflectance. In: Asrar, G. (ed), Theory and applications of optical remote sensing, 14-65. John Wiley & Sons, New York.

Dickinson, R., and Henderson-Sellers, A., 1988, Modeling deforestation: a study of GCM land-surface parameterization, *Quarterly Journal of the Royal Meteorological Society*, **114,** 439–462.

Deardorff, J. W., 1978, Efficient prediction of ground temperature and moisture with inclusion of a layer of vegetation. *Journal of Geophysical Research*, **83,** 1889–1903.

Elvidge, C. D., and Lyon, R. J. P., 1985, Influence of rock- soil variation on the assessment of green biomass, *Remote Sensing of Environment*. **17,**265–279.

Epiphanio, J. C. N., JR, A. C. Almeida, and A. R. Formaggio, 1997, Wheat development evaluated by remote sensing using two vegetation indices. *Anais da Academia Brasileira de Ciencias*, **69**, 471–478.

Epiphanio, J. C. N., and A. R. Huete, 1995, Dependence of NDVI and SAVI on sun/sensor geometry and its effect on fAPAR relationships in Alfalfa. *Remote Sensing of Environment*, **51,** 351± 360.

Fassnacht, K. S., S. T. Gower, E. V. Nordheim, T. M. Lillesand and M. D. MacKenzie ,1997, Estimating the leaf area index of North Central Wisconsin forests using the landsat thematic mapper, *Remote Sensing of Environment* **61,** 229.

Friedl, M., J. Michaelson, F. W. Davis, H. Walker, and D. S. Schimel, 1994, Estimating grassland biomass and leaf area index using ground and satellite data. *International Journal of Remote Sensing*, **15,** 1401- 1420.

Gallo, K.P., Daughtry, C.S.T., and Bauer, M.E. (1985). Spectral estimation of absorbed photosynthetically active radiation in corn canopies. Remote Sensing of Environment, **17**, 221-232.

Gastellu-Etchegorry, J. P., E. Martin, F. Gascon 2004, DART: a 3D model for simulating satellite images and studying surface radiation budget, *International Journal of Remote Sensing*, **25,** 73-96.

Gobron, N., O. Aussedat, B. Pinty, M. Taberner, and M. M. Verstraete 2004, MERIS: level 2 land surface products algorithm theoretical basis document,Access date: 11-10-2005, http://envisat.esa.int/instruments/meris/pdf/.

Gobron, N., , B. Pinty, M. Verstraete, and Y. Govaerts, 1999, The MERIS Global Vegetation Index (MGVI): description and preliminary application, *International Journal of Remote Sensing*, **20**, 1917–1927.

Gobron, N. , B. Pinty and M. M. Vestraete, 1997, Theoretical limits to the estimation of the leaf area index on the basis of visible and near-infrared remote sensing data. IEEE Transactions on Geoscience and Remote Sensing, 35, 1438–1445. Goel, N.S. (1988) Modes of vegetation canopy reflectance and their use in estimation of biophysical parameters from reflectance data, *Remote Sensing of Environment*, **4,** 1-212.

Goel, N.S. (1988) Modes of vegetation canopy reflectance and their use in estimation of biophysical parameters from reflectance data,*Remote Sensing of Environment*, **4,** 1-212.

Govaerts, Y. M., M. M. Verstraete, B. Pinty, and N. Gobron, 1999, Designing optimal spectral indices: a feasibility and proof of concept study, *International Journal of Remote Sensing*, **20**, 1853–1873.

Goward, S. N., B. Markham, D. G. Dye, W. Dulaney, and J. Yang, 1991, Normalized difference vegetation index measurements from the Advanced Very High Resolution Radiometer, *Remote Sensing of Environment,* **35**, 257–277.

Goward, S. N. and K. F. Huemmrich. 1992, Vegetation canopy PAR absorbance and the normalized difference vegetation index: an assessment using the SAIL model, *Remote Sensing of Environment,* **39,** 119-140.

Gower, S.T., C.J. Kucharik, and J.M. Norman, 1999, Direct and indirect estimation of leaf area index, f_{APAR} and net primary production of terrestrial ecosystems. *Remote Sensing of Environmet,* **70**, 29–51.

Guyot, G., X.-F. Gu, 1994, Effect of radiometric corrections on NDVI-determined from SPOT-HRV and Landsat-TM data, *Remote Sensing of Environment* **49**, 169-180.

Hall, F. G., J. R. Townshend, and E. T. Engman, 1995, Status of remote sensing algorithms for estimation of land surface state parameters, *Remote Sensing of Environment,* **51,**138–156.

Hall, F. G., P. J. Sellers, I. MacPherson, R. D. Kelly, S. Verma, B. Markham, B. Blad, J. Wang, and D. E. Strebel. 1989a. FIFE: analysis and results - a review. Advances in Space Research **9,** 275–293.

Hall, J.D., M.L. Murphy, and R.S. Aho. 1989b, An improved design for assessing impacts of watershed practices on small streams. Proc. Int. Ass. Theoret. Appl. Limnol. **20**, 1359-65.

Hatfield, G. Asrar and E. T. Kanemasu, 1984, Intercepted photosynthetically active radiation estimated by spectral reflectance, *Remote Sensing of Environment*, **14**, 65-75.

Hazeu, G. W. 2005, LGN5 crop accuracy estimation, Alterra, Wageningen UR, Wageningen, Access date: 19-08-2005, http://www.lgn.nl.

Hipps, L. E., G. Asrar, and E.Kanemasu, 1983, Assessing the interception of photosynthetically active radiation in winter wheat, *Agricultural and Forest Meteorology*, **28,** 253-259.

Holben, B. N., E. Vermote, Y. J. Kaufman, D. Tanré, and V. Kalb, 1992, Aerosol retrieval over land from AVHRR data—Application for atmospheric correction, *IEEE Transactions on Geoscience and Remote Sensing*,**30**, 212–222.

Holben, B. N., D. S. Kimes, and R. S. Fraser, 1986, Directional reflectance in AVHRR red and near-IR bands for three cover types and varying atmospheric conditions, *Remote Sensing of Environment*, **19,**213-236

Holben, B., C. Justice, 1980, An examination of spectral band ratioing to reduce the topographic effect on remotely sensed data, *International Journal of Remote Sensing*, **2**, 115-133

HOLBEN, B. N., C. J. TUCKER, and C. J., Fan, 1980, Spectral assessment of soybean leaf area and leaf biomass, *Photogrammetric Engineering and Remote Sensing*, **46**, 651–656.

Huemmrich, K. F., and S. N. Goward,. 1997, Vegetation canopy PAR absorbance and NDVI: an assessment for ten tree species with the SAIL model, *Remote Sensing of Environment*, **61,** 254–269.

Huete, A.R and Q. Liu, and, 1995, A feedback based modification of the NDVI to minimize canopy background and atmospheric noise. IEEE Trans. Geosci Remote Sens. 33; 457-465.

Huete, A. R., 1989, Soil influences in remotely sensed vegetation-canopy spectra. In Theory and Applications of Optical Remote Sensing, edited by G. Asrar (New York: Wiley), pp. 119± 128.

Huete, A. R., 1988, A Soil-Adjusted Vegetation Index (SAVI), *Remote Sensing of Environment*, **25**, 295–309.

Huete, A. R., 1987, Soil and Sun angle interactions on partial canopy spectra, *International Journal of Remote Sensing*, **8**, 1307-1317.

Huete, A. R., and R. D. Jackson, 1987, Suitability of spectral indices for evaluating vegetation characteristics on arid rangelands. *Remote Sensing of Environment*, ***23,*** *213-232.*

Jackson, R.D., and A.R. Huete. 1991, Interpreting vegetation indices. Prev. Vet. Med. **11**,185-200

Jackson, R. D. (1986), Spectral response of architecturally different wheat canopies, *Remote Sensing of Environment*, **20,** 43-56.

Jacquemoud, S, 1993, Inversion of the PROSPECT+SAIL canopy reflectance model from AVIRIS equivalent spectra: theoretical study, *Remote Sensing of Environment*, **44**, 281-292.

Jackson, R., Nepali, H.S., and Sherpa, A. R. 1990, Aspects of Wildlife Protection and Utilization in the Makalu-Barun Conservation Area. Report 11, Working Paper Publication Series, Makalu-Barun Conservation Project, Dept. of National Parks & Wildlife Conservation, H.M.G. Katrhmandu, Nepal.

Jasinski, M.F., and P.S. Eagleson. 1989. The structure of red-infrared scattergrams of semivegetated landscapes, *IEEE Transactions on Geoscience and Remote Sensing*, **27**, 441–451

Johnson, L. F., 1999, Response of grape leaf spectra to Phylloxera infestation, NASA Report #CR-208765, NASA Center for AeroSpace Information, Hanover, MD 21076-1320, USA.

Justice C.O., E. Vermote, J. R. G. Townshend, R. Defries, D. P. Roy, D. K. Hall, V. V. Salomonson, J. L. Privette, G. Riggs, A. Strahler, W. Lucht, R. B. Myneni, Y. Knyazikhin, S. W. Running, R. R. Nemani, Z. Wan, A. R. Huete, W. Leeuwen, R.E. Wolfe, L. Giglio, J-P Muller, P. Lewis, and M. J. Barnsley, 1998, The Moderated Resolution Imaging Spectroradiometer (MODIS): Land Remote Sensing for Global Change Research, *IEEE Transactions on Geoscience and Remote Sensing*, **36**, 1228-1249.

Justice, C. O., and J. R. G. Townshend, 1994, Data sets for global remote sensing: lessons learnt, *International Journal of Remote Sensing*, **15**, 3621– 3639.

Justice, C.O., S.W. Wharton, B.N, Holben, 1981, Application of digital terrain data to quantify and reduce the topographic effect on Landsat data*, International Journal of Remote Sensing*, **2,** 213-230.

Kaufman, Y. J. 1989, The atmospheric effect on remote sensing and its corrections, in Theory and Applications of Optical Remote Sensing, (G. Asrar, Ed.), Wiley, New York, 336- 428.

Kimes, Daniel S., Norman, John M., Walthall, Charles L., 1985, MODELING THE RADIANT TRANSFERS OF SPARSE VEGETATION CANOPIES, *IEEE Transactions on Geoscience and Remote Sensing*, **23**, 695-704.

Kite, G.W. and A. Pietrorino, 1996, Remote sensing applications in hydrological modelling. *Hydrological Sciences Journal*, **41**, 563–587.

Lamb, D. W., M. Steyn-Ross, P. Schaare, M. M. Hanna, W. Silvesterr, and ,A.Steynross, 2002, Estimating leaf nitrogen concentration in ryegrass (Lolium spp) pasture using chlorophyll red-edge: theoretical modelling and experimental observation, *International Journal of Remote Sensing*, **23**, 3619–3648.

Lean, J., and, D. Warilow, 1989, Simulation of the regional climatic impact of Amazon deforestation. *Nature*, **342**, 411–413.

Leblanc, S. G., J. M. Chen, H. P. White, R. Latifovic, R. Fernandes, J. L. Roujean and R. Lacaze, 2002, Mapping leaf area index heterogeneity over Canada using directional reflectance and anisotropy canopy reflectance models, *International Geoscience and Remote Sensing Symposium (IGARSS).*

Leprieur, C., Kerry, Y.H., Mastorchio, S. and Meunier, J.C., 2000, Monitoring vegetation cover across semi-arid regions: Comparison of remote observations from various scales. *International Journal of Remote Sensing*, **21,** 281-300.

Liras, E., 2005, Retreival of information on Land Use Cover, Soil, Vegetaion, Atmosphere and Water from Imaging spectroscopy data, Geo-Information Science. Wageningen, Wageningen University and Research Centre. *MSc thesis report***:** 06

Liu, J., J. M. Chen, J. Cihlar and W. M. Park, 1997, A process-based boreal ecosystem productivity simulator using remote sensing inputs *Remote Sensing of Environment*, **62,** 158.

Mengesha, T. G., 2005, Validation of ground biophysical products using imaging specroscopy in a soft wood forest, Geo-Information Science. Wageningen, Wageningen University and Research Centre. **MSc thesis report:** 78.

McVicar, T.R. and D.L.B. Jupp, 1998, The current and potential operational uses of remote sensing to aid decisions on drought exceptional circumstances in Australia: a review, *Agricultural Systems* **57**, 399–468.

Middleton, E.M. 1991, Solar zenith angle effects on vegetation indices in tallgrass prairie. *Remote Sensing of Environment,* **38**, 45-62.

Morisette, J. T., F. Baret, J. L. Privette, R. B. Myneni, J. Nickeson, S. Garrigues, N. Shabanov, M. Weiss, R. Fernandes, S. Leblanc, M. Kalacska, G. A. Sánchez-Azofeifa, M. Chubey, B. Rivard, P. Stenberg, M. Rautiainen, P. Voipio, T. Manninen, A. Pilant, T. Lewis, J. Iiames, R. Colombo, M. Meroni, L. Busetto, W. Cohen, D. Turner, E. D. Warner, G. W. Petersen, G. Seufert and R. Cook. (2005). "Validation of global moderate resolution LAI Products: a framework proposed within the CEOS Land Product Validation subgroup." LAI Intercomparison Overview Submission – *LPV special issue* Retrieved 20-*August, 2005, from http://cliveg.bu.edu/download/manuscripts/morisette01.pdf.*

Myneni, R. B., Ramakrishna, R., Nemani, R., & Running, S. 1997, Estimation of global leaf area index and absorbed par using radiative transfer models, *IEEE Transactions on Geoscience and Remote Sensing*, **35,** 1380-1393.

Myneni, R. B., S. Maggion, J. Iaquinta, J., Privette, J. L., Gobron, N., Pinty, B., Verstraete, M. M., Kimes, D. S. and Williams, D. L 1995, Optical remote sensing of vegetation: modeling, cavaets, and algorithms, *Remote Sensing of Environment,* **51**, 169–188.

Myneni, R. B., F. G. Hall, P. J. Sellers, and A. L. Marshak, 1995, The interpretation of spectral vegetation indexes, *IEEE Transactions on Geoscience and Remote Sensing*, 33, 481-496.

Myneni R. B. and G. Asrar 1994, Atmospheric Effects and Spectral Vegetation Indices. *Remote Sensing of Environment*, **47,** 390-402

Nemani, R. R., L., Pierce, S. W., Running, and L., Band, 1993, Forest ecosystem processes at the watershed scale: sensitivity to remotely-sensed leaf area index estimates, *International Journal of Remote Sensing*, **14**, 2519–2534.

Olioso, A., I. Braud , A. Chanzt, D. Courault, J. Demarty,, L. Kergoat, E. Lewanf, C. Ottle, L.t Prevot, W. G. Zhaoa, J-C Cavlet, P. Cayrol, R. Jongschaap, S.Moulin,, J. Noilhan, J-P Wigneron . 2002, SVAT modeling over the Alpilles-ReSeDA experiment: comparing SVAT models over wheat fields, *Agronomie* **22,** 651-668.

Peterson, D. L., M. A Spanner,., S. W., Running, and K. B. Teuber, 1987, Relationship of thematic mapper simulator data to leaf area index of temperate coniferous forests, *Remote Sensing of Environment*, **22**, 323–341.

Pinter Jr, P.J., G. Zipoli, G. Maracchi, R.J. Reginato, 1987, Influence of topography and sensor view angles on NIR/ red ratio and greenness vegetation indices of wheat, *International Journal of Remote Sensing*, **8**, 953-957.

Pinty, B., and M. M., Verstraete, 1991, Bidirectional reflectance and surface albedo: physical modeling and inversion, Fifth International Colloquim—Physical measurements and signatures in remote sensing, 14–18 January 1991 (Courchevel: ESA SP-391), pp. 383–386.

Pinty, B., C. Leprieur, and M. M. Verstraete, 1993, Towards a quantitative interpretation of vegetation indices." Part I: biophysical canopy properties and classical indices, *Remote Sensing of Environment*, **7**, 127–150.

Price J.C. and Bausch W.C 1995. Leaf area index estimation from visible and near-infrared reflectance data, *Remote Sensing of Environment*, **52**, 55-65

Prince, S.D., 1991a, Satellite remote sensing of primary production: comparison of results for Sahelian grasslands 1981–1988. *International Journal of Remote Sensing*, **12**, 1301–1311.

Prince, S.D., 1991b, A model of regional primary production for use with coarse resolution satellite data, *International Journal of Remote Sensing* **12**, 1313–1330.

Privette, J. L., Myneni, R. B., Emery, W. J., & Hall, F. G. (1996), Optimal sampling conditions for estimating grassland parameters via reflectance model inversions. *IEEE Transactions on Geoscience and Remote Sensing*, **34**, 272-284.

Privette J.L., Myneni, R. B.,Tucker, C.J. and Emery W.J., 1994, Invertibility of a 1-D discrete ordinates canopy reflectance model, *Remote Sensing of Environment*, l. **48**, 89 – 105.

Pu, R., Q. Yu, P. Gong and G. S. Biging 2005, EO-1 Hyperion, ALI and Landsat

7 ETM+ data comparison for estimating forest crown closure and leaf area

index." International Journal of Remote Sensing **26,** 457-474.

Pu, R., P. Gong, G.S. Biging, 2003, Simple calibration of AVIRIS data and LAI mapping of forest plantation in southern Argentina, *International Journal of Remote Sensing*, **24**, 4699-4714.

Qi, J., M. Weltz, A. R. Huete, S. Sorooshian, R. Bryant, Y. H. Kerr, and M. S. Moran, 2000, Leaf area index estimates using remotely sensed data and BRDF models in a semiarid region. *Remote Sensing of Environment*, **73**, 18–30.

Qi, J., A. Chehbouni, A. R. Huete, and Y. H. Kerr, 1994, Modiffied Soil Adjusted Vegetation Index (MSAVI), *Remote Sensing of Environment*, **48**, 119–126.

Qi, J., A., A. Huete, M. Moran, A. Chehbouni, and R. Jackson, 1993, Interpretation of vegetation indices derived from multi-temporal SPOT images, *Remote Sensing of Environment*, **44** , 89-107.

Richardson, A. J., and C. L. Wiegand, 1977, Distinguishing vegetation from soil background information, *Photogrammetric Engineering and Remote Sensing,* **43**, 1541–1552.

Ridao E., Conde J.R., Minguez M.I. Estimating fAPAR from nine vegetation indices for irrigated and non-irrigated faba bean and semileafless pea canopies. *Remote Sensing of Environment,* 1998, **66**, 87-100

Rondeaux, G., M.D. Steven,. and F.Baret, 1996, Optimization of Soil-Adjusted vegetation indices, *Remote Sensing of Environment,* **55**, 95-107.

Ross, J., 1981. The radiation regime and architecture of plant stands. The Hague, 391

Roujean J-L, F-M Breon, 1995, Estimating PAR absorbed by vegetation from bi-directional reflectance measurements. *Remote Sensing of Environment,* **51,** 375–384

Roujean, J.-L., M. Leroy, P.-Y. Deschamps, 1992, A bidirectional reflectance model of the Earth's surface for the correction of remote sensing data, *Journal of Geophysical Research,* **97**, 20,455-20,468.

Running, S. W., R., Nemani, , J. M.Glassy and P. E. Thornton, 1999. MODIS daily photosynthesis (PSN) and annual net primary production (NPP) product (MOD17), Algorithm Theoretical Basis Document Version 3.0.

Sellers, P.J., S.O., Los, , C.J. Tucker, C.O. Justice, D.A. Dazlich, G.J. Collatz, and D.A. Randall, 1996, A revised land surface parameterization (SiB2) for atmospheric GCMs: Part II. The generation of global fields of terrestrial biophysical parameters from satellite data, *Journal of Climate,* **9**, 706–737.

Sellers, P.J., R.E. Dickinson, D.A. Randall, A.K. Betts, F.G. Hall, J.A. Berry, C.J., Collatz, A.S. Denning, H.A.Mooney, C.A. Nobre, and N. Sato, 1997. Modelling the exchanges of energy, water, and carbon between the continents and the atmosphere, *Science,* **275**, 502–509.

Sellers, P. J., B. W. Meeson, F.G Hall, 1995, Remote-sensing of the land-surface for studies of global change-models, algorithms experiments, *Remote Sensing of Environment,* **51,** 3-26.

Sellers, P. J., 1987, Canopy reflectance, photosynthesis and transpiration II: The role of biophysics in the linearity of their interdependence, *International Journal Of Remote Sensing.*, **6,** 1335–1372.

Sellers, P.J., 1985, Canopy reflectance, photosynthesis and transpiration. *International Journal Of Remote Sensing*, **6**, 1335-1372

Shabanov, N. V., Y. Wang, W. Buermann, J. Dong, S. Hoffman, G.R. Smith, Y. Tian,

Y. Knyazikhin, R.B. Myneni . ,2003, Effect of foliage spatial heterogeneity in the MODIS LAI and FPAR algorithm over broadleaf forests, *Remote Sensing of Environment*, **85,** 410-423.

Slama, C., 1980, Manual of Photogrammetry, *American Society of Photogrammetry and Remote Sensing*, Falls Church, Virginia,USA.

Spanner, M. A., L. L. Pierce, D. L. Peterson, and S. W. Running 1990, Remote sensing of temperate coniferous forest leaf area index: the influence of canopy closure, understory vegetation and background reflectance, *International Journal Of Remote Sensing,*, **11,** 95–111.

Tan, B., Hu, J., Zhang, P., Huang, D., Shavanov, V.N., Weiss, M., Knyazikhin, Y., Myneni, R.B., 2005. Validation of MODIS LAI product in croplands of Alpilles, France. J. Geophys. Res. 110,D0110710.1029/2004JD004860.

Teillet, P.M., K., Staenz, D.J. Williams, 1997. Effects of spectral, spatial, and radiometric characteristics on remote sensing vegetation indices of forested regions. *Remote Sensing of Environment*, **61**, 139-149.

Tucker, C. J. and P. J.Sellers, 1986, Satellite remote sensing of primary productivity, *International Journal Of Remote Sensing*, **7,** 1395-1416.

Tucker, C. J., 1979, Red and photographic infrared linear combinations for monitoring vegetation, *Remote Sensing of Environment*, **10**, 127–150.

Turner, D. P., W. B. Cohen, et al. 1999, Relationships between leaf area index and Landsat TM spectral vegetation indices across three temperate zone sites, *Remote Sensing of Environment* ,**70,** 52-68.

United Nations, 1992, UNITED NATIONS FRAMEWORK CONVENTION ON CLIMATE CHANGE. http://unfccc.int/resource/docs/convkp/conveng.pdf.

Verhoef , W. and H. Bach ,2003, Remote sensing data assimilation using coupled radiative transfer models, *Phys. Chem. Earth, Parts A/B/C,* **28**, 3-13.

Vermote E.F**.**, Tanré D., Herman M., 1990, Atmospheric effects on satellite imagery: Correction algorithms for ocean color or vegetation monitoring. MANAUS/ISPRS In: *International archives of photogrammetry and remote sensing*, **28**, 1, 46-55.

Verstraete, M. M., B. Pinty, P. J. Curran 1999, MERIS Potential for land applications, *International Journal of Remote Sensing*, **20,** 1747-1756.

Wang, Y., C. E. Woodcock, W. Buermann, Y. Tian, J. Hu, Y. Knyazikhin, R. B. Myneni, P. Stenberg, P. Voipio, H. Smolander and T. Häme (2004), Evaluation of the MODIS LAI algorithm at a coniferous forest site in Finland, *Remote Sensing of Environment,* **91,** 114.

Weiss, M., L. Beaufor, F. Baret, , D. Allard, N. Bruguier, and O. Marloie, , 2001, Leaf area index measurements at different scales for the validation of large swath satellite sensors: first results of the VALERI project. Proceeding of the 8th international symposium on physical measurements and signatures in remote sensing (pp. 125– 130).

White, M.A., P.E. Thornton and S.W. Running, 1997. A continental phenology model for monitoring vegetation response to interannual climatic variability, *Global Biogeochemical Cycles,* **11,** 217–234.

Wiegand, C.L., A.J Richardson, D.E Escobar, A.H. Gerbermann, 1991, Vegetation indices in crop assessments. *Remote Sensing of Environment*, **35**, 105-119,

Zarco-Tejada, P. J., J. C. Pushnik, S. Dobrowski , S.L. Ustin 2003, Steady-state chlorophyll a fluorescence detection from canopy derivative reflectance and double-peak red-edge effects, *Remote Sensing of Environment***, 84,** 283-294.

WWW References

[WWW 1] CEOS LPV, http://landval.gsfc.nasa.gov/LPVS/

[WWW 2] MERIS-Envisat 2005, http://envisat.esa.int/dataproducts/).

[WWW 3] MERIS-Envisat 2005, http://envisat.esa.int/dataproducts/).

[WWW 4] MERIS-Envisat 2005, http://envisat.esa.int/dataproducts/).

[WWW 5] MERIS-Envisat 2005, http://envisat.esa.int/dataproducts/).

[WWW 6] MERIS-Envisat 2005, http://envisat.esa.int/dataproducts/).

[WWW 7] MERIS-Envisat 2005, http://envisat.esa.int/dataproducts/).

APPENDIX

Appendix 1. Full resolution product structure

MPH
Level 1b - SPH (includes DSDs)
Level 1b Summary Quality ADS (SQ ADS)
Level 1b GADS Scaling Factors and General Info
Level 1b ADS Tie Points Location & Aux. Data
Level 1b MDS (1) TOA Radiance
Level 1b MDS (2) TOA Radiance
Level 1b MDS (3) TOA Radiance
Level 1b MDS (4) TOA Radiance
Level 1b MDS (5) TOA Radiance
Level 1b MDS (6) TOA Radiance
Level 1b MDS (7) TOA Radiance
Level 1b MDS (8) TOA Radiance
Level 1b MDS (9) TOA Radiance
Level 1b MDS (10) TOA Radiance
Level 1b MDS (11) TOA Radiance
Level 1b MDS (12) TOA Radiance
Level 1b MDS (13) TOA Radiance
Level 1b MDS (14) TOA Radiance
Level 1b MDS (15) TOA Radiance

MPH
Level 1b MDS (16) Flags & Spectral Shift Index

Specific Product Header (SPH): The SPH is in ASCII format and contains information which describes the specific product as a whole. The SPH also contains Data Set Descriptors (DSDs).

Data Set Descriptor (DSD): Data Set Descriptors are used to describe an attached Data Set or to provide reference to external files relevant to the current product (e.g. auxiliary data used in processing but not included with the product). There must be one DSD per Data Set or per reference to an external file.

ADS: Annotation Data Set

SQADS: Summary Quality Annotation Data Set

GADS: Global Annotation DataSet

Measurement Data Set (MDS): a defined data entity within a product.

Main Product Header (MPH): the main description record at the start of every product, it follows a generic format.

Appendix 2. Main characteristics of the MERIS L1b dataset that was used in this study

Product name	_FR__1PNEPA20040808_104153_000000982029_00180_12759_0162.N1
Product type	MER_FR__1P
Product description	MERIS Full Resolution Geolocated and Calibrated TOA Radiance
Product format	ENVISAT
Product scene width	2241 pixels
Product scene height	2241 pixels
File size	~158 MB

Appendix 3. Main characteristics of the MERIS L2 dataset that was used in this study.

Product name	MER_FR__2PNUPA20040808_104153_000000982029_00180_12759_0147.N1
Product type	MER_FR__2P
Product description	MERIS Full Resolution Geophysical Product
Product format	ENVISAT
Product scene width	2241 pixels
Product scene height	2241 pixels
File size	~177 MB

Appendix 4. Spectral signatures for land cover types derived from MERIS level 1b TOA Radiances

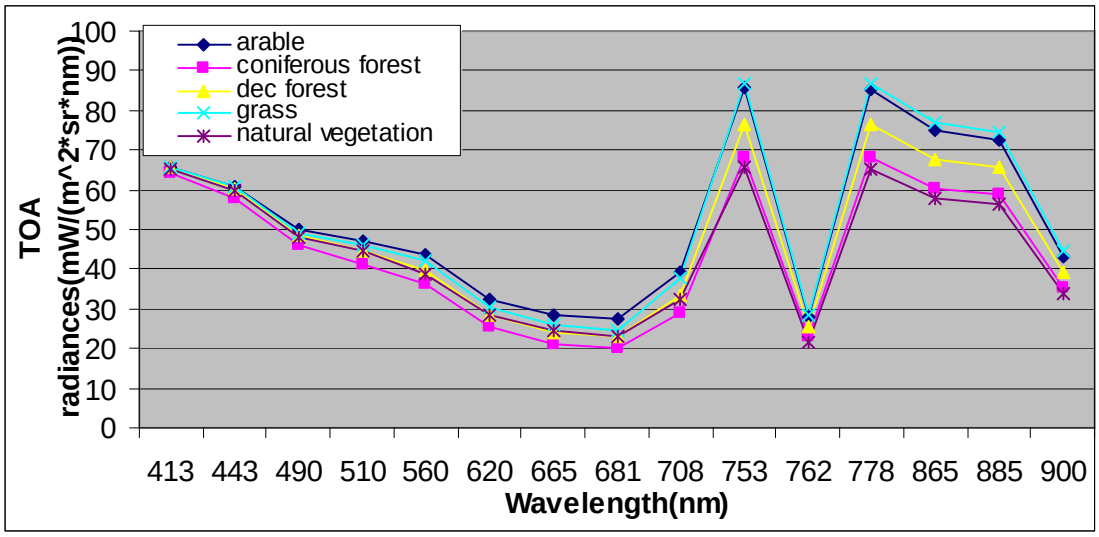

Appendix 5. Spectral signatures for land cover types derived from MERIS level 2 TOC reflectances

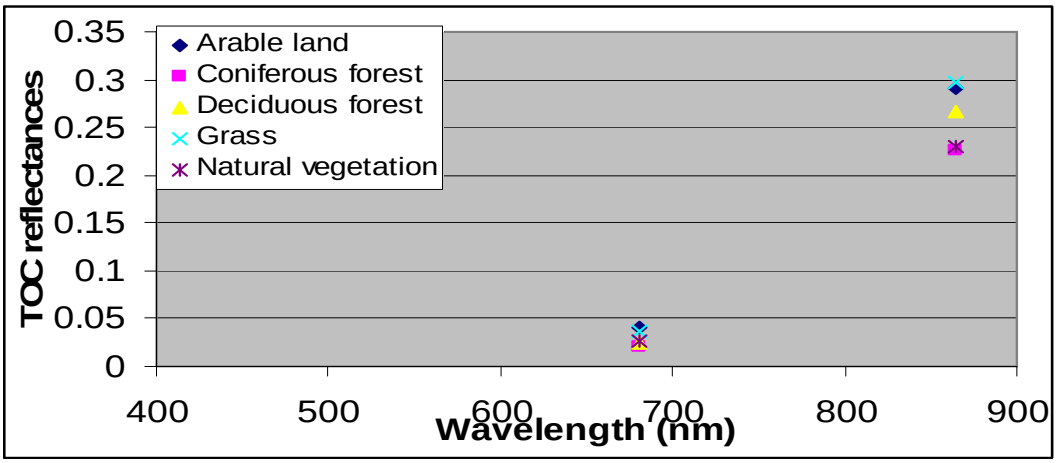

Appendix 6. Correlation matrix for the L2 MERIS image of August 8th, 2004

Band	1	2	3	4	5	6	7	8	9	10	12	13	14	Rec. Red	Rec. NIR
[nm]	412	442	490	510	560	620	665	681	705	754	775	865	890		
1	1														
2	1	1													
3	0.97	0.98	1												
4	0.96	0.98	1	1											
5	0.92	0.94	0.95	0.97	1										
6	0.93	0.95	0.97	0.98	0.97	1									
7	0.92	0.94	0.97	0.97	0.94	1	1								
8	0.92	0.94	0.97	0.97	0.94	0.98	1	1							
9	0.70	0.72	0.75	0.78	0.88	0.82	0.78	0.78	1						
10	-0.30	-0.30	-0.31	-0.28	-0.10	-0.27	-0.34	-0.34	0.21	1					
12	-0.32	-0.32	-0.32	-0.30	-0.13	-0.31	-0.36	-0.37	0.18	1	1				
13	-0.36	-0.36	-0.36	-0.32	-0.14	-0.32	-0.39	-0.39	0.18	0.99	1	1			
14	-0.36	-0.36	-0.36	-0.33	-0.14	-0.32	-0.39	-0.39	0.18	0.99	0.99	1	1		
Rect. Red	0.83	0.87	0.90	0.91	0.89	0.94	0.95	0.95	0.78	-0.29	-0.31	-0.32	-0.32	1	
Rect. NIR	-0.27	-0.28	-0.27	-0.24	-0.07	-0.25	-0.31	-0.31	0.23	0.97	0.97	0.98	0.98	-0.23	1

Appendix 7. Presents the scatterplots and the correlation matrix of the comparison of a) NDVI (TOArReflectances) - NDVI (TOC Reflectance), b) NDVI (TOA Radiances) - NDVI (TOC Reflectances), c) NDVI (TOA Radiances) - NDVI (TOAr Reflectances). Correlation matrix for the NDVI.

a)

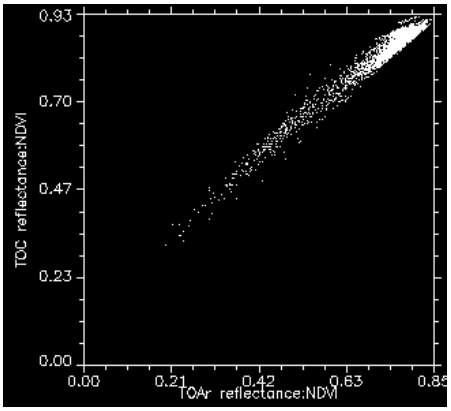

b)

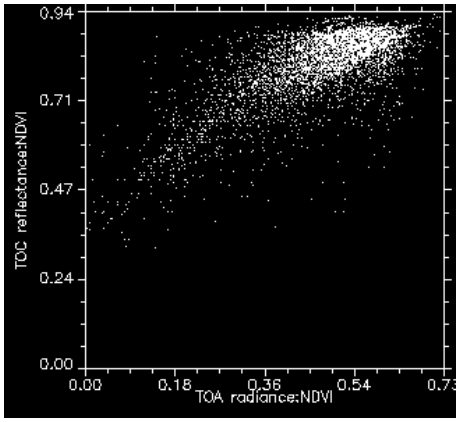

c)

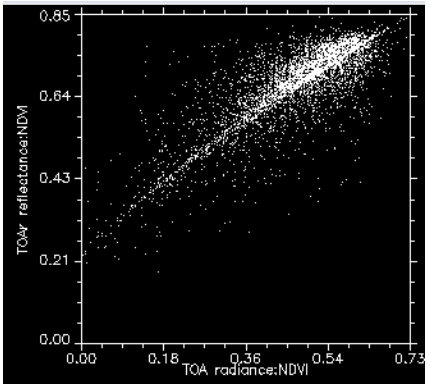

Correlation matrix for the NDVI

Correlation	NDVI TOA Rad.	NDVI TOAr Refl.	NDVI TOC Refl.
NDVI TOA Rad.	1		
NDVI TOAr Refl.	0.84	1	
NDVI TOC Refl.	0.80	0.98	1

Appendix 8. Presents the scatterplots and the correlation matrix of the comparison of a) GEMI (TOArReflectances) - GEMI (TOC Reflectance), b) GEMI (TOA Radiances) - GEMI (TOC Reflectances), c) GEMI (TOA Radiances) - GEMI (TOAr Reflectances).

a)

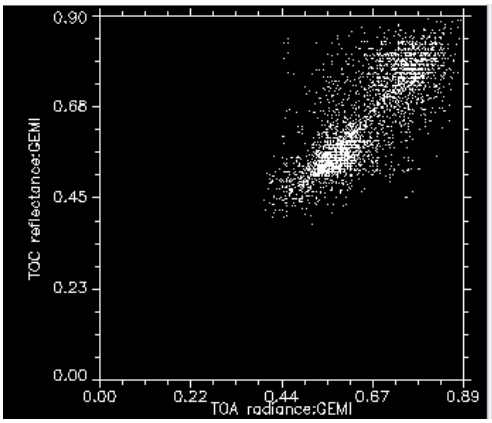

b)

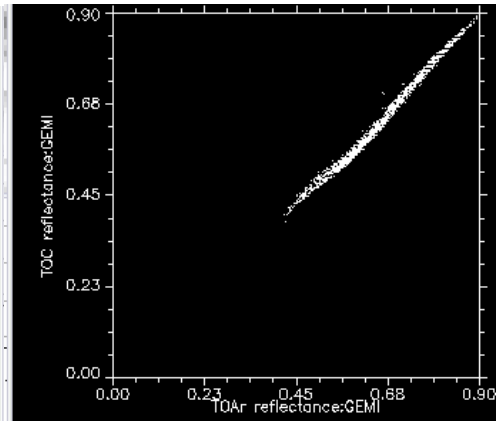

c)

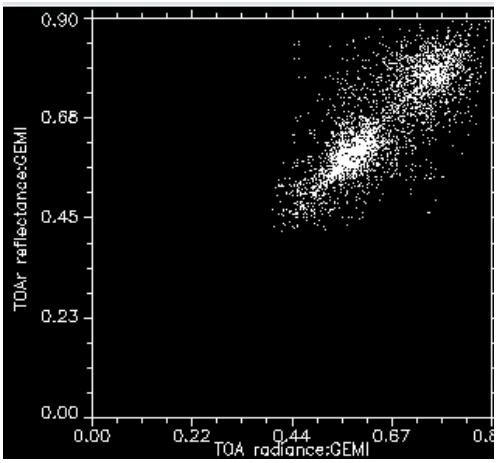

Correlation matrix for the GEMI

Correlation	GEMI TOA Rad.	GEMI TOAr Refl.	GEMI I TOC Refl.
GEMI TOA Rad.	1		
GEMI TOAr Refl.	0.90	1	
GEMI TOC Refl.	0.89	0.99	1

Appendix 9. Scatterplots of the VI_{MERIS}-VI_{HyMap} relationship using the derivations of VI_{MERIS} from TOC reflectances (TOC refl.) for the arable land-dominated pixels of Millingerwaard. Lines are least squares fit to a linear model.

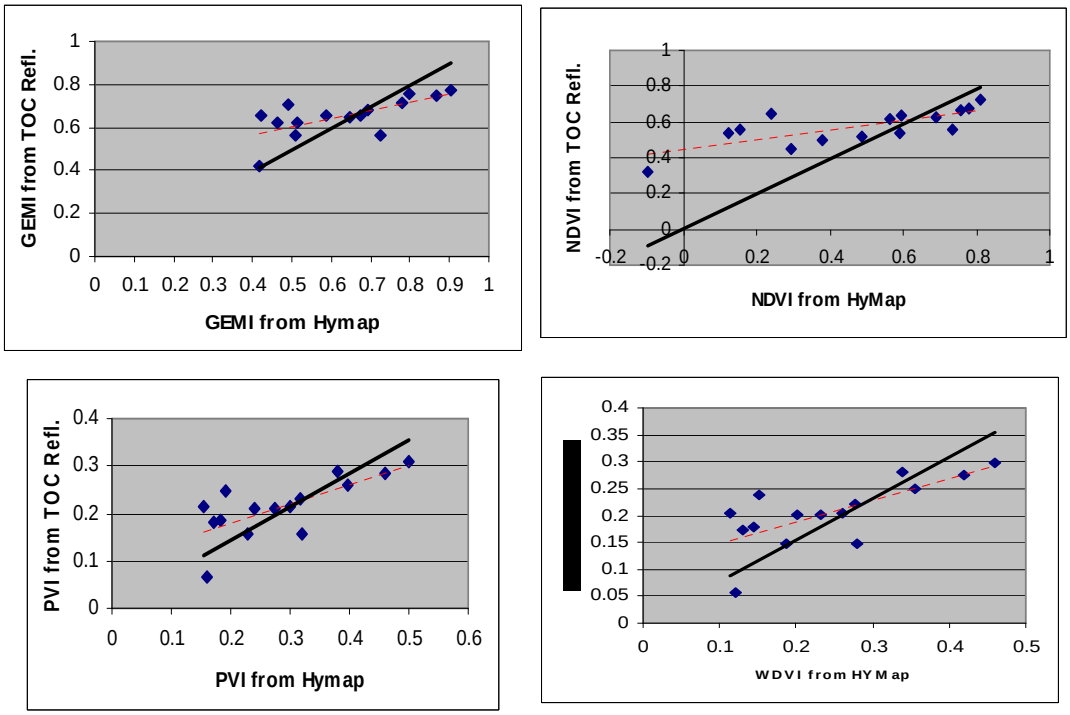

Appendix 10. Scatterplots of the VI_{MERIS}-VI_{HyMap} relationship using the derivations of VI_{MERIS} from TOC reflectances (TOC refl.) for the arable land-dominated pixels of Millingerwaard..

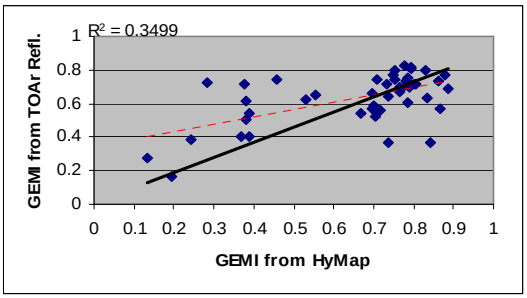

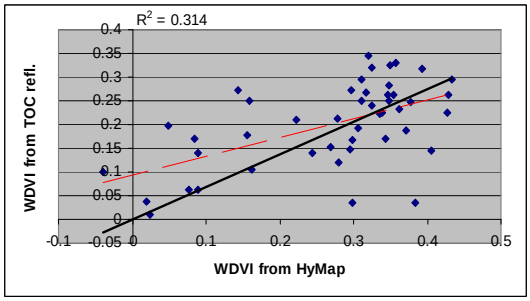

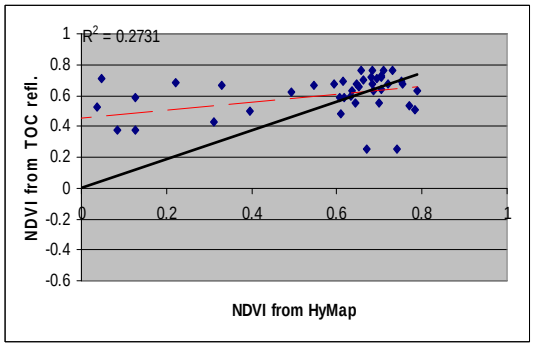

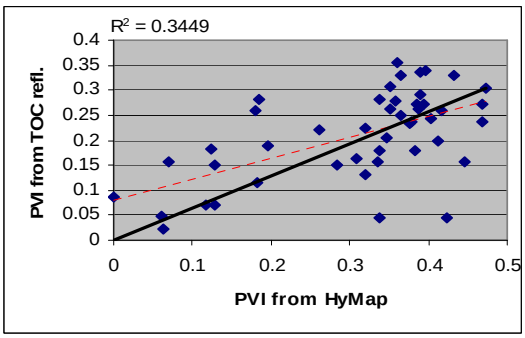

Appendix 11. Effects of different stages of image processing on the LAI–VI relationship across all sites: TOC reflectance of arable. See Table 23. for the model and *R*2 in each case.

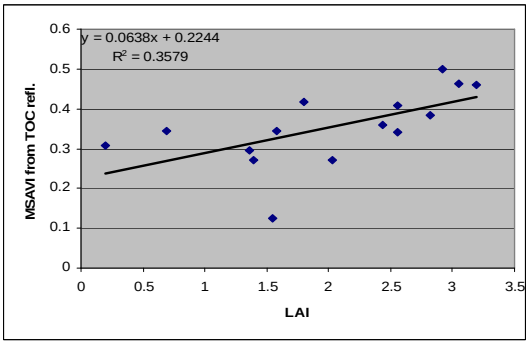

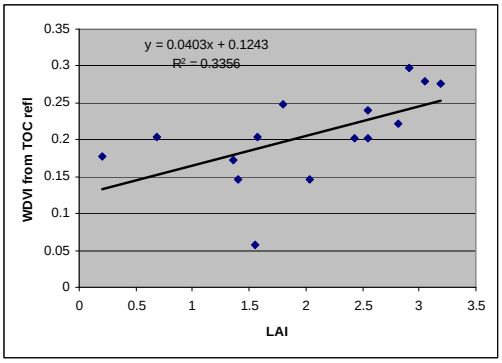

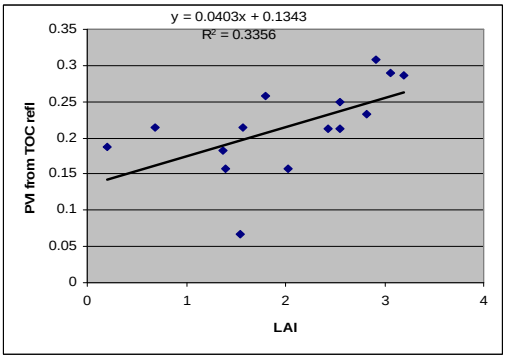

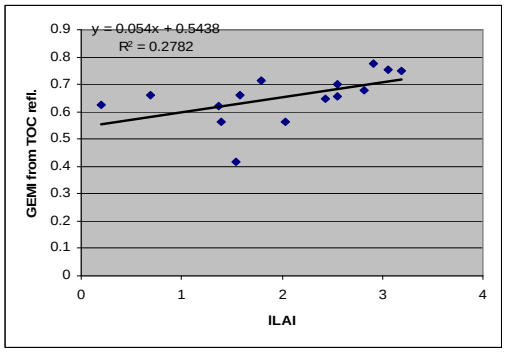

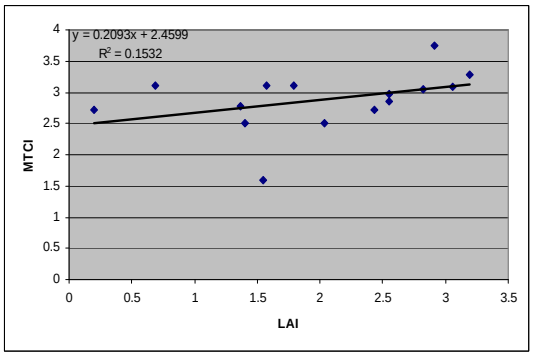

Appendix 12. Effects of different stages of image processing on the LAI–VI relationship across all sites: TOC reflectance of grass. See Table23. for the model and R^2 in each case.

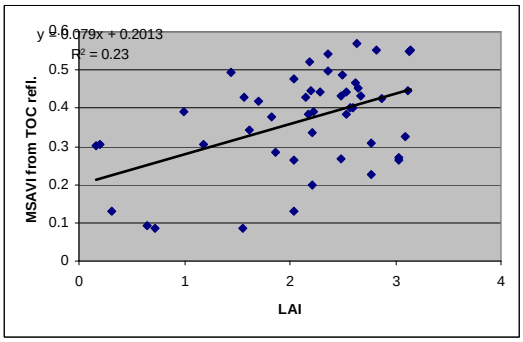

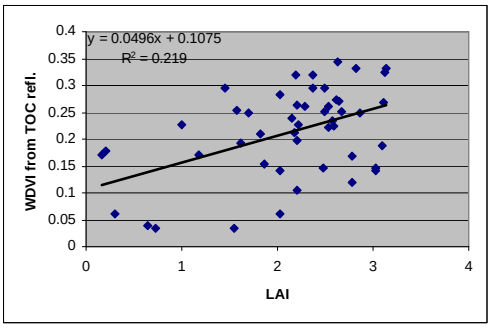

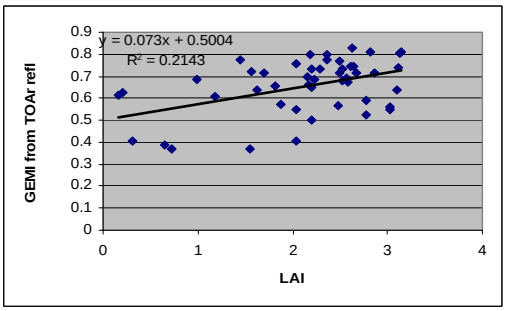

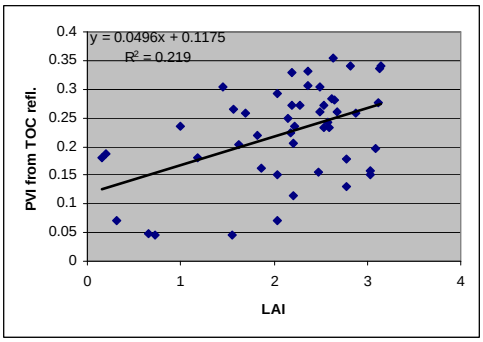

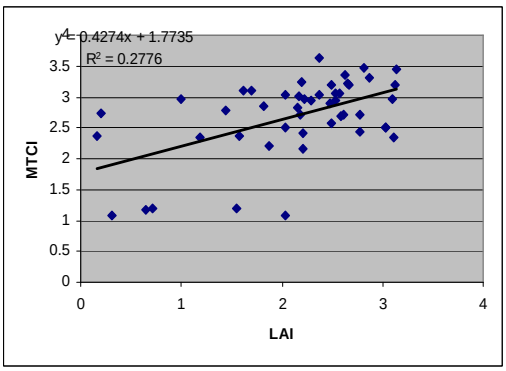

Appendix 13. Effects of different stages of image processing on the MGVI–VI relationship across all sites: TOC reflectance of arable land. See Table 25 for the model and R^2 in each case.

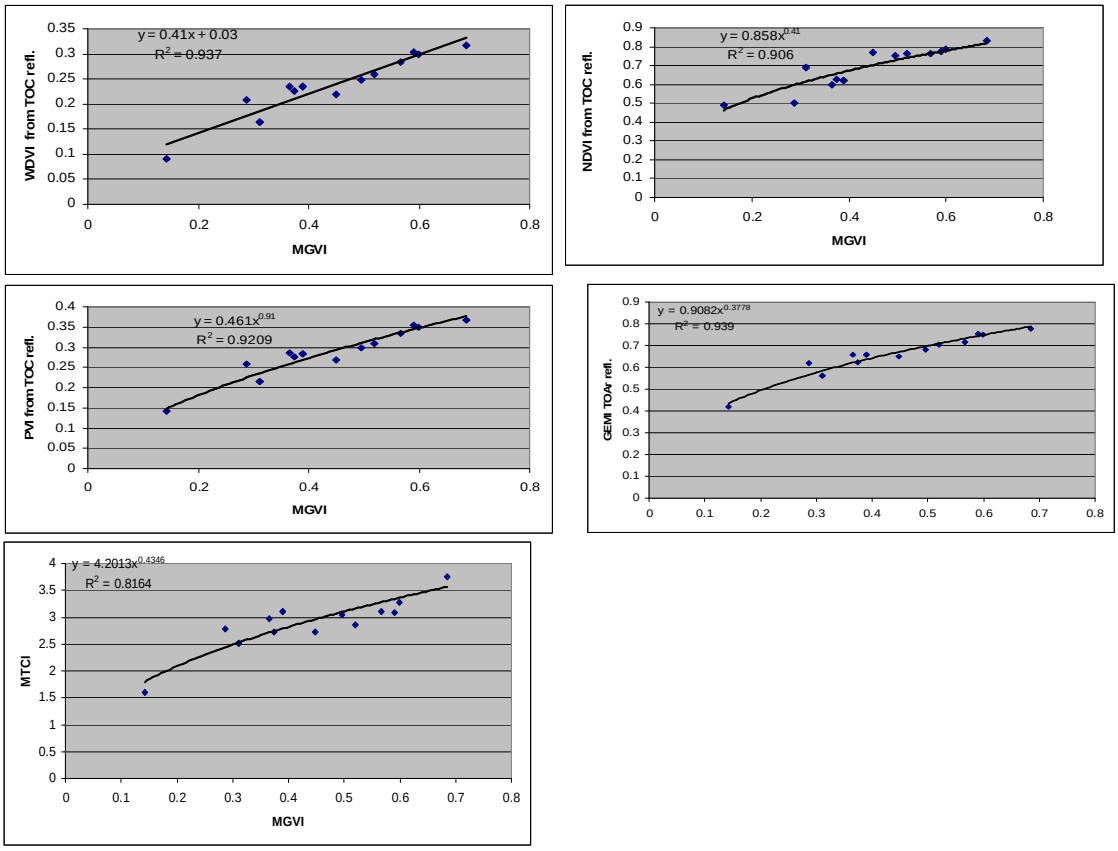

Appendix 14. Effects of different stages of image processing on the MGVI–VI relationship across all sites: TOC reflectance of grass. See Table 25 for the model and R^2 in each case